Aspects of QCD thermodynamics with exact chiral fermions on the lattice.

A Thesis

Submitted to the
Tata Institute of Fundamental Research, Mumbai
for the degree of Doctor of Philosophy
in Physics

by

Sayantan Sharma

School of Natural Sciences,
Tata Institute of Fundamental Research
Mumbai

August, 2011

Dedicated to my
Ma and Baba

DECLARATION

This Ph.D. thesis is a presentation of my original research work. Wherever contributions of others are involved, every effort is made to indicate this clearly, with due reference to the literature, and acknowledgement of collaborative research and discussions.
The work was done under the guidance of Professor Rajiv V. Gavai, at the Tata Institute of Fundamental Research, Mumbai.

Sayantan Sharma

In my capacity as supervisor of the candidates thesis, I certify that the above statements are true to the best of my knowledge.

Rajiv V. Gavai

Contents

List of Tables

List of Figures

Acknowledgements

I would like to express my gratitude to my thesis advisor Prof. Rajiv Gavai for all that I learnt from him during my Ph. D. work. It has been a wonderful experience working with him. His insight and enthusiasm for the subject was inspiring for me. I hope I have been able to better myself over the years through his constant encouragement as well as critical evaluation of my work. I am also grateful to him for his support and advice related to matters both in academics and beyond. It was very enjoyable collaborating with Prof. Rajamani Narayanan and I gratefully acknowledge all that I learnt from him. I would like to thank Prof. Sourendu Gupta for the excellent courses he taught to me both in TIFR as well as in other schools during these years and for the many things on Lattice that I learnt from him. I would also like to thank Dr. Saumen Datta and Dr. Nilmani Mathur for all their help and encouragement during these years. It was very enjoyable interacting with them and learning from them. Thanks to Debasish, my collaborator, and specially to the junior most members of my group Nikhil and Padmanath for all their help. I would like to acknowledge the support during the course of my Ph. D. from the Council of Scientific and Industrial Research(CSIR), Government of India through the SPM fellowship.

It was a great experience to be a part of the Department of Theoretical Physics at TIFR. We had some very good courses as well as regular seminars which gave me a good exposure to the current research in theoretical physics. I would like to thank all the members and the former and current students of my department for a creating a good ambiance of learning. I had a great opportunity to be a part of the 2006 batch of physics and I have enjoyed interacting with my batchmates. I specially appreciate and acknowledge the constant help, encouragement and support from Kusum, Prithvi, Satya and Vibhor and all that I learnt from them; my stay at TIFR would not have been so much enjoyable without their presence.

It was a pleasure interacting with Loganayagam and learning so many things from him. I also enjoyed the company of Anindita, Kishor, Saswata and Somnath from outside my department. I would also like to thank my very lively juniors Amaresh, Arka, Atul, Dipan, Nilay, Sambuddha, Sanmay and Tarun among others whom I have not named explicitly, who have been my support over these years and also helped me in so many ways. My thesis is dedicated to my parents who have been with me throughout. I thank them, my dear sister and my family members whose support and encouragement helped me in my academics over all these years.

Synopsis

Introduction

Protons and neutrons constitute 99.9% of the visible matter in our universe. Understanding the nature and interactions of these particles or of the hadronic matter is one of the important areas of research in fundamental physics. From the experiments at SLAC linear collider in the early 1970 s, where high energy electrons were bombarded on proton targets, it was observed that the scattering of the electrons were caused by point-like particles inside the protons called partons. This also established the fact that the coupling constant that governs the strength of interactions between these partons, now called quarks and gluons, falls with increasing momentum giving rise to almost free partons at large momenta. Experimental searches [1] for free quarks have so far yielded negative results. Thus they are confined to hadrons at low energies. Quantum chromodynamics(QCD) has been a successful theory that can explain both these phenomena of confinement and asymptotic freedom.

If the hadrons are subjected to very high temperatures like that would have occurred in the early universe or can occur in the Heavy-Ion colliders in the present time, one expects that the quarks and the gluons would be liberated from them. The Heavy ion collision experiments at Relativistic Heavy Ion Collider(RHIC) at the Brookhaven National Laboratory have recently found promising signatures of an equilibrated state of matter called the Quark-Gluon Plasma(QGP) formed from the melting of the hadrons at high temperatures. Predicting the different phases of the strongly interacting matter at finite temperatures and density theoretically is of great importance to understand the exciting results coming form the RHIC and expected to come from the upcoming heavy-ion collider facilities at LHC(ALICE experiment) at CERN, GSI in Germany and NICA in Russia. Currently large

portion of the phase diagram of the strongly interacting matter is speculative and most of it known from model calculations which fall in the same universality class as QCD or are expected to be valid for low energy QCD.

Lattice Quantum Chromodynamics(LQCD) has so far provided the most reliable theoretical predictions for the thermodynamics of quarks and gluons important for the ongoing experiments at RHIC, BNL and LHC, CERN. It involves discretizing the continuum QCD Lagrangian on a spacetime lattice. All the operators become finite dimensional matrices and different thermodynamic quantities can be computed in terms of the finite dimensional operators. The lattice spacing acts as an ultraviolet regulator and the theory is finite. However one has to perform a continuum extrapolation of the observables computed on the lattice to mimic the real world and confirm that the renormalization is done properly.

One of the important predictions of LQCD is the existence of QCD critical point at high temperature and small baryon density beyond which, at vanishing baryon density, the transition from hadron phase to QGP becomes a crossover for two light and one heavy quark flavour. The critical point seems to be associated with the chiral symmetry restoration transition. It would be desirable to use fermions with exact chiral symmetry for lattice studies on the critical point. Moreover the location, and even the existence of the critical point in the phase diagram is expected [2] to depend crucially on N_f, as a result of the dependence of the order of the chiral transitions on N_f. The popular choices of the fermions employed in simulations so far like the Wilson fermions, have no chiral symmetry on the lattice or the staggered fermions, which have only a partial chiral symmetry. For the staggered fermions, more often used in finite temperature and density QCD simulations due to this partial chiral symmetry, even N_f is undefined. Of course, these issues are expected to become irrelevant in the continuum limit of vanishing lattice spacing. But they are likely to affect the current available lattice results, sometimes even qualitatively. On the other hand fermions with exact chiral symmetry on the lattice like the Overlap [3] and Domain wall fermions [4] are very expensive to simulate even on reasonably small size lattices. Apart from the advances in both algorithms and the computer hardware, it would be important to look for improvements of the chiral fermion operators for large scale QCD simulations. In view of the practical importance of the applicability of chiral fermions in LQCD, the present thesis work addresses the following issues:

- Whether chiral symmetry is intact when chemical potential is introduced. One of the main conclusions of this work is that the chiral symmetry is not respected by the existing chiral fermion operators at finite density.
- Understanding the lattice discretization effects in the different thermodynamic observables computed using the exact chiral fermions on the lattice both analytically and numerically.
- Reducing these discretization effects for small lattices either by tree level improvement or by appropriate choice of the irrelevant parameter present in the chiral fermion operators.
- Understanding the non-perturbative dependence of chiral anomaly on the fermion chemical potential and its implications for guidance in the choice of lattice chiral operators.
- New and better ways of incorporating chemical potential in chiral fermion operators which may preserve explicit chiral symmetry on the lattice.
- Formulating suitable fermion operators at finite density with remnant chiral symmetry that would allow for faster computation of thermodynamic quantities like the quark number susceptibilities(QNS) to enable precise predictions for the QCD critical point by computing higher order QNS.

Thermodynamics of Overlap fermions

The Overlap fermions [3] preserve chiral symmetry on the lattice by circumventing the famous No-go theorem [5], sacrificing the ultralocality of the fermion operator. The non-locality of the Overlap fermions makes its applicability for large scale QCD simulations difficult. It would thus be important to study different thermodynamic observables on the lattice with free Overlap fermions both analytically and numerically to understand the discretization effects. One may attempt to reduce them by tree level improvements or by fine tuning the irrelevant parameters in the Overlap operator. Also Overlap operators at finite fermion density is still a nascent area of research. One of the main results of the thesis is that all

existing Overlap operators break chiral symmetry explicitly on the lattice for finite chemical potential.

We consider a lattice with N^3 sites and lattice spacing a along the three spatial directions and N_T sites and lattice spacing a_4 along the temporal direction. The volume of the box is $V = N^3a^3$ and the temperature of the system is $T = (N_T a_4)^{-1}$. The Overlap Dirac operator [3] has the following definition for massless fermions,

$$D_{ov} = 1 + \gamma_5 sgn(\gamma_5 D_W) \ , \ sgn(\gamma_5 D_W) = \frac{\gamma_5 D_W}{\sqrt{\gamma_5 D_W \gamma_5 D_W}} \ . \tag{1}$$

where sgn denotes the sign function. The naive discretization of the continuum Dirac operator on a lattice leads to the fermion doubling problem. One of the ways to remove the doublers is to add a second derivative term with the naive Dirac operator which gives us the Wilson-Dirac operator,

$$\begin{aligned} D_W(x,y) &= (3 + \frac{a}{a_4} - M)\delta_{x,y} - \frac{a}{a_4}[U_4^\dagger(x-\hat{4})\delta_{x-\hat{4},y}\frac{1+\gamma_4}{2} + \frac{1-\gamma_4}{2}U_4(x)\delta_{x+\hat{4},y}] \\ &- \sum_{i=1}^{3}[U_i^\dagger(x-\hat{i})\delta_{x-\hat{i},y}\frac{1+\gamma_i}{2} + \frac{1-\gamma_i}{2}U_i(x)\delta_{x+\hat{i},y}] \end{aligned} \tag{2}$$

where the U_μ are the gauge links that connects two adjacent sites on the lattice and is an element of SU(3) colour group. The D_W has a negative mass term M, which is an irrelevant parameter of the Overlap operator. It needs to be restricted between 0 to 2 for simulating a single quark flavour on the lattice. The Overlap operator satisfies the Ginsparg-Wilson relation [6] ensuring exact chiral symmetry on the lattice. The corresponding energy density can be obtained from the partition function,

$$Z = \int \mathcal{D}U \ \mathrm{e}^{-\mathrm{S_{gluon}}} \ \mathrm{det\ D_{ov}} = \langle \mathrm{det\ D_{ov}} \rangle, \tag{3}$$

by taking derivatives with respect to the temperature:

$$\epsilon = \frac{T^2}{V} \left. \frac{\partial \ln Z(V,T)}{\partial T} \right|_V ,$$

We restrict ourselves to $U = 1$ here to focus on the ideal gas limit.

We [16] showed that the energy density can be expressed in terms of the functions g,

f and d are given by,

$$\begin{aligned} g &= M - 4 + b, \text{ with} \\ b &= \cos(ap_1) + \cos(ap_2) + \cos(ap_3) \\ f &= h_1^2 + h_2^2 + h_3^2 \\ d &= 4 + (M-4)^2 + 2(M-4)b + c, \text{ with} \\ c &= \sum_{i<j<4} 2\cos(ap_i)\cos(ap_j) \ . \end{aligned} \tag{4}$$

These functions g, d and f depend only on discrete spatial momenta p_j , j =1-3. This enables us to write down the $ap_4 = \omega_n$-dependence of the energy density explicitly as,

$$\begin{aligned} \epsilon a^4 = \frac{2}{N^3 N_T} \sum_{p_j,n} \left[(g + \cos\omega_n) + \sqrt{d + 2g\cos\omega_n} \right] \\ \times \quad \left[\frac{(1-\cos\omega_n)}{d + 2g\cos\omega_n} + \frac{\sin^2\omega_n (g + \cos\omega_n)}{(d + 2g\cos\omega_n)(f + \sin^2\omega_n)} \right] \ . \end{aligned} \tag{5}$$

The summation over the Matsubara frequencies ω_n, can be converted to a contour integral [16] resulting in the energy density on the lattice to be,

$$\epsilon a^4 = \frac{4}{N^3} \sum_{p_j} \left[\frac{\sqrt{f}}{\sqrt{1+f}} \right] \frac{1}{e^{N_T \sinh^{-1}\sqrt{f}} + 1} + \epsilon_3 + \epsilon_4 \ , \tag{6}$$

Unlike the case of Wilson or staggered fermions where only the physical poles at $\pm i \sinh^{-1}\sqrt{f}$ contribute to the energy density, for the Overlap there are additional branch cuts that contribute to the integrals. These are symbolically denoted as ϵ_3 and ϵ_4. Both the additional lattice artifacts are M dependent. Judicious choice of M can minimize their contributions to the energy density on the lattice.

In the continuum limit of $a \to 0$, the integration variable $\omega = ap_4$ can be traded for p_4, pushing the branch points at $\pm\pi \pm i\cosh^{-1}\frac{d}{2g}$ to infinity faster and hence the terms ϵ_3 and ϵ_4 vanish. Since the poles at $i \sinh^{-1}\sqrt{f}$ scale as a in this limit, they continue to be enclosed in the contour at a finite p_4 and contribute to the energy density giving the correct continuum value, $\epsilon_{SB} = 7\pi^2 T^4/60$.

The numerical estimates of different thermodynamics quantities were also studied, with the aim of finding out,

- the importance of the terms ϵ_3 and ϵ_4 in it on lattices of practical sizes, and
- the role the irrelevant parameter M plays on finite lattices.

In particular, it would be good to know if there exists a range of the parameter M for which the energy density converges to that of the continuum ideal Fermi gas on computationally inexpensive, lattice sizes. The energy density for the Overlap fermions was estimated numerically by summing over all the momenta. In general, the dimensionless lattice energy density will be of the form,

$$E = A(M) + \frac{B}{N_T^4} + \frac{C(M)}{N_T^6} + \frac{D(M)}{N_T^8} + ... \tag{7}$$

where the coefficients $A(M)$ and B are the usual vacuum and the T^4 contributions respectively and $C(M)$ and $D(M)$ are finite lattice spacing artifacts. For each value of the aspect ratio, defined as $\zeta = N/N_T$ and M, the energy density on the lattice was calculated as a function of the N_T. $A(M)$ is the dominant contribution and its removal turned out to be a tricky issue governed by the precision of our computations. This zero temperature part of the energy density was calculated from Eq.(5) by taking $N_T \to \infty$ and a large spatial extent, keeping the lattice spacing finite. The resulting integral over ω was done numerically for each M to estimate the zero temperature contribution. Subtracting the zero temperature part from the energy density and dividing the resultant ϵ by ϵ_{SB} was used to study the ζ and N_T dependence. For any fixed value of M, the ratio appeared to become independent of ζ for $\zeta \geq 3$ signalling the onset of the thermodynamic limit. For a fixed $\zeta = 5$, the range of $1.5 \leq M \leq 1.6$ was found to be the favoured one because all the M-dependent terms were seen to be minimum there.

The chemical potential is usually introduced as the Lagrange multiplier for the constant conserved number in the Lagrangian. On the lattice the chemical potential is written as a dimensionless quantity, $\hat{\mu} = \mu a_4$. Divergences were known to arise [7, 8, 9] for staggered and Wilson fermions, if $\hat{\mu}$ was introduced naively as a coefficient of the conserved number. These were eliminated by putting $\hat{\mu}$ as multiplying factors $\exp(\hat{\mu})$ and $\exp(-\hat{\mu})$ to the timelike links U_4 and $U_4^\dagger$ respectively in Eq.(2). A more general way to introduce the chemical potential is, of course, to introduce functions $K(\hat{\mu})$ and $L(\hat{\mu})$ in place of the factors $\exp(\hat{\mu})$ and $\exp(-\hat{\mu})$ respectively such that $K(\hat{\mu}) = 1 + \hat{\mu} + \mathcal{O}(\hat{\mu}^2)$ and $L(\hat{\mu}) = 1 - \hat{\mu} + \mathcal{O}(\hat{\mu}^2)$. It was shown [10] that the quadratic divergences are avoided if $K(\hat{\mu}) \cdot L(\hat{\mu}) = 1$.

Constructing the conserved number operator for the Overlap Dirac fermions is not easy due to its nonlocality [11] and the corresponding currents may not even be unique [12]. Instead of deriving the conserved number, an inspired guess for it could be made such that it has the right continuum limit. One such proposal for introducing the chemical potential for the Overlap operator is [13] to introduce it in the D_W as one would for the usual Wilson fermions:

$$D_{ov} = 1 + \gamma^5 sgn(\gamma^5 D_W(\hat{\mu})) \ , \tag{8}$$

where the timelike links U_4 and $U_4^\dagger$ respectively in $D_W(\hat{\mu})$ are multiplied with $\exp(\pm\hat{\mu})$. This, of course, renders $\gamma_5 D_W(\hat{\mu})$ non-Hermitian, necessitating an extension of the usual definition of the sign function. It was argued in [13] that the natural choice is to use the sign of the real part of the eigenvalues of $\gamma_5 D_W(\hat{\mu})$ in the equation above. It is important to note that the extended sign function it is not defined for purely imaginary eigenvalues. Numerical simulations were performed [14, 15] for an ideal gas of Overlap fermions to show that in the above way of introducing $\hat{\mu}$, one does not encounter any quadratic divergences at zero temperature for $M = 1$. We [16] have extended the studies at finite μ for different M values. The optimum M range at finite density for which the observables like energy density and susceptibility converge to the continuum results at reasonable lattice sizes is the same as in the $\mu = 0$ case. Furthermore it has been shown [17] analytically that the divergences in the thermodynamic observables are absent for the Overlap fermions for the same set of conditions on $K(\hat{\mu}), L(\hat{\mu})$ as for the staggered fermion case.

A crucial difference is that the introduction of the functions K and L for the staggered fermions still leaves the QCD action invariant under the chiral transformations due to the locality of the action. On the contrary, one can easily check that one breaks the chiral invariance in the case of the Overlap fermions by these functions K, L, or $\exp(\pm\hat{\mu})$. As pointed out earlier, the Overlap operator satisfies the Ginsparg-Wilson relation [6]:

$$\{\gamma_5, D_{ov}(0)\} = D_{ov}(0)\gamma_5 D_{ov}(0). \tag{9}$$

Under the lattice chiral transformation defined by [18],

$$\delta\psi = i\alpha\gamma_5(1 - \frac{1}{2}D_{ov}(0))\psi \quad \text{and} \quad \delta\bar{\psi} = i\alpha\bar{\psi}(1 - \frac{1}{2}D_{ov}(0))\gamma_5 \ , \tag{10}$$

the Overlap action at $\hat{\mu} = 0$, $\sum_{x,y} \ \bar{\psi}_x [D_{ov}(0)]_{xy}\psi_y$ remains invariant and thus have an exact chiral symmetry on the lattice. By construction, the $D_{ov}(\hat{\mu})$ also satisfy the following

relation:

$$\{\gamma_5, D_{ov}(\hat{\mu})\} = D_{ov}(\hat{\mu})\gamma_5 D_{ov}(\hat{\mu}). \tag{11}$$

We have pointed out [16], that this condition is inadequate to ensure chiral symmetry on the lattice since the action at finite chemical potential $S = \sum_{x,y}\ \bar{\psi}_x[D_{ov}(\hat{\mu})]_{xy}\psi_y$ is longer invariant under Luscher transformations in Eq.(10). The variation given as,

$$\delta S = i\frac{a\alpha}{2}\sum_{x,y}\bar{\psi}_x\big[2D_{ov}(\hat{\mu})\gamma_5 D_{ov}(\hat{\mu}) - D_{ov}(0)\gamma_5 D_{ov}(\hat{\mu}) - D_{ov}(\hat{\mu})\gamma_5 D_{ov}(0)\big]_{xy}\psi_y \neq 0\ .$$

is of the $\mathcal{O}(a)$ and the symmetry is restored only in the continuum limit. One may argue that by modifying the chiral transformations as,

$$\delta\psi = i\alpha\gamma_5(1 - \frac{1}{2}D_{ov}(\hat{\mu}))\psi \quad \text{and} \quad \delta\bar{\psi} = i\alpha\bar{\psi}(1 - \frac{1}{2}D_{ov}(\hat{\mu}))\gamma_5\ , \tag{12}$$

one would ensure that $\delta S(\hat{\mu}) = 0$. Altering the symmetry transformations as above has undesirable physical consequences, as discussed in detail in [19]. The main points are:

- Non-Hermiticity of $\gamma_5 D_{ov}(\hat{\mu})$ makes the transformations nonunitary.
- The symmetry group itself changes with μ, leaving no physical order parameter which will characterize the chiral phase transition as a function of μ. In contrast, the chiral symmetry group remains the same at nonzero temperature and zero density, allowing us to infer that vanishing of the chiral condensate would correspond to restoration of the symmetry for the vacuum.
- The chiral anomaly is affected and is addressed in detail in the later part of this thesis.

Thermodynamics of Domain wall fermions

The use of the Overlap fermions for large scale QCD simulations is still limited. This is due to the fact that for the interacting theory, computing the inverse square root of the Dirac operator is quite expensive for the current lattice sizes in use. It would be therefore interesting to explore other variant of fermions with exact chiral symmetry on the lattice namely the Domain wall fermions. It was observed that a theory of fermions in a 5 dimensional spacetime with a domain wall type mass term $M(s) \sim \tanh(ks)$, s being the coordinate

along the fifth dimension, would have a massless mode localized on the domain wall when the fifth dimension is infinite. Hence the 4-D chiral fermion localized on the wall is named so. The lattice realization of this 4-D chiral fermions was first formulated by Kaplan [4] and later refined by Shamir [20]. On a finite 5-D lattice of dimensions $N^3 \times N_T \times N_5$, there would a tower of states with the lowest energy mode being the linear superposition of the left and the right handed chiral fermion. There would always be mixing between the left and right chiral modes on a finite lattice but this overlap between the states falls as $\sim e^{-N_5}$ at zero temperature [21]. In this section we try to address the following issues using Domain wall fermions:

- Estimation of the value of N_5 for which the mixing between the chiral zero modes is minimum. Also it would be important to check whether the exponential fall-off of the overlap between the chiral modes is valid also at finite temperatures by studying different thermodynamic quantities.

- For small lattice sizes, could the cut-off effects be reduced in the Domain wall operator such that we obtain results consistent with the continuum thermodynamic quantities within $5 - 10\%$.

To obtain thermodynamical quantities of a 4-D chiral fermion on the lattice, we need to divide out contribution of the heavy fermion modes which exist in the fifth dimension. This was done by introducing a pseudo-fermion action [20] in the standard 5-D fermion action. The fifth dimensional degrees of freedom can be integrated out to yield the Domain wall operator [22, 23] for massless fermions on a $N^3 \times N_T \times N_5$ lattice with lattice spacings of a, a_4 and a_5 in the three spatial, the temporal and the fifth dimension respectively, as

$$D_{DW} = 1 - \gamma_5 \tanh(\frac{N_5}{2} \ln |T|), \tag{13}$$

where the transfer matrix T that communicates between the fermions on adjacent slices along the fifth dimension;

$$T = (1 + \frac{a_5}{a}\gamma_5 D_W P_+)^{-1}(1 - \frac{a_5}{a}\gamma_5 D_W P_-). \tag{14}$$

and $P_\pm = \frac{1 \pm \gamma_5}{2}$ are the chiral projectors. For the non-interacting fermions, the Domain wall operator was diagonalized [24]. It is to be noted that M is the height of the domain wall on

the lattice which is again fixed to be between 0& 2 for simulating one flavour quark on the lattice. The energy density which is the temperature derivative of partition function was shown to be [24],

$$\epsilon = \frac{2}{N^3 a^4 N_T} \sum_{p_j, p_4} \left(\frac{t^{'}}{t} + \frac{2^{N_5} u^{'}}{2^{2N_5+1} + 2^{N_5} u} - \frac{t u^{'} + u t^{'} - x q^{'} - (q-2) x^{'}}{t u - (q-2) x} \right) \tag{15}$$

where the quantities q, t, u and x are functions of d, f, g and $q^{'}, t^{'}, u^{'}, x^{'}$ are their respective a_4 derivatives,

$$\begin{aligned} s^2 &= d + 2g\cos\omega_n \ , \ t = s\sqrt{s^2 - 4(g+\cos\omega_n) + 4} \ , \ q = s^2 - 2(g+\cos\omega_n) + 2 \\ u/x &= \left(\frac{t-q}{h_5 - 1} \right)^{N_5} + / - \left(\frac{t+q}{1-h_5} \right)^{N_5} \ , \ h_5 = g + \cos\omega_n \ . \end{aligned}$$

In the above expressions a_4 is set to a after evaluating the a_4-derivative. It is difficult to calculate the energy density given in Eq.(15) analytically. In the limit $N_5 \to \infty, a_5 \neq 0$, the energy density expression simplifies to the form,

$$\begin{aligned} \epsilon a^4 &= -\frac{1}{N^3 N_T} \sum_{p_j, n} \left(\frac{4h_5\gamma + 4ss^{'}(1+s^2) + 2ss^{'}t + s^2 t^{'} - 4\gamma s^2 - 8h_5 ss^{'} - 2\gamma t - 2h_5 t^{'}}{2h_5^2 + 2s^2 + s^4 + s^2 t - 4h_5 s^2 - 2h_5 t} \right. \\ &\left. - \frac{2t^{'}}{t} \right) \equiv \frac{1}{N^3 N_T} \sum_{p_j, n} F(R, \omega_n, \vec{p}) \ . \end{aligned} \tag{16}$$

This expression can be computed analytically using the contour integral trick as was outlined for the Overlap fermions. However there are some major differences between the non-analyticities of the function $F(R, \omega_n, \vec{p})$. As in the Overlap case [16], there are poles at $\cos^{-1}(-\sqrt{d-g^2}) = \pm\pi \pm i \sinh^{-1}\sqrt{f}$ and branch cuts at $\pm\pi \pm i\cosh^{-1}\frac{d}{2g}(\pm i\cosh^{-1}\frac{d}{2g})$ for $\frac{d}{2g} > 0 (< 0)$. However in this case, there are additional(unphysical) poles and cuts at at $\pm i\cosh^{-1}\omega_1$ where $\omega_1 = (d+4-4g)/2(g-2)$. Since the latter lie below the previous branch cuts in the complex ω plane we have to close the contour within the bounds set by $\pm i\cosh^{-1}\omega_1$. The resultant energy density expression for the Domain wall fermions on a finite lattice would be,

$$\epsilon a^4 = \frac{1}{N^3} \sum_{p_j} \left[4\frac{\sqrt{f}}{\sqrt{1+f}} + \frac{\sqrt{1+f}-1}{\sqrt{f(1+f)}} G(M) \right] \times \frac{1}{e^{N_T \sinh^{-1}\sqrt{f}} + 1} + \epsilon_3 + \epsilon_4 \ ,$$

Due to a different functional form of F and a different choice of contour, the corresponding lattice correction terms ϵ_3, ϵ_4 are different from the Overlap fermions, leading to different

cut-off effects. This would change the value of the optimal M range for the Domain wall fermions in which the effect of these cut-off effects is minimum. To find the optimal M range, the energy density was computed numerically by summing over the discrete momenta along the spatial and temporal directions. The zero temperature part of the energy density was determined in the same way as was done for the Overlap fermions. Holding the physical volume constant in units of T by keeping $V^{1/3}T = N/N_T = \zeta$ fixed, the continuum limit is achieved when $N_T \to \infty$. The thermodynamic limit is attained for ζ =4-5 for this fermion operator too. The ratio ϵ/ϵ_{SB} become N_5-independent by $N_5 = 18$, making it an optimum choice for obtaining continuum results on the lattice. The optimum range of M is however marginally shifted to 1.45-1.50 where the results obtained are within 3-4 % of the continuum value on the smallest possible lattice of extent $N_T \geq 10$.

At finite density, we considered two quantities of study, first being $\Delta\epsilon(\hat{\mu}, T) = \epsilon(\hat{\mu}, T) - \epsilon(0, T)$ and the quark number susceptibility at $\hat{\mu} = 0$ using the Domain wall operator at finite $\hat{\mu}$ [25]. We have showed analytically that no divergences exist for general choice of functions $K(\hat{\mu})\&L(\hat{\mu})$ satisfying $K.L = 1$ and $K - L \sim \hat{\mu}$. We estimated numerically $\Delta\epsilon(\mu, T)$ for $\mu/T = \hat{\mu}N_T$ fixed at 0.5. No μ^2 divergences were found in these quantities on a finite lattice, as expected [7]. The deviation from the continuum limit was again seen to be small for the same optimum range of $1.45 \leq M \leq 1.50$ for both the observables, as obtained in the zero chemical potential case.

The thermodynamic quantities computed with the Domain wall fermions have large $1/N_T^2$ corrections for small N_T. While we found that the continuum limit for various thermodynamic quantities can be approached faster by choosing the irrelevant parameter M in the range 1.45-1.50, the correction terms for N_T =4-6 are about twice that of the Stefan-Boltzmann result for such a choice of M too. To improve the convergence to the continuum results for small N_T and even for $M = 1.0$ we added three-link terms to the D_W inspired by the attempts to improve the staggered fermions [26]. This amounts to replacing each γ_μ by $(c_1 + c_3/3)\gamma_\mu$. The Wilson mass term, added to remove the doublers, is kept unchanged. The modified D_W operator is still γ_5-hermitian for arbitrary real values of the coefficients c_1 and c_3. The coefficients $c_1\&c_3$ were fixed by demanding the dispersion relation for free fermions in the continuum limit has no terms at $O(a^3 p_j^3)$. This is satisfied for the values of coefficients $c_1 = 9/8,\ c_3 = -1/8$. The ratio of quark number susceptibilities, χ/χ_{SB}, computed

using the above modified Domain wall operator, was studied as a function of $1/N_T^2$. It was observed that the contribution of the correction terms at N_T =6-8 reduced from $\sim 45\%$ for the usual Domain wall operator to about 7-8 %. The improvements for the energy density were quantitatively similar for the improved fermions.

This set of optimum parameters is anticipated to produce similar results in full QCD simulations with chiral fermions. In presence of interactions, the optimum M range may alter but we expect that such changes would not be drastic.

Anomaly and chiral fermions on the lattice

We have showed in this work, that in order to maintain the exact chiral invariance of the Overlap and the Domain wall actions at finite density, one has to modify the chiral transformation on the lattice to those given in Eq.(12). Apart from the unphysical consequences mentioned earlier, it would also result in the chiral anomaly being μ-dependent on the lattice. In view of this we wanted to study what happens to the chiral anomaly at finite temperature and density non-perturbatively.

Anomalies arise when certain symmetries of the action at the classical level are violated when quantum corrections are taken into account. Chiral anomalies are a well-known example of this phenomenon. The flavourless axial current of the fermions is classically conserved but is violated at one-loop level, as was shown in the famous calculation of the Adler-Bell-Jackiw(ABJ) triangle diagram [27, 28]. The anomalous contribution is a universal feature of the theory and is independent of the ultraviolet regulator used for the quantum theory. Fujikawa provided a new insight on chiral anomalies by showing that they arise due to the change of the fermion measure under the corresponding transformation of the fermion fields [29] in the path integral method.

The size of the coefficient of the chiral anomaly term may affect the order of phase transition. Hence preserving the chiral anomaly in an interacting theory is important. If the anomaly contribution is sizeable even at finite temperature [30], the chiral phase transition is of second order, with critical exponents of the $O(4)$ spin model, for the physically interesting case of two massless flavour QCD ($N_f = 2$). One could expect a QCD-critical point in the $T - \mu$ plane for light quarks in that case. It is thus important to ascertain what change

occurs in the anomaly in the presence of finite temperature and densities.

Perturbative calculations of the ABJ anomaly were reported earlier in the *real* time formalism at finite temperature [31]. It turned out that the non-perturbative calculation of the chiral anomaly was not done earlier for QCD at finite density. In the thesis, we studied both the perturbative and nonperturbative aspects of the chiral anomaly at finite temperature/density. The perturbative calculation was done in the imaginary time formalism as this is directly related to the lattice calculations in the weak coupling. Firstly, we have calculated the expectation value of the gradient of flavour singlet axial vector current of QCD perturbatively in the presence of finite fermion density to check how the anomaly equation is affected in the presence of a nonzero chemical potential. The lowest order diagrams are the ABJ triangle diagrams. We have calculated the triangle diagrams at finite density. Our starting point is the QCD Lagrangian in the Euclidean space with the finite number density term:

$$\mathcal{L} = -\bar{\psi}(\not{D} + m)\psi - \frac{1}{2}\mathrm{Tr}\ \ F_{\alpha\beta}F_{\alpha\beta} + \mu\bar{\psi}\gamma_4\psi\ , \tag{17}$$

where $\not{D} = \gamma_\nu(\partial_\nu - igA^a_\nu T_a)$ with T_a being the generators of the SU(3) gauge group. The ghost terms are not important in such a calculation as these do not directly couple to the fermions. The inverse free fermion propagator is seen to acquire a μ dependence and become $[i\not{p} - m + \mu\gamma_4]$. The rest of the Feynman rules remain the same [34]. In order to find out whether the chiral current $j_{\mu 5} = \bar{\psi}\gamma_\mu\gamma_5\psi$ for massless quarks is conserved at finite density in one-loop perturbation theory, we compute the quantum mechanical expectation value of the derivative of the chiral current i.e. ,

$$\langle\partial_\mu j_{\mu,5}\rangle = -\frac{1}{2}\int d^4x_1 d^4x_2 \partial_\lambda\langle T\{j_{5,\lambda}(x)j_\rho(x_1)j_\sigma(x_2)\}\rangle A^\rho(x_1)A^\sigma(x_2)\ . \tag{18}$$

where the expectation value of the time ordered product of the three currents at one-loop level is the axialvector-vector-vector (AVV) triangle diagram or the ABJ diagram. Any deviation of this quantity from its classical value would give us the anomaly. Using the Euclidean space Feynman rules, the amplitude of the AVV triangle diagram can be computed. The crossed diagram with the gluon legs exchanged among the two vector (VV) vertices, is also considered as this process is quantum mechanically equally favored.

Denoting by $\Delta^{\lambda\rho\sigma}(k_1, k_2)$ the total amplitude and contracting it with q_λ, Eq.(18) can

be written in the momentum space for massless quarks as,

$$
\begin{aligned}
q_\lambda \Delta^{\lambda\rho\sigma} &= (-i)g^2 \mathrm{tr}[T^a T^b] \int \frac{d^4p}{(2\pi)^4} \mathrm{Tr} \Big[\gamma^5 \frac{1}{\not{p} - \not{q} - i\mu\gamma^4} \gamma^\sigma \frac{1}{\not{p} - \not{k}_1 - i\mu\gamma^4} \gamma^\rho - \\
&\quad \gamma^5 \frac{1}{\not{p} - i\mu\gamma^4} \gamma^\sigma \frac{1}{\not{p} - \not{k}_1 - i\mu\gamma^4} \gamma^\rho + \gamma^5 \frac{1}{\not{p} - \not{q} - i\mu\gamma^4} \gamma^\rho \frac{1}{\not{p} - \not{k}_2 - i\mu\gamma^4} \gamma^\sigma \\
&- \gamma^5 \frac{1}{\not{p} - i\mu\gamma^4} \gamma^\rho \frac{1}{\not{p} - \not{k}_2 - i\mu\gamma^4} \gamma^\sigma \Big] , \qquad (19)
\end{aligned}
$$

with the tr (Tr) denoting trace over colour (spin) indices. Suitable rearrangement of the expression in Eq.(19), leads to 3 different terms as a function of powers of μ in the numerator of the above expression:

i) The term independent of μ which gives us the result for the zero density case when a cut-off regulator is used and conservation of vector current is imposed.

ii) term linear in μ which vanishes using the above procedure, and

iii) term which is quadratic in μ which vanishes identically by gamma matrix trace identities.

The vector current conservation condition and suitable method of regulating the the linearly divergent integrals in Eq.(19) gives us the canonical result even for $\mu \neq 0$,

$$
q_\lambda \Delta^{\lambda\rho\sigma} = -\mathrm{tr}[T^a T^b] \frac{ig^2}{2\pi^2} \epsilon^{\alpha\beta\sigma\rho} k_{1\alpha} k_{2\beta} \ . \qquad (20)
$$

It is easy to generalize the same computation to nonzero temperatures. At finite temperature, the temporal part of the momentum gets quantized as the well-known Matsubara frequencies : $p_4 = (2n+1)\pi T$. Correspondingly, $\int_{-\infty}^{\infty} \frac{dp_4}{2\pi}$ gets replaced by $T\sum_n$, where $n = \pm 1, \pm 2, ..., \pm\infty$. The sum over discrete energy eigenvalues, can as usual, be split as a zero temperature contribution and the finite temperature contributions weighted by the Fermi-Dirac distribution functions for the particles and antiparticles. The finite temperature contributions would fall off to zero in the ultraviolet limit because these are regulated by the distribution functions. Thus,

$$
\begin{aligned}
&\int \frac{d^3\vec{p}}{(2\pi)^3} \left[k_1^i \partial_i \left[f(|\vec{p}|) \left(\frac{1}{e^{\beta(|\vec{p}|-\mu)}+1} + \frac{1}{e^{\beta(|\vec{p}|+\mu)}+1} \right) \right] + \{\rho, k_1 \leftrightarrow \sigma, k_2\} \right] \\
&= \mathcal{L}t_{|\vec{p}|\to\infty} \frac{4\pi|\vec{p}|}{(2\pi)^3} \left[(\vec{k}_1 \cdot \vec{p}) f(|\vec{p}|) \left(\frac{1}{e^{\beta(|\vec{p}|-\mu)}+1} + \frac{1}{e^{\beta(|\vec{p}|+\mu)}+1} \right) + \{\rho, k_1 \leftrightarrow \sigma, k_2\} \right] \to 0.
\end{aligned}
$$

We [35] have applied the Fujikawa's method of anomaly calculation in the path integral formalism [29], to the finite fermion density case and derived the anomaly at $\mu \neq 0$ non-perturbatively. In the presence of finite chemical potential, the Dirac operator in the action

is changed from $\not{D}$ to $\not{D} - \mu\gamma_4 = \not{D}(\mu)$. Under chiral transformation of the fermion fields, the action still remains invariant as in the zero density case. This is due to the fact that the μ dependent term of the action anticommutes with γ_5: $\{\gamma_5, \mu\gamma_4\} = 0$. The fermion measure again changes by the same Jacobian factor $\mathrm{Tr}\gamma_5$. The corresponding $\mathrm{Tr}\gamma_5$ is now evaluated in the space of eigenvectors of the new Dirac operator $\not{D}(\mu)$. This is because the measure is defined by the complete set of states of the Dirac operator which appears in the action. Although $\not{D}(\mu)$ has an anti-Hermitian and a Hermitian term, it can be shown diagonalizable. Let ϕ_m be an eigenvector of $\not{D}(0)$ with an eigenvalue λ_m. Since $\not{D}(0)$ is anti-Hermitian, $\{\phi_m\}$ form a complete set of orthonormal vectors. We defined two new vectors, ζ_m and υ_m as follows:

$$\zeta_m(\mathbf{x},\tau) = \mathrm{e}^{\mu\tau}\phi_{\mathrm{m}}(\mathbf{x},\tau) \quad , \quad \upsilon^\dagger_{\mathrm{m}}(\mathbf{x},\tau) = \phi^\dagger_{\mathrm{m}}(\mathbf{x},\tau)\mathrm{e}^{-\mu\tau} \ , \tag{21}$$

and showed that ζ_m is the eigenvector of $\not{D}(\mu)$ with the same (purely imaginary) eigenvalue λ_m,

$$\not{D}(\mu)\zeta_m = \lambda_m\zeta_m \ , \tag{22}$$

and $\upsilon^\dagger_m$ is the eigenvector of $\not{D}(\mu)^\dagger$ with the eigenvalue $\lambda^*_m = -\lambda_m$,

$$\upsilon^\dagger_m\not{D}^\dagger(\mu) = -\lambda_m\upsilon^\dagger_m. \tag{23}$$

The sets of eigenvectors $\{\zeta\}$ and $\{\upsilon\}$ are in one-to-one correspondence with the complete set $\{\phi\}$. Using the completeness relation for the latter,

$$\sum_m \phi_m(x)\phi^\dagger_m(y) = \delta^4(x-y) \ , \tag{24}$$

it can be proved that

$$\sum_m \zeta_m(x)\upsilon^\dagger_m(y) = \sum_m \phi_m(x)\mathrm{e}^{\mu\tau_{\mathrm{x}}}\mathrm{e}^{-\mu\tau_{\mathrm{y}}}\phi^\dagger_{\mathrm{m}}(\mathrm{y})\ \mathrm{d}^4\mathrm{x} = \delta^4(\mathrm{x}-\mathrm{y}). \tag{25}$$

Moreover, $\{\zeta\}$ and $\{\upsilon\}$ satisfy the following normality condition,

$$\int \upsilon^\dagger_m(\mathbf{x},\tau)\zeta_m(\mathbf{x},\tau)\ d^4x = \int \phi^\dagger_m\mathrm{e}^{-\mu\tau}\mathrm{e}^{\mu\tau}\phi_{\mathrm{m}}\ \mathrm{d}^4\mathrm{x} = \int \phi^\dagger_{\mathrm{m}}(\mathbf{x},\tau)\phi_{\mathrm{m}}(\mathbf{x},\tau)\ \mathrm{d}^4\mathrm{x} = 1 \ , \tag{26}$$

leading to

$$\upsilon^\dagger_m(\mathbf{x},\tau)\gamma_5\zeta_m(\mathbf{x},\tau) = \phi^\dagger_m\mathrm{e}^{-\mu\tau}\gamma_5\mathrm{e}^{\mu\tau}\phi_{\mathrm{m}} = \ \phi^\dagger_{\mathrm{m}}(\mathbf{x},\tau)\gamma_5\phi_{\mathrm{m}}(\mathbf{x},\tau) \ , \tag{27}$$

Using these eigenvectors of $\not{D}(\mu)$, the calculation of $\mathrm{Tr}\gamma_5$ goes through in the same way as for $\not{D}(0)$ above. Since the new operator still anticommutes with γ_5 i.e $\{\gamma_5, \not{D}(\mu)\} = 0$, for each eigenvector ζ_m with eigenvalue λ_m there is an eigenvector $\gamma_5\zeta_m$ with the eigenvalue $-\lambda_m$. Thus the trace of γ_5 is zero for all nonzero λ_m. In the basis of the zero modes of $\not{D}(\mu)$, given by ζ_n and $\upsilon_n^\dagger$, the change in the fermion measure is given as,

$$\int \mathrm{Tr}\gamma_5 \; d^4x = \int \; d^4x \sum_n \upsilon_n^\dagger \gamma_5 \zeta_n = \int \; d^4x \sum_n \phi_n^\dagger \mathrm{e}^{-\mu\tau}\gamma_5 \mathrm{e}^{\mu\tau}\phi_\mathrm{n} = \mathrm{n}_+ - \mathrm{n}_- . \qquad (28)$$

Thus the change in the fermion measure due to the chiral transformations is the same as in the zero density case with no additional μ dependent terms. Hence the anomaly is unaffected in the presence of μ even non-perturbatively. The definition of the vectors ζ_m and υ_m in Eq.(21) assumes that neither μ nor τ is infinite. The same assumption is also utilized in various steps in Eqs.(25)-(28). Clearly at strictly zero temperature, this is not possible. However, an infinitesimally small temperature suffices for the proof to go through. One then takes the zero temperature limit.

The scaling of the eigenvectors, including the chiral zero modes, by the $\exp(\pm\mu\tau)$ factors can be related to a nonunitary transformation of the fermion fields in the QCD action in the presence of μ, given by

$$\psi^{'}(\mathbf{x},\tau) = \mathrm{e}^{\mu\tau}\psi(\mathbf{x},\tau) \quad , \quad \bar{\psi}^{'}(\mathbf{x},\tau) = \bar{\psi}(\mathbf{x},\tau)\mathrm{e}^{-\mu\tau} \; , \qquad (29)$$

which makes the action μ-independent:

$$S = \int d^4x \; \bar{\psi}^{'}[\not{D} - \mu\gamma_4]\psi^{'} = \int d^4x \; \bar{\psi}\mathrm{e}^{-\mu\tau} \; [\not{\mathrm{D}} - \mu\gamma_4] \; \mathrm{e}^{\mu\tau}\psi = \int \mathrm{d^4x} \; \bar{\psi} \; \not{\mathrm{D}} \; \psi \; . \qquad (30)$$

The fields ψ and $\bar{\psi}$ at the same space-time point scale differently in the transformation in Eq.(29) which is permissible in the Euclidean field theory since they are mutually independent fields. The transformations in Eq.(29) are not unitary and thus not physical. It merely relates the actions in two different physical situations of zero and nonzero μ. We have shown above that the transformation suggests how to extend the cancellation argument for nonzero eigenvalues of the Dirac operator for $\mu = 0$ to the nonzero μ case as well. Furthermore, since the transformation commutes with both flavour singlet and nonsinglet chiral transformations, employing it as a prescription to introduce the chemical potential will likely lead to a μ dependent action which has the same chiral invariance as for $\mu = 0$.

By preserving the transformation in Eq.(29) on the lattice, one may expect to obtain a lattice Dirac action at finite density for local operators. Considering the naıve massless fermion action on the lattice,

$$S = \sum_{x,y} \bar{\psi}_x \left[-U_4^\dagger(y)\frac{\gamma_4}{2}\delta_{x,y+\hat{4}} + U_4(x)\frac{\gamma_4}{2}\delta_{x,y-\hat{4}} - \sum_{i=1}^{3}\left(U_i^\dagger(y)\frac{\gamma_i}{2}\delta_{x,y+\hat{i}} - U_i(x)\frac{\gamma_i}{2}\delta_{x,y-\hat{i}}\right)\right]\psi_y \ . \tag{31}$$

and replacing the ψ and $\bar{\psi}$ fields in the above action by ψ' and $\bar{\psi}'$ respectively, using the lattice analogue of the transformation (29), we indeed obtain a fermionic action on the lattice at finite density,

$$\sum_{x,y} \bar{\psi}'_x \left[\frac{\gamma_4}{2}\left(-\mathrm{e}^{-\hat{\mu}}\mathrm{U}_4^\dagger(\mathrm{y})\delta_{\mathrm{x,y}+\hat{4}} + \mathrm{e}^{\hat{\mu}}\mathrm{U}_4(\mathrm{x})\delta_{\mathrm{x,y}-\hat{4}}\right) - \sum_{i=1}^{3}\frac{\gamma_i}{2}\left(U_i^\dagger(y)\delta_{x,y+\hat{i}} - U_i(x)\delta_{x,y-\hat{i}}\right)\right]\psi'_y \ . \tag{32}$$

This fermion action is the same as proposed [7, 8] from the arguments of cancellation of spurious $\hat{\mu}^2$ divergences on the lattice. Unfortunately, the infamous fermion doubling problem is related to the fact that the anomaly on the lattice is canceled exactly for such naıve fermions. The commonly used fermions on the lattice, like the Wilson and the staggered fermions do not have flavour singlet $U_A(1)$ chiral symmetry, and so there is no anomaly to speak of. The Overlap fermion action however have an exact chiral symmetry on the lattice and remains invariant under the Luscher transformation at zero temperature and density. The change in the measure computed on the lattice due to the Luscher transformations was shown to be related to the index of the fermion operator [36, 18, 37] ,

$$\mathrm{Tr}\ [2\gamma_5(1-\frac{1}{2}D_{ov})] = -\mathrm{Tr}\ (\gamma_5 D_{ov}) = n_+ - n_- = \ 2\ \mathrm{Index}D_{ov}\ , \tag{33}$$

where $n_\pm$ are right and left handed fermion zero modes respectively. We have previously argued that the Bloch-Wettig version of the Overlap operator at finite density has no chiral symmetry. Physical arguments were proposed as to why the transformation of the fermion fields cannot be made μ dependent as in Eq.(12) to keep the Overlap action invariant at finite density. We now elaborate on the chiral anomaly argument. Under the transformations in Eq.(12) the fermion measure changes by a Jacobian factor Tr $[2\gamma_5(1-1/2D_{ov}(\mu))]$. The anomaly equation $-$Tr $(\gamma_5 D_{ov}(\mu)) = 2$ Index$D_{ov}(\mu)$ is still valid [25] on the lattice but the relevant zero modes are now those of the $D_{ov}(\mu)$, and are thus μ dependent, in contrast to our continuum non-perturbative result.

Since the Bloch-Wettig operator in Eq.(8) does not respect chiral symmetry, we explored the simpler and well defined Overlap operator at $\hat{\mu} \neq 0$ which has chiral symmetry violations at the same order in a, the lattice spacing. The Bloch-Wettig proposal [25] turns out to couple $\hat{\mu}$ as the Lagrange multiplier for fermions on each slice of the fifth dimension. This means that **all** the unphysical "bulk" modes are considered with the same weightage in the partition function as the zero modes which eventually correspond to the massless quarks in four dimensions. The subsequent cancellation of the bulk contributions using Pauli-Villars fields to single out the contribution of a single chiral fermion thus becomes μ dependent on the lattice. Motivated by this physical fact, we proposed to introduce the chemical potential only to count the fermions confined to the domain wall [35]. The effective Overlap operator then is given as,

$$D_{ov}(\hat{\mu})_{xy} = (D_{ov})_{xy} - \frac{a\hat{\mu}}{2a_4\ M}\left[(\gamma_4+1)U_4^{\dagger}(y)\delta_{x,y+\hat{4}} - (1-\gamma_4)U_4(x)\delta_{x,y-\hat{4}}\right] \ . \qquad (34)$$

Here D_{ov} is the same Neuberger-Dirac operator of Eq.(1). The term containing the chemical potential however, is not unique. Improved density operators could be used for faster approach to the continuum limit, e.g., addition of three-link terms. We could have chosen $\hat{\mu}/\sqrt{D_W^{\dagger}D_W}$ instead of $\hat{\mu}/M$ as the multiplying factor for the conserved number part. All such choices of actions are constrained by the fact that these have the correct continuum limit. However the finite lattice spacing errors in each of these operators would be different and would affect the numerical results.

This operator too, breaks exact chiral invariance at the same $\mathcal{O}(a)$ as the Bloch-Wettig proposal. As a result, the anomaly equation on the lattice will unfortunately get μ -dependent corrections anyway. A significant difference may be the fact that the change in the measure is μ independent for our proposal, as in the case of the continuum. It may therefore have less severe corrections to the anomaly equation on the lattice. Moreover it is simpler and easier to implement because one does not have to compute the sign function of a non-Hermitian matrix, with its inherent ambiguities, as in the Bloch-Wettig way of incorporating the chemical potential.

This way of incorporating chemical potential is completely general and can be used for any fermion operator on the lattice. To find out the efficiency of the method we would be using staggered fermions.The choice of staggered fermions was motivated from the fact that

computation of quark number susceptibilities(QNS) using Overlap operator would be computationally out of reach and that the staggered fermions have a remnant chiral symmetry on the lattice. The QNS for two quark flavours is defined as,

$$\chi_{ij}(\mu_u, \mu_d) = \frac{T}{V}\frac{\partial^{i+j} \ln Z(T, \mu_{u,d}, m)}{\partial \mu_u^i \mu_d^j} = \frac{T}{V}\frac{\partial^{i+j} \langle Tr \ln D(\mu_{u,d}, m)\rangle}{\partial \mu_u^i \mu_d^j} \ , \tag{35}$$

where Z is the QCD partition function.

The second order QNS computed using the staggered version operator in Eq. (34) would have $\mathcal{O}(1/a^2)$ terms which would diverge as the lattice spacing, $a \to 0$. To remove these artifacts, one has to perform a zero temperature simulation of the observable which are otherwise absent in the standard prescription [7, 8]. The main advantage of this Dirac operator is that it has term only linear in $\hat{\mu}$, hence second and higher order derivatives of this operator with respect to μ vanishes. In contrast, in the usual prescription, all derivatives of the Dirac operator are finite. Each derivative comes with the inverse of Dirac operator in the expression of QNS, and the inversion is the most expensive step in a lattice calculation. Hence we argued in [35], that considerable amount of time would be saved in computing higher order QNS using the operator used here. The ratios of higher order QNS are important as these provide us with an estimate of the location of critical point in the QCD phase diagram by the Taylor series method [38].

To estimate the cut-off effects, the QNS were computed for free fermions on a $24^3 \times 6$ lattice using the operator in Eq.(34) with D_{ov} replaced by $D_{staggered}$. The expressions for χ_{n0} would have zero temperature $\mathcal{O}(a^{n-4})$ lattice artifacts which have to be subtracted to give physical values on the lattice. All such subtraction terms were computed on a 24^3 lattice with an infinite temporal extent. When compared with the results obtained from the standard operator, the QNS computed with the operator in our work has smaller cut-off effects as evident in Fig. (1).

The baryon number susceptibilities for two flavour QCD were computed using this operator on a $24^3 \times 6$ lattice. In this work, all the QNS are computed at zero baryon density so one does not encounter any "sign problem". Also exact isospin symmetry was considered hence, $\mu_u = \mu_d = 3\mu_B$, where μ_B is the baryon chemical potential. Standard Wilson action was used for the gluon sector and naive staggered fermion action for the fermion part. The input pion mass used was 230 MeV. The details of the method and the configurations used

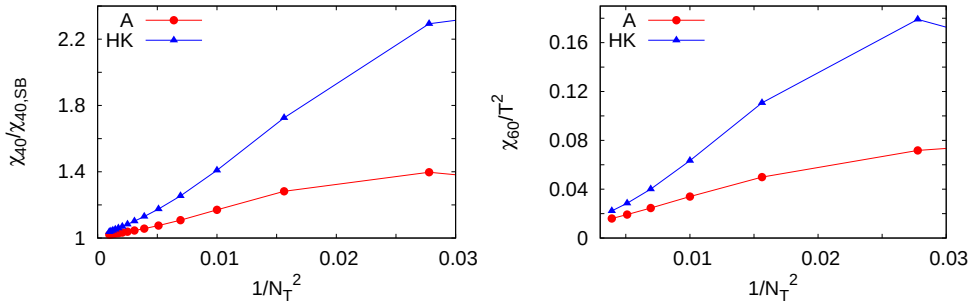

Figure 1: The fourth order(left panel) and the sixth order QNS(right panel) for free fermions as a function of $1/N_T^2$ using the HK prescription and the subtraction method A detailed below.

are mentioned in [39]. In order to estimate the zero temperature lattice artifacts, one should ideally perform QCD simulations on a symmetric lattice of size 24^4 for each value of the coupling constant. This may reduce the estimated gain in time. To remove such terms without any additional computational cost, we propose the following two subtraction schemes:

- A: subtracting the zero temperature value of χ_{20} for free fermions computed by numerically summing over the momentum modes on a 24^3 lattice with infinite temporal extent.

- B: subtracting χ_{20} for free fermions computed numerically on a 24^4 lattice.

We expect that the free theory artifacts would approximately be similar in magnitude to that in the interacting theory in the high temperature regime. Furthermore, the continuum QCD is known to have no additional divergences dependent μ and T perturbatively once the free theory divergences are subtracted. One may expect this to hold true on the lattice as well. This was evident in Fig. (2) where the ratio of $\chi_{20}/\chi_{20,SB}$ is independent of the subtraction scheme at temperatures $T > T_c$, T_c being the crossover temperature. The method B however gave smaller cut-off errors and consistent with those using improved fermion actions like p4 and Asqtad [40, 41]. The values of the fourth and sixth order susceptibilities were obtained by performing similar subtraction by methods A & B. It was observed that both the methods

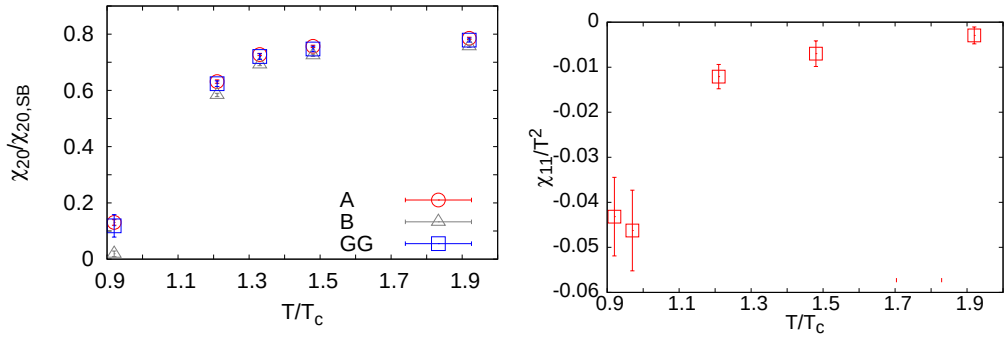

Figure 2: The diagonal $\chi_{20}/\chi_{20,SB}$(left panel) and off-diagonal χ_{11}/T^2(right panel) as a function of T/T_c.

give results in reasonable agreement with the existing results(GG) for $T > T_c$. The difference between the results at $1.92T_c$ between these two methods is at the level of the free theory cut-off effects, emphasizing the fact that at such temperatures the QGP phase becomes almost non-interacting.

The important observables that measure the strength of the interactions are the off-diagonal susceptibilities. This is because these quantities are zero for the non-interacting theory. Also the off-diagonal susceptibilities measure the correlations between the quasi-particles in the QCD medium. The second order off diagonal susceptibility, χ_{11}, should be identical for both the operators used and provides a check for our results. The rapid drop of χ_{11} towards zero at $T > \ 1.2T_c$, as in the right panel of Fig. (2) signify rapid decorrelation among the quark flavours. As the different quark flavours become almost uncorrelated, there would be no further subtraction required for the fourth order off-diagonal QNS. The χ_{22} is a sensitive indicator of the critical point as it peaks sharply at T_c, determined from the Polyakov loop susceptibility, whereas the χ_{31} remains close to zero for $T > T_c$, again signalling almost no correlation between the light quark flavours.

In order to asses these subtraction methods for $T < T_c$, we need to estimate the subtraction term for the interacting theory on a symmetric lattice, for each value of the coupling constant. We expect that the operator used in our work would still be efficient for continuum extrapolation for eighth and higher order QNS, which would be investigated in a

future study.

Overlap fermions at finite chemical potential

In view of the non-locality of the Overlap operator, it would be desirable to introduce the chemical potential by preserving the continuum symmetries on the lattice. External fermion sources are introduced in the Overlap action, which are invariant under continuum chiral transformations, to explicitly bring out the meaning of chiral symmetry in the Overlap context. For motivating the procedure, the concept of the Overlap fermions at zero fermion density is briefly outlined. If we have fermions in a five dimensional Euclidean spacetime with a single domain wall profile, we can consider the fifth dimension as timelike and construct the Hamiltonian $\mathcal{H} = \gamma_5(D+M(s))$, D being the four dimensional Dirac operator and s being the time coordinate. If the domain wall in the fifth dimension is of the form $M(s) = -M, s > 0$ and $M(s) = \Lambda, s < 0$, then the overlap between the ground states $|+\rangle$ and $|-\rangle$ of the two many body Hamiltonians $\mathcal{H}_+ = \gamma_5(D - M)$ and $\mathcal{H}_- = \gamma_5(D + \Lambda)$, respectively, gives us a chiral fermion for $s \to \infty$. This idea can be generalized on the lattice by replacing D by the Wilson Dirac operator, D_W, and choosing $\Lambda \to \infty$. The resultant superposition between the ground states of the lattice Hamiltonians gives the corresponding determinant of the Overlap operator of Eq.(1). On a lattice of size $n = N^3 \times N_T \times N_c$, the many body Hamiltonian is a $2n \times 2n$ matrix,

$$\mathcal{H}_+ = \begin{pmatrix} B - M & C \\ C^\dagger & -B + M \end{pmatrix}$$

with $B_{xy} = \frac{1}{2}\sum_{\mu=1}^{4}\left(2\delta_{y,x} - U_\mu(x)\delta_{y,x+\mu} - U_\mu^\dagger(y)\delta_{y,x-\mu}\right)$ being the Wilson term and $C_{xy} = \frac{1}{2}\sum_\mu \sigma_\mu\left(U_\mu(x)\delta_{y,x+\mu} - U_\mu^\dagger(y)\delta_{y,x-\mu}\right)$, the nearest neighbour hopping term and σ being the standard Pauli matrices in n-dimensions. The Hamiltonian can be diagonalized by the unitary operator,

$$U = \begin{pmatrix} \alpha & \gamma \\ \beta & \delta \end{pmatrix}$$

with all the elements of U are $n \times n$ matrices. If $d^\dagger$ and $u^\dagger$ be the creation operators of the Hamiltonian $\mathcal{H}_-$ that create a fermion and an anti-fermion and $d'^\dagger$ and $u'^\dagger$ be the corresponding ones for $\mathcal{H}_+$, then the lowest states of $\mathcal{H}_\pm$ for left and right handed particles

are respectively,

$$|+\rangle_{R,L} = u'^{\dagger}_{R,L_n} u'^{\dagger}_{R,L_{n-1}} \cdots u'^{\dagger}_{R,L_2} u'^{\dagger}_{R,L_1} |0\rangle \tag{36}$$

and

$$|-\rangle_{R,L} = u^{\dagger}_{R,L_n} u^{\dagger}_{R,L_{n-1}} \cdots u^{\dagger}_{R,L_2} u^{\dagger}_{R,L_1} |0\rangle \tag{37}$$

Introduction of chemical potential would require that the fermion number is conserved so it should couple with a term that creates a chiral fermion on one side of the wall annihilates corresponding fermion. The generating functional for the Overlap operator in terms of chiral fermion sources $\xi_{R,L}$ at finite density is given as,

$$Z(\bar{\xi}_R, \bar{\xi}_L, \xi_R, \xi_L; \mu_R, \mu_L) = {}_R\langle -|e^{\bar{\xi}_R d_R + \xi_R u^{\dagger}_R + u^{\dagger}_R \mu_R d_R}|+\rangle_{RL}\langle +|e^{\xi_L d^{\dagger}_L + \bar{\xi}_L u_L - d^{\dagger}_L \mu_L u_L}|-\rangle_L, \tag{38}$$

For a vectorlike theory like QCD, $\mu_L = \mu_R = \mu$. On a lattice, many choices of the chemical potential operator is possible for which the corresponding Dirac operators have the correct continuum limit. The most naive choice is $\mu = i\hat{\mu}/2M$. The left and the right chiral sectors are distinctly separate in the partition function and the chemical potential term do not mix these two sectors. The resultant partition function can be evaluated explicitly in terms of sources to give us,

$$Z = \int \mathcal{D}U \mathrm{e}^{-\mathrm{S_G}} \det\alpha \det\left(1 + \mu\beta\alpha^{-1}\right) \det\alpha^{\dagger} \det\left(1 - \mu\left[\beta\alpha^{-1}\right]^{\dagger}\right) \mathrm{e}^{\bar{\xi}_\mathrm{R} \frac{1}{\alpha\beta^{-1}+\mu} \xi_\mathrm{R}} \mathrm{e}^{\bar{\xi}_\mathrm{L} \frac{1}{[\alpha\beta^{-1}]^{\dagger}-\mu} \xi_\mathrm{L}} . \tag{39}$$

The term within the determinant could be written in terms of the standard Overlap operator for the naive choice for μ, as,

$$D_{ov}(\hat{\mu}) = D_{ov}(0) + \frac{\hat{\mu}}{2M}\gamma_4(2 - D_{ov}(0)). \tag{40}$$

The term in the exponent can be formulated in terms of the standard four dimensional spinor notation. The Lagrangian in presence of the sources then turn out to be,

$$\mathcal{L} = \bar{\eta}\left(\frac{D_{ov}(0)}{2 - D_{ov}(0)} + \frac{\hat{\mu}\gamma_4}{2M}\right)^{-1} \eta \ , \ \eta \equiv \begin{pmatrix} \xi_R & \xi_L \end{pmatrix} . \tag{41}$$

We showed the following in this work,

- Under the global chiral transformation of the sources,

$$\xi_R \to e^{i\varphi_R}\xi_R \ , \ \bar{\xi}_R \to \bar{\xi}_R e^{-i\varphi_R} \ , \ \xi_L \to e^{i\varphi_L}\xi_L \ , \ \bar{\xi}_L \to \bar{\xi}_L e^{-i\varphi_L} \ , \tag{42}$$

the action remains invariant for massless source fermion fields. Thus the exact chiral symmetry on the lattice for the Overlap operator is realized in the sense that the chiral sources have the continuum chiral symmetry even on the lattice.

- In terms of four dimensional gamma matrices, the action is invariant under the global chiral transformation $\eta \rightarrow \exp(-i\gamma_5\varphi)\eta$ of the sources, since the inverse of the Overlap propagator anticommutes with γ_5 i.e., $\{\gamma_5, \left(\frac{D_{ov}}{2-D_{ov}} + \frac{\hat{\mu}\gamma_4}{2M}\right)^{-1}\} = 0$.

- The Overlap operator can be diagonalized exactly for the free fermions. For the choice of $\mu \sim \hat{\mu}$, the quark number susceptibility at zero density computed from the partition function in Eq.(39), has terms like $1/a^2$ which diverge in the continuum limit. A zero temperature subtraction has to be performed to remove such lattice artifacts for continuum extrapolation. Point split [7] prescription which is popularly used to remove such divergences on the lattice does not work for the Overlap fermions. A suitable method to address the divergence issue is under study.

- The Overlap determinant could also be derived from the domain wall formalism considering that the chemical potential couples to only the physical fermions localized on the walls. If the unphysical bulk modes are integrated over and removed from the physical partition function, the corresponding fermion operator thus obtained has the same form as that in Eq.(40).

List of Publications contributing to this thesis

1. Debasish Banerjee, R. V. Gavai, Sayantan Sharma,
   "Thermodynamics of the ideal overlap quarks on the lattice,"
   Phys. Rev. D 78, 014506 (2008), [arXiv:0803.3925].

2. R. V. Gavai, Sayantan Sharma,
   "Thermodynamics of free Domain Wall fermions,"
   Phys. Rev. D 79, 074502 (2009), [arXiv:0811.3026].

3. R. V. Gavai, Sayantan Sharma,
   "Anomalies at finite density and chiral fermions,"
   Phys. Rev. D 81, 034501 (2010), [arXiv:0906.5188].

4. R. Narayanan, Sayantan Sharma
   "Introduction of the chemical potential in the overlap formalism ",
   JHEP 1110, 151 (2011), [arXiv:1108.2667].

Publications in Conference proceedings

1. R. V. Gavai, Sayantan Sharma,
   "Towards QCD thermodynamics using exact chiral symmetry on lattice,"
   J.Phys.G35:104097, 2008, [arXiv:0805.2866].

2. Debasish Banerjee, Rajiv V. Gavai, Sayantan Sharma,
   "Exact Chiral Fermions and Finite Density on Lattice,"
   PoS (LATTICE 2008), 177, Proceedings of Lattice 2008, [arXiv:0809.4535].

3. Rajiv V. Gavai, Sayantan Sharma,
   "Anomaly at finite density and chiral fermions on lattice,"
   PoS (LATTICE 2009), 177, Proceedings of Lattice 2009, [arXiv:0910.2784].

4. R. V. Gavai, Sayantan Sharma,
   "Towards faster computation of higher order quark number susceptibilities in QCD,"

Conference Proceedings for ICPAQGP 2010,
Nucl. Phys. A, 862-863 CF, 355 (2011).
Results in this work are yet unpublished and included in this thesis.

Bibliography

[1] K. Nakamura et al. (Particle Data Group), *J. Phys.* G 37, 075021 (2010).

[2] K. Rajagopal and F. Wilczek, in "At the Frontier of Particle Physics / Handbook of QCD", Vol. 3, M. Shifman, ed., (World Scientific), p2061.

[3] R. Narayanan and H. Neuberger, *Phys. Rev. Lett.* 71, 3251 (1993);
R. Narayanan and H. Neuberger, *Nucl. Phys.* B 443, 305 (1995).

[4] D. B. Kaplan, *Phys. Lett.* B288, 342 (1992).

[5] S. B. Nielsen and M. Ninomiya, *Nucl. Phys.* B 185, 20(1981).

[6] P. H. Ginsparg and K. G. Wilson, *Phys. Rev.* D25, 2649(1982).

[7] P. Hasenfratz and F. Karsch, *Phys. Lett.* 125B, 308 (1983).

[8] J. Kogut *et al.*, *Nucl. Phys.* B 225, 93(1983).

[9] N. Bilic and Rajiv V. Gavai, *Z. Phys.* C23, 77 (1984).

[10] R. V. Gavai, *Phys. Rev.* D32, 519 (1985).

[11] Y. Kikukawa and A. Yamada, *e-Print : hep-lat/9810024*;
P. Hasenfratz *et al.*, *Nucl. Phys.* B643, 280 (2002).

[12] J. E. Mandula, `e-Print: arXiv:0712.0651` [hep-lat].

[13] J. Bloch and T. Wettig, *Phys. Rev. Lett.* 97, 012003 (2006).

[14] C. Gattringer and L. Liptak, *Phys. Rev.* D76, 054502 (2007).

[15] P. Hegde *et al.*, *Eur. Phys. J.* C55, 423 (2008).

[16] D. Banerjee, R. V. Gavai and S. Sharma, *Phys. Rev.* D78, 014506 (2008).

[17] D. Banerjee, Ph.D. thesis.

[18] M. Luscher, *Phys. Lett.* B428, 342 (1998).

[19] D. Banerjee, R. V. Gavai and S. Sharma, *PoS (LATTICE 2008)*, 177.

[20] Y. Shamir, *Nucl. Phys.* B406, 90 (1993).

[21] P. M. Vranas, *Phys. Rev.* D57, 1415(1998).

[22] H. Neuberger, *Phys. Rev.* D57, 5417 (1998).

[23] R. G. Edwards and U. M. Heller, *Phys. Rev.* D63, 094505 (2001).

[24] R. V. Gavai and S. Sharma, *Phys. Rev.* D79, 074502 (2009).

[25] J. Bloch and T. Wettig, *Phys. Rev.* D76, 114511 (2007).

[26] S. Naik, *Nucl. Phys.* B 316, 238 (1989).

[27] S. L. Adler, *Phys. Rev.* 177, 2426 (1969).

[28] J. Bell and R. Jackiw, *Nuovo. Cim.* A60, 47 (1969).

[29] K. Fujikawa, *Phys. Rev.* D21, 2848 (1980).

[30] R. D. Pisarski and F. Wilczek, *Phys. Rev.* D29, 338(1984).

[31] H. Itoyama and A. H. Meuller, *Nucl. Phys.* B 218, 349(1983).

[32] Z. Qian, R. Su and P. K. N. Yu, *Z. Phys.* C63, 651 (1994).

[33] S. Gupta and S. N. Nayak, hep-ph/9702205.

[34] M. Kapusta, *Finite Temperature Field Theory* , Cambridge University Press, Cambridge, England, (1985), pp. 124-125.

[35] R. V. Gavai and S. Sharma, *Phys. Rev.* D81, 034501 (2010).

[36] P. Hasenfratz, V. Laliena and F. Neidermeyer, *Phys. Lett.* B 427, 125 (1998).

[37] K. Fujikawa, *Nucl. Phys.* B 546, 480 (1999).

[38] R. V. Gavai and S. Gupta, *Phys. Rev.* D68, 034506 (2003).

[39] R. V. Gavai and S. Gupta, *Phys. Rev.* D78, 114503 (2008).

[40] M. Cheng *et al.*, *Phys. Rev.* D79, 074505 (2009).

[41] C. DeTar *et. al.* , *Phys. Rev.* D81, 114504 (2010).

Chapter 1

Introduction

Understanding fundamental building blocks of matter and the interactions between them is a primary goal of theoretical physics. The visible matter around us comprises mainly of protons and neutrons. They are themselves made up of even more basic particles called the quarks and gluons. These particles carry a new quantum number called the colour and their dynamics and interactions are described by a field theory known as Quantum Chromodynamics(QCD). The quarks and gluons, collectively called partons, transform under different representation of SU(3) colour group and hence carry specific colour charge. In our world, the quarks are confined to form colour singlet hadrons at low energies. At very high energies, the strength of the interactions between these particles become small due to asymptotic freedom. These particles become almost free as observed from the Bjorken scaling of the parton distribution functions in the electron proton collision experiments at SLAC [1]. It is expected that at very high temperatures too, the hadrons would melt to form a new equilibrated state of matter called the Quark Gluon Plasma(QGP). The conditions of temperature and energy density in the very early universe within first 20-25 μs of the Big Bang would have resulted in such a state to exist. Such conditions can also be recreated in terrestrial laboratories. Signatures of such a phase have been apparently seen in the heavy ion collision experiments at the Relativistic Heavy Ion Collider(RHIC) in Brookhaven National Laboratory(BNL) [2]. Thus understanding the nature of the different phases of QCD and the interactions is important both from the theoretical as well as practical point of view. The different phases can be charted out in the space of the parameters of finite

temperature QCD which are the temperature and the chemical potentials corresponding to the conserved quantum numbers. The baryon number is always conserved in nature. Strangeness is also a conserved quantity but the strange particles are not present in the initial stages of heavy ion collisions so the relevant intensive parameters which defines the axes for the phase diagram are the temperature and the baryon chemical potential, μ_B. The phase diagram of QCD has rich features. Much of it only known from models which have the same symmetries as QCD. This is because the interactions between the particles are strong enough that the perturbative techniques fail at these energy regime. Lattice QCD is a non-perturbative technique that can give first principles predictions for the phase diagram. In fact, the existence of the critical point at high temperatures and small baryon density has been already predicted from lattice studies [3, 4]. This would set the reference for the ongoing experimental searches for the critical point at RHIC in BNL and to start at FAIR in GSI and NICA in Dubna. In a thermodynamically equilibrated system, one of the signatures of the existence of the critical point is the divergence of the correlation length(ξ). Since in a heavy-ion collision the equilibrated matter is formed in a finite volume for a finite time span, the ξ cannot diverge. So higher moments of conserved charges like the baryon number can be more sensitive to the existence of the critical point as these have a stronger dependence of ξ [5]. Recently it was proposed that the ratios of moments of baryon number is a more useful observable to measure as the finite volume effects cancel [6] allowing direct comparison of the experimental observations with the lattice results. In the heavy ion experiments, the center of mass energy $\sqrt{s}$ of the colliding nuclei is varied to scan a range of temperature and baryon chemical potential. A non-monotonic variation of the ratios of moments of suitable quantity like the proton number as a function of $\sqrt{s}$ would indicate that the system has evolved to the vicinity of the critical point. The ratios of moments of the net proton distribution observed in the Au+Au collisions in the STAR experiment at RHIC, for $\sqrt{s} = 19.6,\ 62.4$ and 200 Gev [7] at mid-rapidity, are clearly in agreement with the lattice results [8] as well as predictions from the models without a critical point. STAR measurements [7] have not yet found any non-monotonicity in the behaviour of ratios of higher moments for $\mu_B \lesssim 200$ MeV indicating that the critical point may not exist for this range of μ_B. Recent STAR results [9] on the ratios show a deviation from the Hadron Resonance gas model for $\sqrt{s} < 39$ GeV and there would be new set of data for $\sqrt{s} = 19.6,\ 27$ GeV which would allow for a comprehensive understanding of the location of the QCD critical point.

The starting point for thermodynamic computations in QCD at finite temperature T and density is the grand canonical partition function,

$$Z = \text{tr} \;\; \mathrm{e}^{-\frac{\mathcal{H}_{QCD}-\mu N}{T}} \;\; . \tag{1.1}$$

where $\mathcal{H}_{QCD}$ is the QCD Hamiltonian, N is the conserved baryon number operator and μ is the corresponding baryon chemical potential. The partition function can be expressed as a path integral of the QCD action over a four dimensional Euclidean spacetime with a compact temporal direction of extent $1/T$,

$$Z = \int \mathcal{D}\bar{\psi}\mathcal{D}\psi\mathcal{D}A_\mu \;\; \mathrm{e}^{-\mathrm{S}} \;\; , \tag{1.2}$$

where the S is the QCD action,

$$S = -\int_0^{1/T} d\tau \int d^3x \left[\bar{\psi}(\not{D} + m)\psi - \frac{1}{2}\mathrm{Tr} \;\; F_{\alpha\beta}F_{\alpha\beta} - \mu\bar{\psi}\gamma_4\psi\right] \;\; , \tag{1.3}$$

with $\not{D} = \gamma_\mu(\partial_\mu - igA^a_\mu T^a)$ and the field tensor $F_{\alpha\beta} = \partial_\alpha A_\beta - \partial_\beta A_\alpha + ig[T^a, T^b]A^a_\alpha A^b_\beta$. The matrices T^a are the generators of $SU(3)$ colour group satisfying the commutation relation $[T^a, T^b] = if^{abc}T_c$. The fermion fields transform as fundamental representation of the colour gauge group $SU(3)$, whereas the gauge fields transform as adjoint of the same group. In addition, at finite temperature, the fermion and the gauge fields must satisfy anti-periodic and periodic boundary conditions along the compact temporal direction respectively due to the trace relation in Eq.(1.2),

$$\psi(\vec{x}, \tau + 1/T) = -\psi(\vec{x}, \tau) \;\; , \;\; A^a_\mu(\vec{x}, \tau + 1/T) = A^a_\mu(\vec{x}, \tau) \;\; . \tag{1.4}$$

Once the partition function is defined we need to look into the symmetries of the QCD Hamiltonian to construct suitable order parameters to characterize the different phases of the system. The QCD Lagrangian for massless quarks has a $SU_V(3) \times SU_A(3) \times U_V(1)$ chiral symmetry. The QCD vacuum breaks this symmetry dynamically to $SU_V(3) \times U_V(1)$ giving rise to Goldstone modes which are the pions and kaons. The order parameter for this transition is the chiral condensate, $\langle\bar{\psi}\psi\rangle$ which acquires a non-zero value in the hadron phase and falls off to zero in the QGP phase. For finite quark masses however, it not an exact order parameter and the transition is a crossover at high temperatures and almost vanishing baryon number density. The pions are now the pseudo-Goldstone modes with

masses proportional to the square root of the quark mass. But considering the fact that the light quark masses, $m_u, m_d << \Lambda_{QCD}$, the light quark condensate is still a good order parameter. The $U_A(1)$ symmetry is anomalous [10, 11, 12] and there is no order parameter corresponding to it. However there is always an axial $Z_A(3)$ flavour symmetry even in the presence of anomaly. The magnitude of the anomaly term is important as it affects the phase diagram qualitatively. From models which have same symmetries as QCD, it is known that the chiral transition is of first order at low temperature and large baryon density ending in a critical end point predicted as well from lattice studies. The existence of the critical point depends crucially on the number of light quark flavours as well as on the anomaly term. From the renormalization group study of the effective Lagrangian having same global symmetries as QCD [13], it is known that for the physically interesting case of two flavour QCD, the size of the anomaly term determines the existence of the critical point. If the anomaly does not change significantly with temperature from its zero temperature value then the first order line ends in a critical end point belonging to the O(4) universality class [13].

Lattice QCD is a first principle non-perturbative approach to study different aspects of the QCD phase diagram. The Lattice approach [14] consists of discretizing the Euclidean QCD Lagrangian on a discrete spacetime with N cells along each of the spatial dimensions and N_T cells along the temporal direction with lattice spacing a. The physical volume of the system is $V = N^3a^3$ and the temperature is $T = 1/(N_T a)$. The derivatives that appear in the kinetic terms are substituted by finite differences. The quantum fermion fields ψ sit on each discrete spacetime point. The continuum gauge fields A_μ are replaced by directed gauge links U_μ that join two adjacent lattice points. The gauge links are elements of $SU(3)$ colour group and are related to the gauge fields by the following relation,

$$U_\mu(x) = P\left(\mathrm{e}^{\mathrm{ia}\mathrm{A}^{\mathrm{a}}_{\mu}(\mathrm{x})\mathrm{T}^{\mathrm{a}}}\right) \text{ . where } \quad x = na \quad , \tag{1.5}$$

where P denotes path ordering. To make the gauge fields dynamical we define a gauge invariant term called plaquette that consists of product of gauge links on four adjacent sites of the lattice.

$$U_{\mathcal{P}} = U_\mu(x)U_\nu(x+\mu)U^\dagger_\mu(x+\nu)U^\dagger_\nu(x) \tag{1.6}$$

In the continuum limit the value of the plaquette is given as,

$$U_{\mathcal{P}} = \mathrm{e}^{\mathrm{ia}^2\mathrm{F}_{\alpha\beta}}. \tag{1.7}$$

The kinetic term on the lattice for the gauge field is thus

$$S_G = \beta \sum_{\mathcal{P}} [1 - \frac{1}{3}\text{Re} \ \ \text{Tr}U_{\mathcal{P}}] \ , \ \beta = \frac{6}{g^2} \ . \tag{1.8}$$

The derivative terms on the lattice can be written in a gauge covariant way with the gauge links such that under $SU(3)$ rotation of the fermion fields, the Lagrangian remains invariant.

$$\bar{\psi}\gamma_\mu D_\mu \psi \rightarrow \bar{\psi}(x)\frac{\gamma_\mu}{2}\left[U_\mu(x)\delta_{x+\hat{\mu},y} - U^\dagger_\mu(y)\delta_{x-\hat{\mu},y}\right]\psi(y) \ . \tag{1.9}$$

The naive discretization of the fermion action leads to the *fermion doubling problem*. This is related to the fact that the lattice propagator for free massless fermions has a pole not only at the point where $p_\mu = 0$ but also at the points $p_\mu = \pi/a$, in the momentum space. Thus for a four dimensional lattice, there are $2^4 = 16$ such poles out of which one of them correspond to the physical fermion and the rest 15 of them are lattice artifacts because we would think that in the continuum limit only the pole at $p_\mu = (0, 0, 0, 0)$ should survive. All these fermions corresponding to the additional poles contribute equally to the different observable quantities. In an interacting theory these species can interact with the gauge fields and cause spurious effects in the different observable quantities. Thus one needs to remove the contribution of the doublers at the operator level itself. The origin of this problem is related to the famous 'No-go' theorem by Nielsen and Ninomiya [15]. It states that the massless lattice fermion operator $D(p)$ in the momentum space representation, cannot satisfy the following relations simultaneously,

- D(p) is a periodic, analytic function of p_μ ;
- D(p)$\propto \gamma_\mu p_\mu$ for $a|p_\mu| << 1$;
- D(p) is invertible everywhere except at $p_\mu = 0$;
- $\{\gamma_5, D(p)\} = 0$;

The first two conditions ensure that the fermion operator in the coordinate space is ultralocal and has the correct continuum limit. The third condition ensures that spectrum is doubler free and fourth implies exact chiral symmetry on the lattice. To remove the doublers, different procedures are followed on the lattice giving rise to different fermion operators. The most commonly used lattice fermion operators are discussed below:

- *Wilson fermions*

  A popular method suggested by Wilson [14] was to add a dimension five operator $a\bar{\psi}\hat{\Box}\psi$ to the naive fermion action, where $\hat{\Box}$ is the double derivative term on the lattice. This double derivative term mixes left and right fermion modes and hence breaks chiral symmetry explicitly on the lattice. In the continuum limit, $a \to 0$, the doublers become infinitely heavy and decouple from the spectrum. The Wilson fermion action can be written in terms of effective coupling $\kappa = 1/(8 + 2ma)$ as,

$$\begin{aligned} S_W &= \sum_{x,y} \bar{\psi}_W(x) D_W(x,y) \psi_W(y) \ , \ \psi_W(x) = \frac{\psi}{\sqrt{2\kappa}} \ , \\ D_W &= 2\delta_{x,y} - \kappa \sum_{\mu} \left[(1-\gamma_\mu) U_\mu(x) \delta_{x+\hat{\mu},y} + (\gamma_\mu + 1) U^\dagger_\mu(y) \delta_{x-\hat{\mu},y}) \right] \ . \end{aligned} \tag{1.10}$$

  where the coordinates $x = na$ and $y = n'a$. The two couplings of the theory are the β, the inverse of the gauge coupling and the hopping parameter κ. The quark mass in the interacting theory can be defined as $ma = 1/\kappa - 1/\kappa_c$. The quark masses are no longer protected from additive renormalization as its value at different gauge coupling depends on both κ and κ_c. It is due to this reason that simulations at very small quark masses are difficult as the quark propagator may become singular. To suppress the contribution of these so called exceptional configurations, one has to either work with heavy quark masses or use large lattice volumes. Moreover the chiral order parameter $\langle\bar{\psi}\psi\rangle$, has large additive correction due to chiral symmetry breaking and one has to do a fine-tuning to get the correct continuum limit.

- *Staggererd fermions*

  The doublers contribute from each corner of the Brillouin zone so one of the method to suppress the doubler contribution is to reduce the Brillouin zone itself. This can be achieved by spin-diagonalizing the spinor fields. This method was originally suggested by Kogut and Susskind and these fermions are called the staggered or the Kogut-Susskind fermions [16]. The free fermion action can be written as,

$$S_{KS} = \sum_{n,\mu} \bar{\chi}(n) \left[\eta_\mu(n) (U_\mu(n) \chi(n+\mu) - U^\dagger_\mu(n-\mu)\chi(n-\mu)) + ma\chi(n) \right] \ , \tag{1.11}$$

where α =1-4 and the $\chi_\alpha(n)$ are one-component spinors. These one-component fields are obtained from the four component Dirac spinors through suitable diagonalization in the spin space. Unitary matrices of the form $T(n) = \gamma_1^{n_1}\gamma_2^{n_2}\gamma_3^{n_3}\gamma_4^{n_4}$ can diagonalize the four dimensional spinors such that

$$\psi(n) = T(n)\chi(n) \ , \ \bar{\psi}(n) = \bar{\chi}(n)T^\dagger(n) \ , \tag{1.12}$$

where,

$$T^\dagger(n)\gamma_\mu T(n+\mu) = (-1)^{n_1+n_2+..+n_{\mu-1}} = \eta_\mu(n)\mathcal{I}. \tag{1.13}$$

and $\mathcal{I}$ is the identity matrix. For four dimensional spinors there were 16 flavours of fermions on the lattice due to doubling. For these one dimensional counterparts the doubling would be minimized to four. This could be explicitly shown by reconstructing the four dimensional fermions from these one component species. The construction for free fermions is simpler and is outlined here. For the interacting theory this procedure could be generalized suitably. The staggered fermions are defined on a 16 dimensional hypercube with the origin at $2N$. Collecting the fermions from the edges of the Brillouin zone to form the four dimensional species $\psi_\alpha(N) = 1/8\sum_\rho T_\alpha(\rho)\chi_\alpha(2N+\rho)$, the fermion action can be rewritten as,

$$S_{KS} = \sum_{n,\mu}\bar{\psi}(n)\left[ma(\mathcal{I}\otimes\mathcal{I}) + \frac{1}{2}(\gamma_\mu\otimes\mathcal{I})\hat{\partial}_\mu + \frac{1}{4}(\gamma_5\otimes t_\mu t_5)\hat{\Box}\right]\psi(n) \ . \tag{1.14}$$

The matrices t_μ and t_5 are similar to the γ matrices except that these are in the flavour space. The $\hat{\partial}_\mu$, $\hat{\Box}$ are the gauge covariant first and second derivative lattice operators respectively. On a finite lattice and for massless fermions the action is invariant under the following U(1) transformations of the fermion fields:

$$\psi = \mathrm{e}^{\mathrm{i}\theta}\psi \quad , \quad \psi = \mathrm{e}^{\mathrm{i}\beta(\gamma_5\otimes \mathrm{t}_5)}\psi \ . \tag{1.15}$$

The action thus has a remnant $U(1)\times U(1)$ chiral symmetry which in the continuum limit gives the full $U(4)\times U(4)$ symmetry. This feature of staggered fermions make it suitable for studying the chiral restoration transition of QCD at finite temperature. However both spin and flavour quantum numbers are not defined on the lattice and these issues may be important for determining the order of phase transition on the lattice.

- *Overlap fermions*

  When one tries to regulate an anomaly free quantum field theory of chiral fermions one requires an infinite set of Pauli-Villars fields. The same is true for non-perturbative regulator like the lattice. One way to realize a chiral fermion on the lattice is through the Overlap formalism developed by Narayanan and Neuberger [17]. In this formalism, the infinite set of flavours can be visualized as bulk modes of a five dimensional theory with an infinite extent along the fifth dimension and a "domain wall like" five dimensional potential. The determinant of the chiral fermion operator, called the Overlap operator, is the superposition between the ground states of the two many body Hamiltonians defined on either side of this domain wall. The form of the 4D Overlap operator on the lattice, first derived by Neuberger [18] is,

$$D_{ov} = 1 + \gamma_5 sgn(H_W) \ , \ H_W = \gamma_5 D_W \ , \quad sgn(H_W) = \frac{H_W}{\sqrt{H_W^2}} \ . \tag{1.16}$$

  where sgn is the matrix sign function and D_W is the standard Wilson-Dirac operator with a parameter M,

$$D_W = \sum_\mu \left[\frac{\gamma_\mu}{2} (U_\mu(x)\delta_{x+\hat{\mu},y} - U_\mu^\dagger(y)\delta_{x-\hat{\mu},y}) - \frac{1}{2}(U_\mu(x)\delta_{x+\hat{\mu},y} + U_\mu^\dagger(y)\delta_{x-\hat{\mu},y}) \right] + (4-M)\delta_{x,y} \tag{1.17}$$

  The M is an irrelevant parameter of the Overlap operator which can be tuned to a specific range of values corresponding to different flavours of quarks on the lattice [19]. It has to be fixed between 0-2 for simulating one flavour of massless quark on the lattice. The sign function involves inverse square root of H_W so it is a matrix that has non-zero entries for all pairs of lattice sites. But it was proved analytically that the Overlap operator falls off exponentially in the position space under the assumption of sufficiently smooth gauge link variables $|1 - U| < 1/30$ [20]. This ensures that the quantum field theory to be designed with the Overlap fermions is not plagued with problems of causality violating interactions present in non-local theories. One of the most important property of this operator is that it satisfies the Ginsparg-Wilson relation [21],

$$\{\gamma_5, D_{ov}\} = a D_{ov} \gamma_5 D_{ov}. \tag{1.18}$$

  which allows one to define chiral symmetry on the lattice. It was originally derived starting with a fermion theory with continuum chiral symmetry and performing a

renormalization group transformation to know the fate of the symmetry relation on a finite lattice. Luscher showed that by defining the chiral transformation on a lattice as [22],

$$\delta\psi = i\alpha\gamma_5(1 - \frac{a}{2}D_{ov})\psi \quad \text{and} \quad \delta\bar{\psi} = i\alpha\bar{\psi}(1 - \frac{a}{2}D_{ov})\gamma_5 \ , \tag{1.19}$$

and using the Ginsparg-Wilson relation, the Overlap action has an exact chiral symmetry. All the previously described fermion actions are ultralocal having upto second derivative terms in the fermion operator. For the Overlap fermions, the ultralocality condition is sacrificed to preserve exact chiral symmetry on the lattice in accordance with the Nielsen-Ninomiya theorem. The advantage of Overlap fermions is that these have an exact chiral and flavour symmetry on the lattice. But since the operator involves a matrix sign function, its numerical implementation is computationally more expensive.

- *Domain wall fermions*

  In a five dimensional spacetime, if we consider a theory of massless fermions interacting with each other through the gauge fields that has no component along the fifth dimension then one can have four dimensional chiral fermions by choosing a suitable mass profile along the fifth dimension. In particular if the mass profile is like that of a domain wall sitting at the origin of the fifth dimension then it can be shown that the chiral fermion is localized on the domain wall for infinite extent of the fifth dimension. This idea of obtaining a 4D chiral fermion of definite handedness from a five dimensional theory was first proposed by Kaplan and extended to the lattice [19]. If the fifth dimension is finite then there would be a mixing between the left and the right chiral modes. The same is true on the lattice. On a finite 5-D lattice of dimensions $N^3 \times N_T \times N_5$, there would a tower of states with the lowest energy mode being the linear superposition of the left and the right handed chiral fermion. One can remove the contribution of the bulk five dimensional modes by using pseudofermions in the partition function leaving only the contribution of the lowest state which is called the Domain wall fermion. The advantage of using these lattice fermions is that, for sufficiently smooth gauge field configurations, the overlap between the left and the right handed states fall exponentially with the number of sites N_5 along the fifth dimension [23]. Thus the chiral and continuum limits are separated with the chiral symmetry

now independently tuned by controlling the number of sites along the fifth dimension, N_5. For sufficiently large extent along the fifth dimension, exact chiral symmetry is realized even for a finite lattice spacing. Due to these attractive features and being computationally less expensive than the Overlap fermions it is being recently used for large scale finite temperature QCD simulations [24].

At finite baryon density one has to work in the grand canonical ensemble. On a lattice, a conserved number density can be constructed for the Wilson and the staggered fermion operators. For the Overlap operator, the conserved currents are not unique [25] and even undefined due to which a suitable conserved charge cannot be defined [26]. Naively adding a μN term to the lattice Dirac operators leads to a spurious μ^2/a^2 term in the expression of the energy density, that diverge in the continuum limit. Such divergences are not observed only on the lattice. It was noted earlier [27] that if the number operator in the continuum field theory is not properly normal ordered then the contribution of the infinite number of fermions in the filled Dirac sea would lead to such divergences in thermodynamic quantities like energy density and the quark number susceptibility. To avoid such divergences on lattice, the chemical potential can be introduced as $exp(\pm\mu a)$ factors multiplying the forward and backward temporal gauge links of the lattice Dirac operator respectively [28, 29]. In fact this method is not unique [30, 31]. One can use the functions [31] $f(\mu a)$ and $g(\mu a)$ multiplying the forward and backward temporal gauge links and satisfying the following properties, $f(\mu a) \cdot g(\mu a) = 1$ and $f(\mu a) - g(\mu a) = \mu a + \mathcal{O}(a^2)$ in the lattice fermion operators leading to the removal of the divergent terms in the various thermodynamic quantities.

Once the partition function is known different thermodynamic quantities can be constructed in terms of the derivatives of the partition function with respect to different intensive quantities. Finally to make predictions relevant for the experiments one has to perform a continuum extrapolation of the lattice results. To take the continuum limit i.e $a \to 0$, one has to increase the size of the lattice such that the physical quantities like the temperature is kept fixed. From asymptotic scaling relation, the variation of the bare coupling constant with the lattice spacing is known so taking continuum limit is equivalent to taking $\beta \to \infty$. In presence of finite quark masses the continuum limit has to be taken along the line of constant physics. This is ensured by maintaining the ratios of hadron masses to be constant while varying the coupling constants of the theory namely the gauge coupling and the quark

masses. For the composite operators like the $\langle\bar{\psi}\psi\rangle$, there could be large additive corrections due to the finite lattice spacing if chiral symmetry is not realized exactly on the lattice. One has to do a fine-tuning of the lattice results to get the correct continuum limit. Hence for studying the thermodynamics near the critical point on the lattice one should have the correct flavour content as well as a well defined order parameter with the correct symmetries. For Wilson fermions, there is no chiral symmetry to begin with and hence there is no order parameter on the lattice. The chiral symmetry is broken at the order $'a'$, the finite lattice spacing. It is therefore very difficult to perform a simultaneous chiral and continuum extrapolation. The various low energy theorems like the Gell Mann-Oakes-Renner relation are not satisfied on the lattice. For the staggered fermions there is a remnant chiral symmetry but the spin and flavour symmetries are broken explicitly. The anomalous Ward identities are not satisfied on the lattice making the definition of anomaly ambiguous. For both the cases it is important to appreciate that the difficulties arise due to the coupling of the chiral and the continuum limits. Though these issues would be irrelevant in the continuum limit, it could affect the current lattice results on the critical point significantly. Current lattice results on the critical point use the staggered fermions [3, 4]. It is therefore important to consider fermions with exact chiral symmetry on the lattice to define a correct order parameter with the right symmetries.

Using fermions with exact chiral symmetry on the lattice to study QCD thermodynamics is computationally quite challenging. For the Overlap fermions, one has to compute the sign function of a large matrix. Though considerable progress has been made in defining matrix sign function in terms of rational polynomials, there are difficulties like the occurrence of nested iterations in inverting the operator and implementing topology changing transitions in the simulations. Domain wall fermions have exact chiral symmetry only when the fifth dimensional extent is infinite so the computational cost increases in making the fifth dimension sufficiently large to reduce the mixing between the chiral states. The lattice cut-off effects for different thermodynamic quantities computed on small lattices currently in use for QCD simulations, are similar is magnitude for the Wilson/staggered and the chiral fermion operators [32]. Using the present resources it seems difficult to perform continuum extrapolation with the chiral fermions.

In this thesis we would like to investigate the different properties of the chiral fermion

operators on the lattice and address various issues regarding their applicability for QCD simulations. The main issues that we tried to look upon in this work are,

- The study of chiral symmetry restoration and the critical point involves probing regions of the phase diagram at finite baryon chemical potential. There has been recent proposal for incorporating finite chemical potential in the Overlap/Domain wall fermion operators [33, 34]. We show in our work that all such operators do not have the exact chiral symmetry on the lattice at finite density due to which the chiral order parameter cannot be defined uniquely.

- The thermodynamic quantities computed using the chiral fermions have large lattice cut-off errors for lattice sizes currently used for the QCD computations. Through *tree level improvements* and suitable fine-tuning of the irrelevant parameter in these operators we have reduced the cut-off effects for the ideal gas of fermions to a few percent level on computationally inexpensive lattice sizes. We expect that these improvements would work for full QCD as well in the high temperature regime when the ideal gas limit is approached. Moreover the corrections to the optimum range of the irrelevant parameter due to interactions is expected to be not so drastic though an explicit check has to be done for full QCD.

- The magnitude of the chiral anomaly term determines the nature of phase transitions in QCD. It is important to have an estimate of this anomaly term at finite temperature and density. We have showed non-perturbatively in continuum QCD that there are no corrections to the anomaly equation due to presence of a finite chemical potential. We have also used perturbative imaginary time formalism technique to show that the anomaly equation has no finite temperature and density correction terms. We expect that the chiral anomaly of the theory of Overlap fermions at finite chemical potential, should be independent of fermion density effects. This allows us to motivate for new or perhaps better chiral fermion operators at finite density.

- In the generating functional of the 4D Overlap fermions, the operator in the fermion determinant is not the inverse of the propagator that is sandwiched between the source terms in the exponent. This is one of the important features of a chiral gauge theory. Hence it is important to understand methods to introduce chemical potential

in Overlap formalism and the meaning of chiral symmetry in this context. We look into incorporating the quark chemical potential in the Overlap operator from the first principle Hamiltonian formalism. A suitable conserved number operator is defined in terms of the many body operators. The meaning of the chiral symmetry is evident in terms of the massless fermion source terms included in the action level. We show that under chiral transformation of the source fields the action remains invariant in presence of finite chemical potential and hence exact chiral symmetry is realized even on a finite lattice.

- If a critical point exist in QCD, then the second order quark number susceptibility(QNS) would diverge at that point. The second order QNS can be expressed as a Taylor series in μ_B/T, where μ_B is the baryon chemical potential, then the radius of convergence of the series would give the location of the singularities like the critical point. The radius of convergence estimates require ratio of different higher order QNS. On a finite lattice however there are no divergences but at the critical point all terms of the series would be positive and their corresponding ratios would all be equal. Accurate estimation of the radius of convergence require us to compute QNS of higher orders beyond the current state-of-the-art of eighth order QNS [3]. Motivated from our efforts of prescribing suitable chiral fermion operators at finite density, we propose a staggered fermion operator at finite density which would allow us to compute higher order QNS with considerably reduced computational effort in the QGP phase. In addition such operators have reduced cut-off effects which allow for a better estimation of the radius of convergence.

The thesis is organized as follows: In chapters two and three we discuss about the thermodynamics of the Overlap and the Domain wall fermions and discuss about the reduction of lattice artifacts by either fine tuning of the irrelevant parameter M or through tree level improvement of the operators itself. We show how the existing Overlap and Domain wall fermion operators break chiral symmetry explicitly on the lattice. In chapter four we discuss about both the perturbative and nonperturbative fate of the chiral anomaly at finite fermion density in the continuum. This motivates us to define new Overlap and Domain wall fermion operators on the lattice which would allow for faster computation of the quark number susceptibilities(QNS) on the lattice. Finally in the fifth chapter of the thesis we

show a method of introducing the chemical potential in the Overlap formalism by respecting chiral symmetry on the lattice in the Hamiltonian method.

Chapter 2

Thermodynamics of ideal Overlap fermions

2.1 Introduction

The equation of state of QCD seems [35] to exhibit robust features as one changes the number of light quarks, N_f but the order of the phase transition and the transition temperature T_c seems [36] to depend on it crucially. The location, and even the existence of the critical point in the $\mu_B - T$ phase diagram is expected [37] to depend on N_f, as a result of this dependence of the order of the transitions on N_f. Since the transition seems to be associated with the restoration of the spontaneously broken chiral symmetry at high temperatures, it is very important to study it using fermions having exact chiral symmetries on the lattice.

In view of the experimental relevance of these issues, it would clearly be ideal to employ fermions with exact chiral symmetry on lattice for investigations of the QCD thermodynamics. As is well-known by now, the Overlap fermions [17] have such good chiral properties even on the lattice. The corresponding fermion operator respects chiral symmetry at the expense of not being ultra-local, making the corresponding computations rather expensive. Advances in both algorithms and the computer hardware may have brought such investigations closer to reality today. We would like to investigate the thermodynamics of the free Overlap fermions with an aim to examine its continuum limit both analytically and numerically. For practical reasons, we investigate numerically whether the irrelevant parameter

M in the operator can be tuned optimally to recover the continuum results on the smallest possible lattice size. These predictions can be used in full QCD simulations with such fermions to do the finite temperature calculations faster. We also comment on the recent efforts to introduce chemical potential in the Overlap fermion operator and show that the chiral symmetry is not respected by this operator.

2.2 Zero chemical potential

The Overlap Dirac operator [17] has the following form for massless fermions on asymmetric lattice with spacing a and a_4 in the spatial and temporal directions:

$$D_{ov} = 1 + \gamma_5 sgn(\gamma_5 D_W) \ , \tag{2.1}$$

where sgn denotes the sign function which is defined as,

$$sgn(H_W) = \frac{H_W}{\sqrt{H_W^2}} \ , \ H_W = \gamma_5 D_W \ , \tag{2.2}$$

and

$$\begin{aligned} D_W(x,y) &= (3 + \frac{a}{a_4} - M)\delta_{x,y} - \frac{a}{a_4}[U_4^\dagger(x-\hat{4})\delta_{x-\hat{4},y}\frac{1+\gamma_4}{2} + \frac{1-\gamma_4}{2}U_4(x)\delta_{x+\hat{4},y}] \\ &- \sum_{i=1}^{3}[U_i^\dagger(x-\hat{i})\delta_{x-\hat{i},y}\frac{1+\gamma_i}{2} + \frac{1-\gamma_i}{2}U_i(x)\delta_{x+\hat{i},y}] \end{aligned} \tag{2.3}$$

is the standard Wilson-Dirac operator on the lattice but with a negative mass term $M \in (0,2)$ for simulating one flavour quark on the lattice. The Overlap operator satisfies the Ginsparg-Wilson relation [21] and has exact chiral symmetry on the lattice. For evaluating different thermodynamic quantities we need to evaluate the partition function,

$$Z(V,T) = \int \mathcal{D}U \mathrm{e}^{-\mathrm{S_G}} \mathrm{detD_{ov}} \ . \tag{2.4}$$

The expression for energy density and pressure can be obtained from the partition function, by integrating the quark-antiquark fields :

$$\begin{aligned} \epsilon &= \frac{T^2}{V}\frac{\partial \ln Z(V,T)}{\partial T}\bigg|_V, \quad \text{and} \\ P &= T\frac{\partial \ln Z(V,T)}{\partial V}\bigg|_T, \end{aligned} \tag{2.5}$$

where the spatial volume $V = N^3a^3$ and the temperature $T = (N_T a_4)^{-1}$ for an $N^3 \times N_T$ lattice. We restrict ourselves to $U = 1$ here to focus on the ideal gas limit. The sign function for a matrix can be defined in terms of its eigenvalues, which allows us to express the energy density as,

$$\epsilon = -\frac{1}{N^3a^3N_T}\left(\frac{\partial ln(\prod_n \lambda_n)}{\partial a_4}\right)_a = -\frac{2}{N^3a^3N_T}\sum_{\lambda_\pm}\left(\frac{\partial ln\lambda_\pm}{\partial a_4}\right)_a , \tag{2.6}$$

where the chiral nature of the eigenvalue spectrum in the free case was used in the last line. The eigenvalues of the free Overlap operator in the momentum space can be easily worked [38, 39] out to be

$$\lambda_\pm = 1 - \frac{sgn\left(\sqrt{h^2 + h_5^2}\right) h_5 \pm i\sqrt{h^2}}{\sqrt{h^2 + h_5^2}} , \tag{2.7}$$

where the variables h above are given by

$$\begin{aligned} h_5 &= M - \sum_{j=1}^{3}(1 - \cos(ap_j)) - \frac{a}{a_4}(1 - \cos(a_4p_4)) \\ h_j &= -\sin(ap_j) \qquad \text{where } j = 1, 2, 3 \\ h_4 &= -\frac{a}{a_4}\sin(a_4p_4) \\ h^2 &= h_1^2 + h_2^2 + h_3^2 + h_4^2 \;\; s^2 = h^2 + h_5^2 \; . \end{aligned} \tag{2.8}$$

From the (anti)periodic fermion boundary conditions in the (time) space directions, the discrete p_μ's appearing in the equations above are seen to have the following allowed values :

$$\begin{aligned} ap_j &= \frac{2n_j\pi}{N}, n_j = 0, .., (N-1), j = 1, 2, 3 \text{ and} \\ ap_4 &= \omega_n = \frac{(2n+1)\pi}{N_T}, n = 0, .., (N_T - 1) \end{aligned} \tag{2.9}$$

The variables h_i are all real. Furthermore, a simple algebra shows that $(h^2 + h_5^2) > 0$ for all ranges of interest for M, a and a_4. Since the sign term in Eq.(2.7) is thus a constant, it does not contribute to the derivative in Eq.(2.6); it merely provides the overall sign for the energy density. Choosing $sgn(\sqrt{h^2 + h_5^2}) = 1$, the energy density becomes

$$\begin{aligned}\epsilon &= \frac{2}{N^3 a^3 N_T}\sum_{p_j,p_4}\frac{\frac{\partial h_5}{\partial a_4}-\frac{h_5}{h^2+h_5^2}\left(h_4\frac{\partial h_4}{\partial a_4}+h_5\frac{\partial h_5}{\partial a_4}\right)}{\sqrt{h^2+h_5^2}-h_5} \\ &= \frac{2}{N^3 a^3 N_T}\sum_{p_j,p_4}\frac{h^2\frac{\partial h_5}{\partial a_4}-h_5 h_4\frac{\partial h_4}{\partial a_4}}{h^2(h^2+h_5^2)}(\sqrt{h^2+h_5^2}+h_5)\ ,\end{aligned}$$

where the summations are over all the discrete sets of momenta on the lattice. The derivatives in the expression above are seen to be

$$\frac{\partial h_4}{\partial a_4}=-\frac{h_4}{a_4}\ ,\ \frac{\partial h_5}{\partial a_4}=\frac{a}{a_4^2}(1-\cos(a_4 p_4)) \tag{2.10}$$

Similarly pressure P can be computed by taking partial derivative with respect to a, holding a_4 constant to obtain

$$P=\frac{-2}{3N^3 a^2 a_4 N_T}\sum_{p_j,p_4}\frac{h^2\frac{\partial h_5}{\partial a}-h_5 h_4\frac{\partial h_4}{\partial a}}{h^2(h^2+h_5^2)}(\sqrt{h^2+h_5^2}+h_5)\ . \tag{2.11}$$

The derivatives in the expression for pressure are

$$\frac{\partial h_4}{\partial a}=\frac{h_4}{a}\ ,\ \frac{\partial h_5}{\partial a}=-\frac{1}{a_4}(1-\cos(a_4 p_4)) \tag{2.12}$$

Substituting the derivatives in Eq.(2.10) and Eq.(2.11), one finds the expected ideal gas equation of state $\epsilon = 3P$, valid for all values of a and a_4. We shall therefore focus in the remainder only on the energy density for free Overlap quarks on the lattice and evaluate it by setting $a_4 = a$. We introduce the functions g, f, d and c defined as,

$$\begin{aligned}g &= M-4+b,\ \text{with} \\ b &= \cos(ap_1)+\cos(ap_2)+\cos(ap_3) \\ f &= h_1^2+h_2^2+h_3^2 \\ d &= 4+(M-4)^2+2(M-4)b+c,\ \text{with} \\ c &= \sum_{i<j<4}2\cos(ap_i)\cos(ap_j)\ .\end{aligned} \tag{2.13}$$

such that the $h's$ can be written in terms of the above functions as,

$$\begin{aligned}h_5 &= g+\cos\omega_n \\ h^2 &= f+\sin^2\omega_n \\ h^2+h_5^2 &= d+2g\cos\omega_n\ ,\end{aligned} \tag{2.14}$$

It may be noted that the g, d and f depend only on spatial momenta p_j and enable us to write down the ω_n-dependence of the energy density explicitly:

$$\begin{aligned}\epsilon a^4 &= \frac{2}{N^3 N_T}\sum_{p_j,n}\left[(g+\cos\omega_n)+\sqrt{d+2g\cos\omega_n}\right] \\ &\times \left[\frac{(1-\cos\omega_n)}{d+2g\cos\omega_n}+\frac{\sin^2\omega_n(g+\cos\omega_n)}{(d+2g\cos\omega_n)(f+\sin^2\omega_n)}\right] . \end{aligned} \tag{2.15}$$

2.2.1 Analytic results

The summation over all Matsubara frequencies $\omega_n = \frac{(2n+1)\pi}{N_T}$ can be done using the standard textbook [42] method of contours in the complex ω-plane. Before we show the details of the energy density calculation, let us list certain useful relations amongst the quantities g,d,b and c introduced in Eq.(2.13), (which will be useful for the calculations below) :

- Since $\cos(ap_j) \leq 1$ for any j, $g < 0$ for $M < 1$,
- $g^2 + f + 1 = d \Longrightarrow d > 0$, since f is a sum of squares,
- $d^2/4g^2 - f - 1 = (g^2 - f - 1)^2/2g^2 \Longrightarrow d^2/2g^2 > 1 + f$,
- $\cosh^{-1}\frac{d}{2g} > \sinh^{-1}\sqrt{f}$. This follows trivially from the line above. Since $\frac{d^2}{4g^2} > (1+f)$, it follows $\frac{d}{2g} > \sqrt{1+f}$ ($\frac{d}{2g} < -\sqrt{1+f}$, for $g < 0$). Noting that $\cosh(\sinh^{-1}\sqrt{f}) = \sqrt{1+f}$, one has $\cosh^{-1}(\frac{d}{2g}) > \sinh^{-1}\sqrt{f}$ ($\cosh^{-1}(\frac{d}{2g}) < -\sinh^{-1}\sqrt{f}$ for $g < 0$).

The last line justifies the drawing of the contour in Figure 2.1 by avoiding the poles/cuts at $\pm i\,\cosh^{-1}(\frac{d}{2g})$. For a general function $F(\omega)$, which depend on variables p_j, but this dependence will not be shown explicitly below, the frequency sum therefore is,

$$\frac{2\pi}{N_T}\sum_n F(\omega_n) = \int_{\pi-i\epsilon}^{-\pi-i\epsilon}\frac{F(\omega)d\omega}{e^{i\omega N_T}+1} + \int_{-\pi+i\epsilon}^{\pi+i\epsilon}\frac{F(\omega)d\omega}{e^{i\omega N_T}+1} , \tag{2.16}$$

where the integrals are evaluated on the contour lines running parallel to the real axis. The second integral can further be re-written as

$$\int_{-\pi+i\epsilon}^{\pi+i\epsilon}\frac{F(\omega)d\omega}{e^{i\omega N_T}+1} = \int_{-\pi+i\epsilon}^{\pi+i\epsilon}F(\omega)d\omega - \int_{-\pi+i\epsilon}^{\pi+i\epsilon}\frac{F(\omega)d\omega}{e^{-i\omega N_T}+1} . \tag{2.17}$$

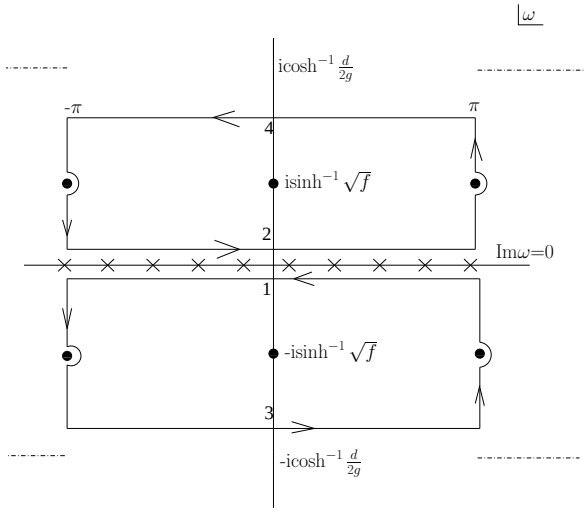

Figure 2.1: The choice of contours for evaluating the ω-sum in Eq.(2.15). The dashed lines represent branch cuts. The crosses denote the Matsubara frequencies ω_n, while the filled circles denote the poles of $F(\omega)$.

The summand $F(\omega)$ in Eq.(2.15) can be split in to two terms,

$$F(\omega) = F_1(\omega) + F_2(\omega) \ ,$$

with

$$F_1(\omega) = \left(\frac{(1-\cos\omega)}{d+2g\cos\omega} + \frac{\sin^2\omega(g+\cos\omega)}{(d+2g\cos\omega)(f+\sin^2\omega)} \right) \times (g+\cos\omega) \ , \tag{2.18}$$

and

$$F_2(\omega) = \left(\frac{(1-\cos\omega)}{d+2g\cos\omega} + \frac{\sin^2\omega(g+\cos\omega)}{(d+2g\cos\omega)(f+\sin^2\omega)} \right) \times \sqrt{d+2g\cos\omega} \ . \tag{2.19}$$

Both the functions F_i have a finite number of poles at $\omega = \pm i \sinh^{-1}\sqrt{f}$ and $\pm m\pi \pm i \sinh^{-1}\sqrt{f}$, where m is an integer. Furthermore, F_1 has poles for $\frac{d}{2g} > 0$ at $\omega = \pm k\pi \pm i \cosh^{-1}\frac{d}{2g}$ while F_2 has branch points at the same locations. Similarly, for $\frac{d}{2g} < 0$ the poles (branch points) of F_1 (F_2) are at $\pm i\cosh^{-1}\frac{d}{2g}$. In the rest of the complex ω plane both the functions are analytic. In view of these properties the contours in Eq.(2.16) can be deformed to the contours shown in Figure 2.1. We chose each contour such that it lies below (above) the cut in the upper (lower) half of the plane. As shown above, $\cosh^{-1}\frac{d}{2g} > \sinh^{-1}\sqrt{f}$.

Defining therefore $2\eta = \cosh^{-1}\frac{d}{2g} - \sinh^{-1}\sqrt{f}$ with $\eta > 0$, the lines 3 and 4 are drawn through the points $\mp(i\sinh^{-1}\sqrt{f} + i\eta)$ respectively to avoid the cuts shown in Figure 2.1.

Consequently, the frequency sum in Eq.(2.16) becomes

$$\begin{aligned}\frac{2\pi}{N_T}\sum_n F(\omega_n) &= -2\pi i \sum_{\text{Im }\omega>0} \frac{\text{Res } F(\omega)}{e^{-i\omega N_T}+1} + 2\pi i \sum_{\text{Im }\omega<0} \frac{\text{Res } F(\omega)}{e^{i\omega N_T}+1} \\ &- \int_3 \frac{F(\omega)d\omega}{e^{i\omega N_T}+1} + \int_4 \frac{F(\omega)d\omega}{e^{-i\omega N_T}+1} + \int_{-\pi+i\epsilon}^{\pi+i\epsilon} F(\omega)d\omega \ .\end{aligned}$$

The line integrals along the vertical lines through π and $-\pi$ cancel each other due to the periodicity of the function $F(\omega)$. Indeed, in general for any function $G(\omega)$ satisfying the property, $G(\pi+i\eta) = G(-\pi+i\eta)$, the sum of integrals of $G(\omega)$ along opposite vertical paths of equal length through $-\pi$ and π is identically zero.

The residues of the function $F_{1,2}(\omega)$ at the poles $\omega = \pm i\sinh^{-1}\sqrt{f}$ are $\pm iR_1$ and $\pm iR_2$ respectively where

$$R_1 = R_2 = \frac{\sqrt{f}}{2\sqrt{1+f}} \tag{2.20}$$

Our choice of the contour also ensures that the poles at $\pm\pi \pm i\sinh^{-1}\sqrt{f}$ do not contribute to the energy density. By taking the limit $N_T \to \infty$ on the lattice, on finds that the last term of Eq.(2.20) gives the quartically divergent vacuum contribution in the continuum limit. Defining the physical energy density by subtracting it off, we have,

$$\epsilon a^4 = \frac{4}{N^3}\sum_{p_j}\left[\frac{\sqrt{f}}{\sqrt{1+f}}\right]\frac{1}{e^{N_T\sinh^{-1}\sqrt{f}}+1} + \epsilon_3 + \epsilon_4 \ , \tag{2.21}$$

where ϵ_3, ϵ_4 terms come from from the line integrals 3 and 4 in Figure 2.1 respectively. Their explicit N_T dependence indicates that they contribute to the energy density on the lattice. However, they do not do so in the continuum limit, as we shall see below.

In order to take the continuum limit of $a \to 0$, we let $N, N_T \to \infty$ such that T and VT^3 is kept constant. Each summation over momenta is replaced by an integral in this limit:

$$\frac{1}{N}\sum_{p_j} \to \frac{a}{2\pi}\int_{-\infty}^{\infty} dp_j. \tag{2.22}$$

Further the integration variable $\omega = ap_4$ can be traded for p_4, pushing the branch points at $\pm\pi \pm i\text{cosh}^{-1}\frac{d}{2g}$ to infinity faster than the contours 3 and 4 are pushed. The line integrals.

and hence the terms ϵ_3 and ϵ_4 vanish. Since the poles at $i \sinh^{-1}\sqrt{f}$ scale as a in this limit, they continue to be enclosed in the contour at a finite p_4 and do contribute to the energy density. This can be explicitly checked algebraically by taking the limit of the Eq.(2.21) to obtain the expression for the continuum energy density as,

$$\epsilon_{SB} = \frac{2}{(2\pi)^3}\left(2\int\prod_{j=1}^{3} dp_j \frac{E}{1+e^{E/T}}\right) = \frac{7\pi^2}{60}T^4 \ , \tag{2.23}$$

where $E = \sqrt{p_1^2 + p_2^2 + p_3^2}$ is the energy of the massless quarks.

2.2.2 Numerical results

In this subsection we investigate the lattice energy density of the Eq.(2.15) numerically by summing over all the momenta. The objectives in this section are:

- to estimate the importance of the terms ϵ_3 and ϵ_4 in it on lattices of practical sizes,
- to find out the role M plays on finite lattices since ϵ_3 and ϵ_4 are functions of M.

In particular, it would be good to know if there exists a range of the irrelevant parameter M for which the energy density converges to that of the continuum ideal Fermi gas on reasonable, i.e. computationally inexpensive, lattice sizes. This would mean that we would be looking for a range of M for which ϵ_3 and ϵ_4 are minimized. Since we have shown the existence of the continuum limit for the entire allowed range of M in the previous subsection, it is clear that a sufficiently fine lattice must eventually yield the correct result for any M.

In general, the dimensionless lattice energy density will be of the form,

$$E = A(M) + \frac{B}{N_T^4} + \frac{C(M)}{N_T^6} + \frac{D(M)}{N_T^8} + ... \tag{2.24}$$

where the coefficients $A(M)$ and B are the usual vacuum and the T^4 contributions, while $C(M)$ and $D(M)$ are finite lattice spacing artifacts. For each value of M and aspect ratio, defined as $\zeta = N/N_T$, the energy density on the lattice was calculated as a function of the N_T. Clearly A is the dominant contribution and its removal turned out to be a tricky issue governed by the precision of our computations. Fitting the above form to obtain C or D was therefore not feasible. The zero temperature part of the energy density was calculated

from Eq.(2.15) by taking $N_T \to \infty$ and a large spatial extent, keeping the lattice spacing finite. The resulting integral over ω was done numerically for each M to estimate the zero temperature contribution. Subtracting the zero temperature part from the energy density and dividing the resultant ϵ by ϵ_{SB} gives us a ratio which we employ for further studies. In the left panel of Figure 2.2, the ratio ϵ/ϵ_{SB} is shown as a function of N_T for $M = 1.55$ and various aspect ratios ζ. A mild dependence on ζ is visible for lower values but in each case the curve approaches to unity by $N_T = 12$, signalling the onset of continuum limit. For $\zeta \geq 3$, the results are within 3-4% of each other signalling the onset of the thermodynamic limit. In the right panel of Figure 2.2, the M-dependence of the same ratio is shown for

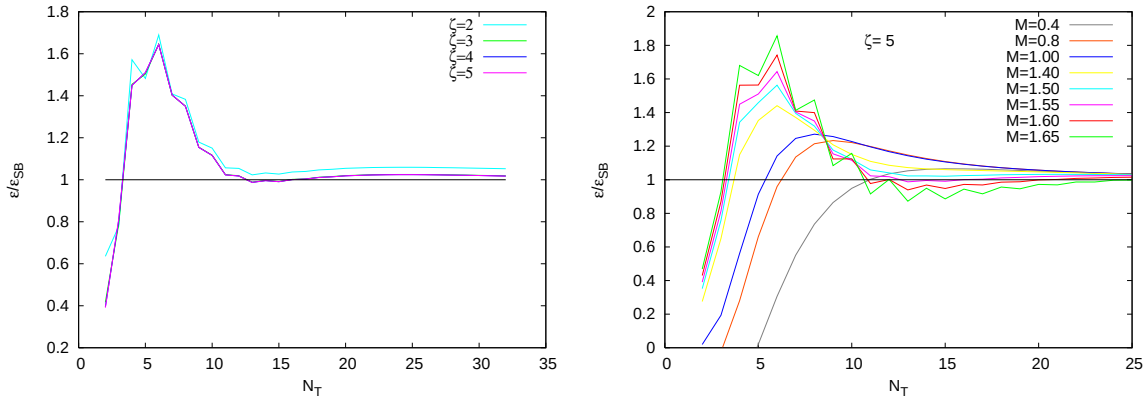

Figure 2.2: The variation of the ratio ϵ/ϵ_{SB} with N_T for $M = 1.55$ and $\zeta = 2 - 5$(left) and the variation of the ratio ϵ/ϵ_{SB} with N_T for different M and $\zeta = 5$(right).

a fixed $\zeta = 5$ for the range $0.4 \leq M \leq 1.65$. A range of $1.5 \leq M \leq 1.6$ emerges as the favoured one because all the M-dependent terms are seen to be minimum there and hence the continuum limit is reached faster. On smaller lattices with $N_T = 4-8$, the lattice results are seen to be 1.6-1.8 times larger in this range of M. For other values of M, the continuum limit is seen to be approached slowly; even an $N_T = 25$ seems not enough. For larger M, we also observed oscillations as N_T changed between odd and even, limiting our effort to increase the M-range further. The values of ϵ/ϵ_{SB} for $N_T = 4 - 16$ and different M are tabulated in Tables 2.1, 2.2 for easy reference.

In order to estimate the size of the $1/N_T^2$ correction term for different values of M, the same ratio is plotted as a function of $1/N_T^2$ in the left panel of Figure 2.3. From the plot,

Table 2.1: ϵ/ϵ_{SB} values for different. M for $\zeta = 2$

N_T	M=1.0	1.50	1.55	1.60	1.65
4	0.630	1.453	1.571	1.697	1.828
6	1.194	1.606	1.690	1.792	1.914
8	1.316	1.355	1.383	1.431	1.506
10	1.268	1.158	1.150	1.156	1.186
12	1.206	1.078	1.054	1.036	1.033
14	1.160	1.060	1.032	1.004	0.983
16	1.129	1.061	1.037	1.008	0.979

it is evident that the correction terms become insignificant very fast for $1.50 \leq M \leq 1.60$ and the continuum limit is reached within 2-3 % already for $N_T = 12$ whereas for $M = 1$ they are relevant even for $N_T \geq 12$. Of course, the continuum extrapolation for $M = 1.0$ is easier than for $1.50 \leq M \leq 1.60$ due to the nonlinearities present for the latter. However, the energy density for at least three different lattice sizes with $N_T = 10, 12, 14$ need to be computed for such an extrapolation. On the other hand, although the extrapolation for $1.50 \leq M \leq 1.60$ is difficult due to the complex variation seen in the left panel of Figure 2.3, the deviation from the continuum value is within the typical accuracy range of the current lattice results, making it an optimal range for simulations. It should also be noted that the corrections for the Overlap fermions for $M \sim 1.55$ for $N_T < 12$ are smaller than compared to the Wilson and the staggered case [32] as well. Ref. [32] deals with p/p_{SB} which we showed above to be identical to the ϵ/ϵ_{SB} for the Overlap ideal gas.

Filled squares in the right panel of Figure 2.3 show the percentage average deviations of the ratio from unity due to lattice artifact terms as a function of M for large N_T values($N_T \geq 18$). It shows marginal dependence on M for $M < 1.2$ but the deviation itself is about 5-6 %. For larger M, the data show a dip, indicating clearly that the thermodynamics of free fermions favours the optimum value of M to lie between 1.50-1.60, with a deviation of only about 2.5 % or lower.

Comparing our results with other studies of thermodynamics of free fermions done with improved actions [40] and also with Overlap fermions ($M = 1$) in 2-D [41] as well

Table 2.2: ϵ/ϵ_{SB} values for different. M for $\zeta = 5$

N_T	M=1.0	1.50	1.55	1.60	1.65
4	0.561	1.342	1.450	1.563	1.681
6	1.141	1.563	1.644	1.742	1.857
8	1.272	1.319	1.350	1.399	1.475
10	1.228	1.122	1.116	1.124	1.157
12	1.167	1.041	1.018	1.001	1.002
14	1.123	1.023	0.996	0.969	0.950
16	1.092	1.025	1.001	0.972	0.944

as in 4-D [39, 32], we find that i) there are larger deviations in higher dimensions and ii) the oft-favoured choice of $M = 1$ favours rather poorly on finite lattices. Indeed, one can significantly reduce the corrections to the energy density of Overlap fermions due to the lattice artifacts with a proper choice of M.

2.3 Nonzero chemical potential

The chemical potential is usually introduced as the Lagrange multiplier to investigate thermodynamics at constant conserved number. Constructing the relevant number operator for the Overlap Dirac fermions is not easy due to its nonlocality [25] and may even be not unique [26]. Instead of deriving the conserved number, one may make an inspired guess for it such that it has the right continuum limit. One such proposal for introducing the chemical potential for the Overlap operator is [33] to introduce it in the D_W as one would for the usual Wilson fermions:

$$D_{ov} = 1 + \gamma^5 sgn(\gamma^5 D_W(\hat{\mu})) \ , \tag{2.25}$$

where the chemical potential $\hat{\mu} = \mu a_4$ appears only as multiplying factors $\exp(\hat{\mu})$ and $\exp(-\hat{\mu})$ to the links U_4 and $U_4^\dagger$ respectively in Eq.(2.3). This, of course, renders $\gamma_5 D_W(\mu)$ to be non-hermitian, necessitating an extension of the usual definition of the sign function. The natural choice [33] was to use the sign of the real part of the eigenvalues of $\gamma_5 D_W(\mu)$ in the equation above. It is important to note that the extended sign function is not defined

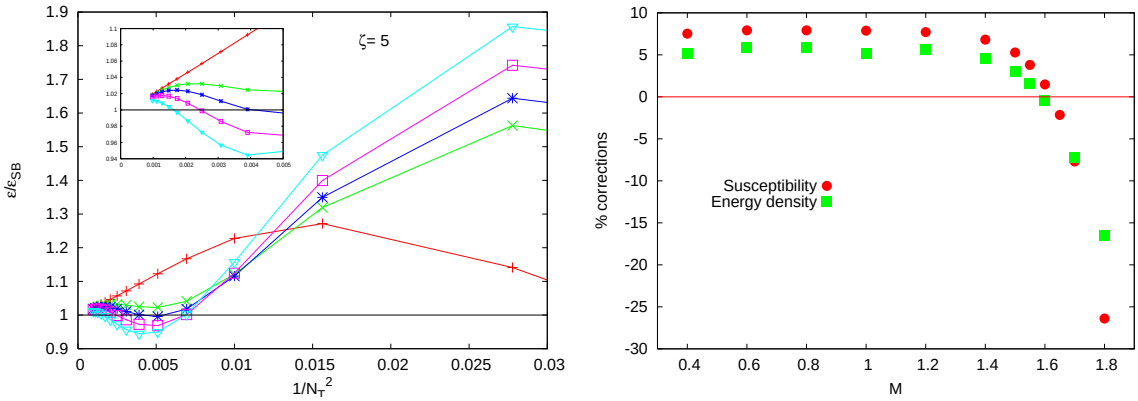

Figure 2.3: The variation of the ratio ϵ/ϵ_{SB} with $1/N_T^2$ for different $M \geq 1$ and $\zeta = 5$. The plusses, crosses, stars, boxes and triangles denote M=1.0, 1.50, 1.55, 1.60 and 1.65 respectively(left) and the estimated finite lattice spacing corrections for the energy density and susceptibility at $\mu = 0$ in percentage as a function of M(right).

for purely imaginary eigenvalues. Numerical simulations were performed [39] for an ideal gas of Overlap fermions to show that the above way of introducing μ does not encounter any quadratic divergences at zero temperature for $M = 1$. Such divergences were known to arise [28, 30] for staggered and Wilson fermions, if μ was introduced naively as a coefficient of the conserved number. These were eliminated by the choice of the $\exp(\pm\hat{\mu})$ factors. A more general way to introduce the chemical potential is, of course, to introduce functions $K(\hat{\mu})$ and $L(\hat{\mu})$ in place of the factors $\exp(\hat{\mu})$ and $\exp(-\hat{\mu})$ respectively such that $K(\hat{\mu}) = 1+\hat{\mu}+\mathcal{O}(\hat{\mu}^2)$ and $L(\hat{\mu}) = 1-\hat{\mu}+\mathcal{O}(\hat{\mu}^2)$, It was shown [31] that the quadratic divergences are avoided if $K(\hat{\mu}) \cdot L(\hat{\mu}) = 1$.

Here we follow that idea and introduce chemical potential in the Overlap Dirac operator through the K and L factors in D_W and study where the condition to eliminate the quadratic divergences remains the same. Introducing

$$\begin{aligned} \frac{K(\hat{\mu}) - L(\hat{\mu})}{2} &= R\sinh\theta \\ \frac{K(\hat{\mu}) + L(\hat{\mu})}{2} &= R\cosh\theta\ , \end{aligned} \tag{2.26}$$

one can follow through the steps of the previous section to find that the free Overlap operator in the momentum space can again be written in terms of the h_i of Eq.(2.8) but with h_4 and

h_5 changed to :

$$\begin{aligned} h_5 &= M - \sum_{j=1}^{3}(1-\cos(ap_j)) - \frac{a}{a_4}(1 - R\cos(a_4 p_4 - i\theta)) \\ h_4 &= -\frac{a}{a_4} R\sin(a_4 p_4 - i\theta) \ . \end{aligned} \tag{2.27}$$

The energy density in presence of finite chemical potential is defined as

$$\epsilon(\mu) = -\frac{1}{N^3 a^3 N_T}\left(\frac{\partial ln\det D}{\partial a_4}\right)_{a,a_4\mu} = -\frac{2}{N^3 a^3 N_T}\left(\frac{\partial ln(\lambda_+\lambda_-)}{\partial a_4}\right)_{a,a_4\mu} \tag{2.28}$$

In the following we assume that the sign function is always defined and is +1, as for the $\mu = 0$ case. We shall comment on this assumption later. The energy density is obtained using Eq.(2.28) and setting $a = a_4$.

$$\begin{aligned} \epsilon a^4 &= \frac{2}{N^3 N_T}\sum_{p_j,n}\left[g + R\cos(\omega_n - i\theta) + \sqrt{d_R + 2gR\cos(\omega_n - i\theta)}\right] \\ &\times \quad \left[\frac{1 - R\cos(\omega_n - i\theta)}{d_R + 2gR\cos(\omega_n - i\theta)} + \frac{R^2\sin^2(\omega_n - i\theta)(g + R\cos(\omega_n - i\theta))}{(d_R + 2gR\cos(\omega_n - i\theta))(f + R^2\sin^2(\omega_n - i\theta))}\right] \ . \end{aligned} \tag{2.29}$$

The summand in the Eq.(2.29) has the same functional form as that in Eq.(2.15). Indeed the only changes are: $d_R = f + g^2 + R^2$ replaces d of Eq.(2.13), $\omega \to \omega - i\theta$ and the factor R multiplies each sine/cosine term. Comparing Eq.(2.27) with Eq.(2.8), and using the expression for the pressure given in Eq.(2.11), one again finds that the equation of state $\epsilon = 3P$ also holds in the presence of a chemical potential, μ. An additional new physical observable that can be computed is the number density, defined as,

$$n = \frac{1}{N^3 a^3 N_T}\left(\frac{\partial ln\det D}{\partial \hat{\mu}}\right)_{a_4} \tag{2.30}$$

In terms of h's the previous expression can be calculated explicitly,

$$\begin{aligned} na^3 &= \frac{-2i}{N^3 N_T}\sum_{p_j,n}\left[R\sin(\omega_n - i\theta) \times \left(\frac{gR\cos(\omega_n - i\theta) + R^2 + f}{(d_R + 2gR\cos(\omega_n - i\theta))(f + R^2\sin^2(\omega_n - i\theta))}\right)\right. \\ &\times \quad \left.\left(g + R\cos(\omega_n - i\theta) + \sqrt{d_R + 2gR\cos(\omega_n - i\theta)}\right)\right] \\ &= \frac{-2i}{N^3 N_T}\sum_{p_j,n} F_N(R, \omega_n - i\theta) \ . \end{aligned} \tag{2.31}$$

It can be shown that the condition to obtain the correct continuum values of $\epsilon = \mu^4/4\pi^2$ and $n = \mu^3/3\pi^2$ are the expected ones, $K(\hat{\mu}) - L(\hat{\mu}) = 2\hat{\mu} + O(\hat{\mu}^2)$. The details are mentioned in this thesis [43]. The earlier work [31] on staggered fermions employed the exact number density on the lattice which is not the case for the Overlap fermions here. That one obtains still identical conditions in both the cases suggests that it is indeed the behaviour near the continuum limit which dictates these conditions. Finally, using the same techniques to evaluate the Matsubara frequencies sum, the energy density at non-zero temperature and chemical potential can be computed analytically. Further details are again given in the thesis [43]. The final expression is,

$$\epsilon a^4 = \frac{2}{N^3} \sum_{p_j} \left[\frac{\sqrt{f}}{\sqrt{1+f}} \frac{1}{e^{(\sinh^{-1}\sqrt{f} - \hat{\mu})N_T} + 1} + \frac{\sqrt{f}}{\sqrt{1+f}} \frac{1}{e^{(\sinh^{-1}\sqrt{f} + \hat{\mu})N_T} + 1} + \epsilon_{3\mu} + \epsilon_{4\mu} \right] \tag{2.32}$$

The terms $\epsilon_{3\mu}$ and $\epsilon_{4\mu}$ are contributions of the line integrals below the branch cuts. We would be investigating the M dependence of these quantities $\epsilon_{3\mu}$ and $\epsilon_{4\mu}$ numerically in Sec. 2.3.2 to check how the optimum range of the parameter M changes in the presence of μ.

2.3.1 Loss of chiral invariance

Another crucial difference is that the introduction of the functions K and L for the staggered fermions still leaves the action invariant under the chiral transformations due to the locality of the action. This is true for the full theory, i.e., even after the link variables , U_x^μ are restored. On the contrary, one can easily check that one breaks the chiral invariance in the case of the Overlap fermions by these functions K, L, or $\exp(\pm\hat{\mu})$. As defined in Eq.(1.19), the chiral transformation involves $D_{ov}(\hat{\mu} = 0)$, while the action for $\mu \neq 0$ for the Overlap fermions has $D_{ov}(\hat{\mu})$ of the Eq.(2.25). By construction, the latter does satisfy the Ginsparg-Wilson relation [21] with the μ-dependent Overlap Dirac operator on both sides :

$$\left\{\gamma_5, D_{ov}(\hat{\mu})\right\} = D_{ov}(\hat{\mu})\gamma_5 D_{ov}(\hat{\mu}) \ . \tag{2.33}$$

Unfortunately though, it is not sufficient to guarantee invariance under the chiral transformation in Eq.(1.19), as it does not have any μ-dependence. Indeed, the variation of action

under the chiral transformation of Eq.(1.19) is

$$\delta S = i\alpha \sum_{x,y} \bar{\psi}_x \big[\gamma_5 D_{ov}(\hat{\mu}) + D_{ov}(\hat{\mu})\gamma_5 - \frac{1}{2} D_{ov}(0)\gamma_5 D_{ov}(\hat{\mu}) - \frac{1}{2} D_{ov}(\hat{\mu})\gamma_5 D_{ov}(0)\big]_{xy} \psi_y \ ,$$

which clearly does not vanish on a finite lattice in spite of Eq.(2.33). One may alternatively propose modified chiral transformations,

$$\delta\psi = i\alpha\gamma_5(1 - \frac{1}{2} D_{ov}(\mu))\psi \quad \text{and} \quad \delta\bar{\psi} = i\alpha\bar{\psi}(1 - \frac{1}{2} D_{ov}(\mu))\gamma_5 \ , \tag{2.34}$$

which will ensure $\delta S = 0$. Furthermore, altering the symmetry transformations as above has undesirable physical consequences [63] which are outlined below. Non-Hermiticity of $\gamma_5 D_{ov}(\mu)$ makes the transformations nonunitary. The symmetry transformations should not depend on the intensive thermodynamic quantity μ, which is a tunable parameter of the physical system. The symmetry group itself changes with μ, leaving no physical order parameter which will characterize the chiral phase transition as a function of μ. In contrast, the chiral symmetry group remains the same at nonzero temperature (and zero density), allowing us to infer that vanishing of the chiral condensate would correspond to restoration of the symmetry for the vacuum.

2.3.2 Numerical results

We compute the sums over all momenta in Eq.(2.32) to find out the importance of lattice artifacts in form of the terms $\epsilon_{3\mu}$ and $\epsilon_{4\mu}$, resulting from the line integrals 3 and 4, and to look for the role of M. The focus here is, of course, on the chemical potential. We therefore consider two observables here. One is the change in the energy density, $\Delta\epsilon(\mu, T) = \epsilon(\mu, T) - \epsilon(0, T)$. In continuum it is given by,

$$\frac{\Delta\epsilon(\mu, T)}{T^4} = \frac{\mu^4}{4\pi^2 T^4} + \frac{\mu^2}{2T^2} \ . \tag{2.35}$$

The other quantity we consider is the quark number susceptibility at $\hat{\mu} = 0$. For the free Overlap fermions, it is given for any $\hat{\mu}$ by

$$\chi = \frac{1}{N^3 a^2 N_T} \left(\frac{\partial^2 ln \det D}{\partial \hat{\mu}^2} \right)_{a_4} \ , \tag{2.36}$$

which can be worked out to be

$$\chi = \frac{2i}{N_T N^3 a^2} \sum_{p_j, p_4} \left[\frac{-\left(h^2 h_4 + h_4 h_5 \cos(ap_4 - i\hat{\mu})\right) u}{s^4 (s - h_5)^2} + \frac{v}{s^2 (s - h_5)} \right] , \tag{2.37}$$

where u and v are in the expression above are

$$\begin{aligned} u &= 2(s - h_5)(h_4 \frac{\partial h_4}{\partial \hat{\mu}} + h_5 \frac{\partial h_5}{\partial \hat{\mu}}) + s^2 (\frac{\partial s}{\partial \hat{\mu}} - \frac{\partial h_5}{\partial \hat{\mu}}) , \\ v &= \frac{\partial h_4}{\partial \hat{\mu}} (2h_4^2 + h^2 + h_5 \cos(ap_4 - i\hat{\mu})) + h_4 \frac{\partial h_5}{\partial \hat{\mu}} \cos(ap_4 - i\hat{\mu}) + i h_4 h_5 \sin(ap_4 - i\hat{\mu}) , \end{aligned}$$

and

$$s^2 = h^2 + h_5^2 . \tag{2.38}$$

Again in the continuum, the susceptibility is known to be

$$\chi(\mu) = \frac{\mu^2}{\pi^2} + \frac{T^2}{3} . \tag{2.39}$$

Our computations for the energy density were performed keeping the ratio $r = \mu/T = \hat{\mu} N_T$ fixed, yielding a constant $\Delta\epsilon/T^4$ in the continuum from Eq.(2.35). Our choices of r were restricted by the fact that on lattices with odd N_T, eigenvalues of $\gamma_5 D_W(\hat{\mu})$ can turn purely imaginary for sufficiently large $\hat{\mu}$. This is related to the fact that $(\gamma_5 D_W)^\dagger \gamma_5 D_W$ has $h^2 + h_5^2$ as eigenvalues and

$$\begin{aligned} \text{Re } (h^2 + h_5^2) &= g^2 + 1 + f + 2g \cos\omega \, \cosh\hat{\mu} \\ \text{Im } (h^2 + h_5^2) &= 2g \sin\omega \, \sinh\hat{\mu} . \end{aligned} \tag{2.40}$$

has zero imaginary part at $\omega = \pi$ with negative real part for $\mu \geq \mu_c$. The sign function is undefined for such cases. Indeed, in the interacting case it may even be possible to get such purely imaginary argument of the sign function of the Overlap Dirac operator for all N_T. From the plots of the ratio of the $\Delta\epsilon/T^4$ on the lattice and in the continuum (Eq.(2.35)), shown in Figure 2.4 we again conclude that the continuum limit is reached for $N_T \geq 12$ for both the cases for essentially all M, with the $1.5 < M < 1.6$ region displaying the smallest deviations in the region $N_T > 12$ as in the $\hat{\mu} = 0$ case. Moreover the results for $\Delta\epsilon$ again appear about 1.6-1.8 times larger on the lattices with $N_T = 4 - 8$ while the susceptibility is close to twice the continuum result. In the left panel of Figure 2.5, we display the ratio

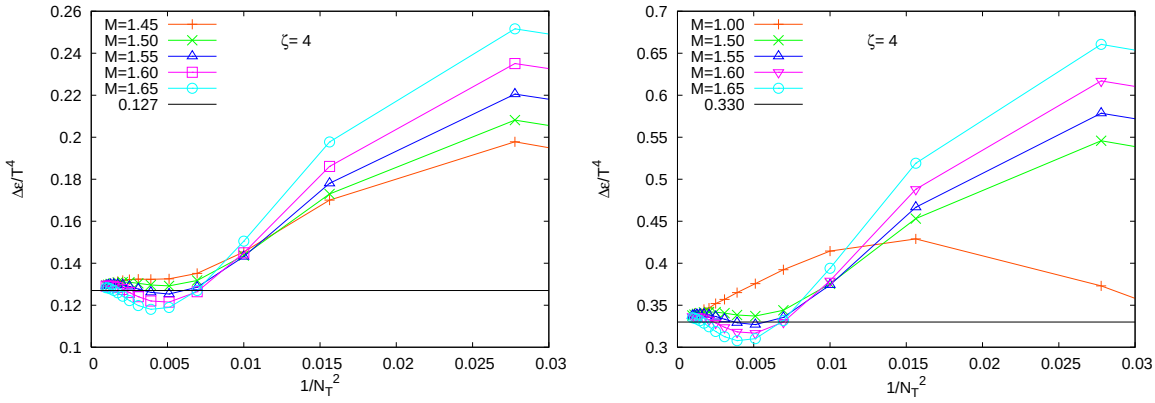

Figure 2.4: The variation of the lattice $\Delta\epsilon/T^4$ with $1/N_T^2$ for $\hat{\mu} = 0.5/N_T$(upper panel) and $\hat{\mu} = 0.8/N_T$(lower panel).

of $\chi(\mu = 0, T)$ on the lattice with the corresponding continuum value from Eq.(2.39). One sees again a similar pattern as for the energy density. As in Eq.(2.24), the susceptibility calculated on the lattice will also have a form,

$$\chi(0) = \frac{B^\chi}{N_T^2} + \frac{C^\chi(M)}{N_T^4} + \frac{D^\chi(M)}{N_T^6} + \ldots \,, \tag{2.41}$$

where the only difference is the absence of a constant term like A. Keeping only the first term, one will again get the effective B^χ to become M-dependent; its deviation from 1/3 will be a measure of the finite lattice spacing effects. The filled circles in the right panel of Figure 2.3 display these artifact effects as a function of M which were obtained by assuming a constant behaviour in the range $18 \leq N_T \leq 32$. The absence of a dominant term like A in the equation above allowed us to re-do the fit with the inclusion of the next term for each M. We found that the resultant B^χ is already M-independent and close to 1/3 in each case. Moreover the C^χ changed with M substantially and was smallest for $M = 1.6$. From all these fits, it also emerged that by $N_T = 64$ the contribution of the C^χ-term becomes negligible. The right panel of Figure 2.5 exhibits the results of our attempt to verify this by extending the computations to larger lattices. We find a convergence to the continuum result irrespective of the value of M from lattice sizes of $320^3 \times 64$. Note that one finds very similar effects of finite lattice spacing for both the susceptibility and the energy density at $\mu = 0$ in the right panel of Figure 2.3, with $M \sim 1.6$ emerging as a good choice for calculations on

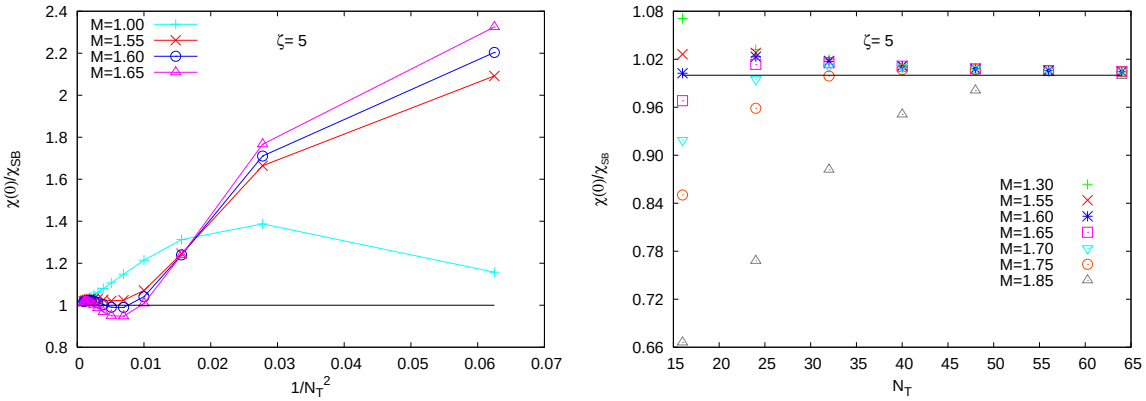

Figure 2.5: The variation of $\chi(0)/\chi_{SB}$ vs $1/N_T^2$(upper panel) and vs N_T(lower panel) for different M and $\zeta = 5$.

lattices with small N_T due to smallest contribution from the correction terms.

2.4 Massive Overlap fermions

While we restricted ourselves to the thermodynamics of massless Overlap fermions, most of our treatment goes through for the massive fermions as well. In this section we outline this for the $\mu = 0$ case. For the sake of novelty, we use an alternative way of doing the computation. The Overlap operator for fermions of mass m is written as,

$$D_{ov} = (1 + \frac{ma}{2M}) + (1 - \frac{ma}{2M}) sgn(\gamma^5 D_W) \ . \tag{2.42}$$

The eigenvalues of the Overlap-Dirac operator change from $\lambda_\pm$ in Eq.(2.7) to $\lambda_\pm \to \lambda_\pm(1 - ma/2M) + ma/M$. As a result the energy density modifies from Eq.(2.10) to

$$\epsilon = \frac{2}{N^3 a^3 N_T} \sum_{p_j, p_4} \frac{\alpha(h^2 \frac{\partial h_5}{\partial a_4} - h_5 h_4 \frac{\partial h_4}{\partial a_4})}{(h^2 + h_5^2)(\gamma\sqrt{h^2 + h_5^2} - \alpha h_5)} \ , \tag{2.43}$$

where

$$\alpha = 2\left(1 - \frac{m^2 a^2}{4M^2}\right) \quad \text{and} \quad \gamma = 2\left(1 + \frac{m^2 a^2}{4M^2}\right) \ .$$

Substituting the values of h_4, h_5 and their derivatives, one obtains

$$\epsilon a^4 = \frac{2\alpha}{N^3 N_T} \sum_{p_j,n} \left[\frac{(1-\cos\omega_n)(f+\sin^2\omega_n) + \sin^2\omega_n(g+\cos\omega_n)}{(d+2g\cos\omega_n)(\gamma^2(d+2g\cos\omega_n) - \alpha^2(g+\cos\omega_n)^2)} \right]$$
$$\times \left[\gamma\sqrt{d+2g\cos\omega_n} + \alpha(g+\cos\omega_n) \right] \ . \tag{2.44}$$

Note that setting $m = 0$, reduces $\alpha = \gamma$. Substituting in the equation above, and using the relation $d = g^2 + f + 1$, it becomes identical to the expression in Eq.(2.15), as expected.

One can again use the same contour method for evaluating the energy density. By comparing with Eq.(2.15), the functions F_1 and F_2 can be identified as the two terms obtained by removing the second pair of brackets of Eq.(2.44). The poles (and branch cuts) of these functions can be seen to be the same except that the poles defined by $\omega = \pm i \sinh^{-1}\sqrt{f}$ are now given by

$$\cos\omega = y \pm z \ , \tag{2.45}$$

where y and z are defined as

$$y = g\left(\frac{\gamma^2}{\alpha^2} - 1\right) \tag{2.46}$$

$$z = \frac{\gamma}{\alpha}\sqrt{g^2\left(\frac{\gamma^2}{\alpha^2} - 1\right) + f + 1} \ . \tag{2.47}$$

We outline below that $z - y > 1$, making abs$(\cos\omega) > 1$ or ω purely imaginary. The pole $\omega = i\cosh^{-1}(y+z)$ lies on the imaginary axis while that for $\omega = i\cosh^{-1}(y-z)$ lie on parallel lines shifted by $\pm\pi$. The following three properties are important for further calculations:

- $y > 0$ since $\gamma > \alpha$.
- Let $\xi = \frac{\gamma^2}{\alpha^2} - 1$, where $\xi > 0$.
- A little algebra shows that $z^2 - (y+1)^2 = \xi[(g-1)^2 + f] + f > 0$ which in turn implies the relation $z - y > 1$.

The choice of contour can be made similar to that in Figure 2.1, allowing only the pole at $\omega = i\cosh^{-1}(y+z)$ to contribute to the energy density. Setting $m = 0$, it is easy to verify that this approach also yields precisely the result in Eq.(2.21) by selecting the contour as in

the upper half plane of Figure 2.1. Its analog for $m \neq 0$ by can be obtained by computing the residue at the pole defined by Eq.(2.45). The full expression is quite complicated, we only indicate how the results in the continuum limit arise. The pole positions can be computed to be

$$\cos\omega = \alpha_1 = 1 + \frac{a^2(\vec{p}^2 + m^2)}{2} \ , \tag{2.48}$$

and denoting by $m' = m(M-2)/M$

$$\cos\omega = \alpha_2 = -\left(1 + \frac{a^2(\vec{p}^2 + m'^2)}{2}\right) \ , \tag{2.49}$$

where $\vec{p}^2 = p_1^2 + p_2^2 + p_3^2$. The pole at α_1 has, at order a, the residue

$$\text{Res } F_1(\alpha_1) = \pm\frac{a\sqrt{\vec{p}^2 + m^2}}{2}$$

All the other poles, including the poles at α_2, and the branch cuts do not contribute to the contour integrals, as seen in Figure 2.1. Therefore the energy density in the continuum comes out to be the same as in Eq.(2.23) but with $E = \sqrt{m^2 + p_1^2 + p_2^2 + p_3^2}$

2.5 Summary

Investigating the thermodynamics of QCD on lattice with fermions which possess both the chiral symmetry and the flavour symmetry relevant to our world has important consequences for both the experimental aspects of the heavy ion collisions and the theoretical aspects of the $\mu_B - T$ phase diagram. Staggered fermions used in the bulk of the work so far are not adequate to resolve some of these issues. Overlap fermions, while computationally more expensive, may prove better in such studies in near future.

We have presented analytical and numerical results on the thermodynamics of free Overlap fermions in 4-D both for zero and numerical results for nonzero (baryonic) chemical potential by varying the irrelevant parameter M. From the energy density computed on the lattice in these cases, we showed that the expected continuum limit is reached. Considering the recently proposed Overlap action [33] for nonzero μ, we demonstrated numerically that the μ^2-divergence in the continuum limit is avoided for the choice $\exp(\pm\hat{\mu})$. However, the chiral invariance of the action is lost for nonzero μ on a finite lattice.

While the sign function in the free Overlap Dirac operator remains a constant in computations for $\mu = 0$, we pointed out that it becomes undefined on lattices with odd number of temporal sites for $\mu \geq \mu_c$, where the value of μ_c depends on M. Our numerical computations were restricted to smaller μ-values. The numerical results were mildly dependent on the aspect ratio of the spatial and temporal direction but changed significantly as a function of the irrelevant parameter M of the Overlap Dirac operator. For the choice of $1.5 \leq M \leq 1.6$, both the energy density and the quark number susceptibility computed for $\mu = 0$ exhibited the smallest deviations from the ideal gas limit, as seen in Figure 2.3. As seen from Figures 2.2, 2.4 and 2.5, lattice results approximate the continuum well for lattices with 12 or more temporal sites, with typically a factor ≈ 1.8 larger results for smaller lattices with 6-8 temporal sites. We expect that M being an irrelevant parameter will not be affected much due to quantum corrections in the interacting theory and it would be interesting to check whether the optimum M-range is still the same in the presence of gauge fields.

Chapter 3

Thermodynamics of ideal Domain Wall fermions

3.1 Introduction

Kaplan [19] proposed a way to define 4-D fermions with exact chiral symmetry on a five-dimensional (5-D) lattice with a mass term M in the form a step function(domain wall) and with an infinite extent along the fifth dimension. The massless 4-D fermions are obtained localized on the wall, and are hence known as the Domain wall fermions. On a finite lattice needed for numerical simulations, however, fermions of both chiralities exist with an exponentially small overlap between the respective chiral states [23] for sufficiently smooth gauge field configurations. Currently, the most popularly used fermions in QCD simulations at finite temperatures/densities are the staggered fermions which have only a remnant chiral symmetry on the lattice. Moreover, they explicitly break spin and flavour symmetries. The full chiral symmetry for these fermions is recovered only in the continuum limit, i.e., in the limit of vanishing lattice spacing. In spite of the (exponentially small in N_5, the number of sites in the fifth dimension) chiral violation on the lattice, the Domain wall fermions are more promising than the staggered fermions due to their exact flavour and spin symmetry on the lattice. Moreover for the Domain wall fermions, the chiral and continuum limits are clearly disentangled, with the chiral symmetry depending on the suitable tuning of N_5. On the other hand these are more expensive to simulate as the computational cost increases

linearly with N_5. One has to optimize N_5 and M for full QCD simulations. In order to gain insights on ways to minimize the lattice cut-off effects, we study various thermodynamic quantities of free Domain wall fermions as a function of M and N_5 with an aim to optimize the irrelevant lattice parameters for faster convergence to their continuum values. We find that by adjusting the domain wall height M in the range $1.45 - 1.55$ rather than the frequently used choice of $M = 1.0$, a faster convergence to the continuum results for both finite and infinite values of N_5 is achieved. However, the cut-off effects are seen to be quite large on small lattices with temporal extent of 6-8 where most of the current QCD simulations are being done. We therefore examine modifications of the domain wall, as well as the Overlap kernel to minimize such corrections for small lattice sizes.

The chapter is divided into four sections. In section 3.2, we compute the energy density of free domain wall quarks on the lattice analytically and verify that it yields the correct continuum limit. In section 3.3, the same quantity is computed numerically and the various lattice parameters for which the convergence to the continuum is fastest are estimated. In section 3.4, we repeat the calculations of energy density in the presence of chemical potential and susceptibility and confirm that this optimum M-range does not shift significantly. In section 3.5, we propose a method of reducing the lattice cut-off corrections to thermodynamic quantities on small lattice sizes, computed using both the chiral fermions, namely the domain wall at infinite N_5 and the Overlap fermions. This helps in faster convergence to the continuum results even for $M = 1.0$ which is significantly different from the optimal M-range.

3.2 Energy Density of Domain wall fermions

The Domain wall fermions [19] in the continuum are defined on a 5-D space-time with the mass term in the fifth dimension in form of a domain wall $\phi(M) = M \tanh(s)$, s being the coordinate in the fifth dimension. This helps in localizing a fermion of definite chirality on the domain wall. The Domain wall operator in the continuum is given as,

$$D_{DW} = \sum_{\mu=1}^{4} \gamma_\mu \partial_\mu + \gamma_5 \partial_5 + \phi(M). \tag{3.1}$$

The massless fermion modes in 4-D are obtained when the following conditions are simultaneously satisfied.

$$\sum_{\mu=1}^{4} \gamma_\mu \partial_\mu \psi = 0 \quad , \quad (\gamma_5 \partial_5 + \phi(M))\psi = 0.$$

It was shown that only one normalizable solution exist, bounded to the wall at $s = 0$ where the $\phi(M)$ changes abruptly. The corresponding analog of the domain wall term on the lattice is of the form

$$\phi(M) = M\Theta(s) \tag{3.2}$$

On the lattice we do not get a single massless mode by discretizing Eq. (3.1). This is because the lattice regulator is anomaly free, so massless fermions of both handedness exist on the lattice. A Wilson term is needed to spatially separate the left and the right handed fermions in the 5th dimension by localizing them on the domain wall and the anti-domain wall respectively which are separated from each other by the lattice extent in the fifth dimension N_5. To obtain thermodynamical quantities of free fermions with exact chiral symmetry on the lattice in 4-D, we need to divide out contribution of the heavy fermion modes which exist in the fifth dimension. This is done by subtracting a pseudo-fermion action [44] from the standard 5-D action. Following Shamir [44], the Domain wall fermion action on a $N^3 \times N_T \times N_5$ anisotropic lattice with lattice spacings of a, a_4 and a_5 in the three spatial, the temporal and the fifth dimension respectively can be written as,

$$S_{DW} = -\sum_{s,s'=1}^{N_5} \sum_{x,x'} \bar{\psi}(x,s) D_{DW}(x,s;x',s',\hat{\mu},\hat{m}_q)\psi(x',s') \tag{3.3}$$

$$= \sum_{s,s'=1}^{N_5} \sum_{x,x'} \bar{\psi}(x,s) \left[-\left(\frac{a_5}{a} D_W(x,x',\hat{\mu}) + 1\right) \delta_{s,s'} + (P_- \delta_{s',s+1} + P_+ \delta_{s',s-1})\, \delta_{x,x'} \right] \psi(x',s'),$$

with the boundary conditions

$$P_- \psi_{N_5+1} = -\hat{m_q} P_- \psi_1, \quad P_+ \psi_0 = -\hat{m_q} P_+ \psi_{N_5} \tag{3.4}$$

where $P_\pm = \frac{1 \pm \gamma_5}{2}$ are the chiral projectors and $\hat{m_q}$ is the bare quark mass in lattice units. D_W is the Wilson-Dirac operator defined on a 4-D lattice. The volume of the system is $V = N^3 a^3$ and $T = 1/(N_T a_4)$ is its temperature. The chemical potential $\mu a_4 = \hat{\mu}$ is usually introduced as a Lagrange multiplier corresponding to the conserved number density in the expression

for the Lagrangian. For the Domain wall fermions we do not have a good prescription for obtaining the conserved number density. Following Bloch and Wettig [34], we incorporate the chemical potential in D_W but in a general form using the functions K and L [31] defined below. These multiply the $1 \pm \gamma_4$ factors in the Wilson-Dirac operator leading to,

$$D_W(x,x',\hat{\mu}) = -\sum_{j=1}^{3}\left(U_j^\dagger(x')\frac{1+\gamma_j}{2}\delta_{x,x'+\hat{j}} + U_j(x)\frac{1-\gamma_j}{2}\delta_{x,x'-\hat{j}}\right)$$
$$+\left(3+\frac{a}{a_4}-M\right)\delta_{x,x'} - \frac{a}{a_4}\left(K(\hat{\mu})U_4^\dagger(x')\frac{1+\gamma_4}{2}\delta_{x,x'+\hat{4}} + L(\hat{\mu})U_4(x)\frac{1-\gamma_4}{2}\delta_{x,x'-\hat{4}}\right).$$

In this chapter we consider the non-interacting fermions, i.e., $U_\mu(x) = 1$. Introducing R and θ by

$$\frac{K(\hat{\mu})+L(\hat{\mu})}{2} = R\cosh\theta \quad \frac{K(\hat{\mu})-L(\hat{\mu})}{2} = R\sinh\theta\ , \tag{3.5}$$

the free Wilson-Dirac operator in Eq.(3.5) can be diagonalized in the momentum space in terms of the functions,

$$\begin{aligned} h_j &= \sin ap_j\ ,\ h_4 = -\frac{a}{a_4}R\sin(a_4p_4 - i\theta)\ , \\ h_5 &= M - \sum_{j=1}^{3}(1-\cos ap_j) - \frac{a}{a_4}(1 - R\cos(a_4p_4 - i\theta)). \end{aligned} \tag{3.6}$$

such that

$$D_W(\vec{p},p_4) = -\sum_{i=1}^{4} i\gamma_i h_i - h_5. \tag{3.7}$$

To study thermodynamics of fermions one has to necessarily take anti-periodic boundary conditions along the temporal direction. Assuming periodic boundary conditions along the spatial directions we obtain

$$\begin{aligned} ap_j &= \frac{2n_j\pi}{N}, n_j = 0,..,(N-1), j = 1,2,3 \text{ and} \\ ap_4 &= \omega_n = \frac{(2n+1)\pi}{N_T}, n = 0,..,(N_T-1) \end{aligned} \tag{3.8}$$

It is to be noted that M, the height of the domain wall on the lattice, is bound to $0 < M < 2$ to simulate one flavour quark on the lattice. To suppress the heavy mode contributions and recover a single chiral fermion, pseudo-fermion fields are introduced which have the same action but with $\hat{m_q} = 1$ i.e with anti-periodic boundary condition in the fifth dimension [23].

The fifth dimensional degrees of freedom can be integrated out to yield an effective Domain wall operator [18, 45]

$$\frac{D_{DW}(\hat{m}_q)}{D_{DW}(1)} = 1 + \hat{m}_q + (1 - \hat{m}_q)\gamma_5 \frac{1 - T^{N_5}}{1 + T^{N_5}}, \tag{3.9}$$

where the transfer matrix T is

$$T = (1 + \frac{a_5}{a}\gamma_5 D_W P_+)^{-1}(1 - \frac{a_5}{a}\gamma_5 D_W P_-). \tag{3.10}$$

Since T can be shown to be Hermitian for $\hat{\mu} = 0$, and therefore has real eigenvalues, T^{N_5} has only positive eigenvalues for even N_5. Introducing [45] a notation $|T|$, the function $\frac{1-T^{N_5}}{1+T^{N_5}}$ in the Domain wall operator can be expressed in the form of a tanh function as in Eq.(3.11).

$$\frac{D_{DW}(\hat{m}_q)}{D_{DW}(1)} = 1 + \hat{m}_q - (1 - \hat{m}_q)\gamma_5 \tanh(\frac{N_5}{2} \ln |T|). \tag{3.11}$$

The above derivation of the effective domain wall operator assumes that $1 + T^{N_5}$ does not have any zero eigenvalues. For if it does, then the contribution of the heavy modes is zero. If λ be an eigenvalue of T, then this assumption requires that

$$\ln \lambda \neq i\frac{(2n+1)\pi}{N_5} \ . \tag{3.12}$$

This is clearly true for $\hat{\mu} = 0$ for even the interacting fermions where T is Hermitian and thus any λ is real. However, once chemical potential is introduced in the Wilson-Dirac operator, as above, D_W and T are not Hermitian any longer for the free fermions themselves, leaving open the possibility that this condition will not be met.

It is easy to see that three distinct limits are of interest in which we should compute the various thermodynamic quantities for massless domain wall operator. These are as follows:

1. $N_5 \to \infty, a_5 \neq 0$, where one obtains exact chiral fermions for $\hat{m_q} = 0$,

2. $N_5 \to \infty, a_5 \to 0$ such that the L_5 is finite, where $L_5 = N_5 a_5$, leading to an approximate form for the Overlap fermions [34, 17], and

3. $N_5 =$ finite, $a_5 =$ finite, corresponding to the form of Domain wall operator directly relevant for practical simulations on the lattice.

3.2.1 $N_5 \to \infty, a_5 \neq 0$

In this limit, the tanh function in Eq.(3.11) becomes sign function and the resultant effective Domain wall operator is given as

$$D_{DW}^{eff} = 1 + \hat{m}_q - (1 - \hat{m}_q)\gamma_5 sgn(\ln|T|) \tag{3.13}$$

The operator T has an explicit a_5 dependence as shown in Eq.(3.10). For $\hat{m}_q = 0$, this form of the Domain wall operator satisfies the Ginsparg-Wilson relation [21]. Indeed, it is just like the Overlap operator, but with a different argument of the sign function. The operator T is not Hermitian in presence of $\hat{\mu}$ and hence the sign function has to be defined carefully. We follow the definition as in Bloch and Wettig [34]. The finite size corrections to various thermodynamic quantities computed with this lattice operator are expected to be different from the Overlap case. For this type of Ginsparg Wilson fermion too the introduction of chemical potential necessarily leads to chiral symmetry breaking [46] on the lattice because the action in presence of $\hat{\mu}$ is not invariant under the chiral transformations [22] on lattice. Like in the case of the Overlap fermions, chiral symmetry is exactly realized for these wall fermions only in the absence of chemical potential.

The energy density ϵ of the Domain wall fermions in the chiral limit is evaluated from the partial derivative with respect to inverse temperature, of the partition function, $Z = \mathrm{Det}(D_{DW}^{eff})$. This is equivalent to taking a partial derivative with respect to a_4 on a lattice of fixed size N_T. The energy density,

$$\epsilon = -\frac{1}{N^3 a^3 N_T}\left(\frac{\partial}{\partial a_4}\ln\, Z\right)_{a,\hat{\mu}}. \tag{3.14}$$

can be evaluated analytically in terms of the quantities q, s, t and $s^{'}, t^{'}$ defined below in

Eq.(3.15), where the dash denotes the a_4-derivative of the respective quantities. Defining

$$\begin{aligned} h^2 &= \sum_{i=1}^{4} h_i^2 \ , \ s^2 = h^2 + h_5^2 \ , \\ t &= s\sqrt{s^2 - 4h_5 + 4} \ , \quad q = s^2 - 2h_5 + 2 \ , \\ \alpha &= \frac{\partial h_4}{\partial a_4} = \frac{a}{a_4^2} R\sin(a_4 p_4 - i\theta) \ , \\ \gamma &= \frac{\partial h_5}{\partial a_4} = \frac{a}{a_4^2}(1 - R\cos(a_4 p_4 - i\theta)) \\ s^{'} &= \frac{h_4\alpha + h_5\gamma}{s} \ , \ t^{'} = \frac{s^{'}t}{s} + \frac{s^2(ss^{'} - 2\gamma)}{t} \end{aligned} \tag{3.15}$$

one has,

$$\epsilon a^4 = \frac{1}{N^3 N_T} \quad \sum_{p_j,n} \Bigg(- \frac{4h_5\gamma + 4ss^{'}(1+s^2) + 2ss^{'}t + s^2t^{'} - 4\gamma s^2 - 8h_5 ss^{'} - 2\gamma t - 2h_5 t^{'}}{2h_5^2 + 2s^2 + s^4 + s^2 t - 4h_5 s^2 - 2h_5 t} + \frac{2t^{'}}{t} \Bigg) \equiv \frac{1}{N^3 N_T} \sum_{p_j,n} F(R, \omega_n, \vec{p}) \ . \tag{3.16}$$

In all the equations above and in the following subsections, a_5 is set to unity in the units of a. Furthermore, setting $a_4 = a$ after evaluating the a_4-derivatives, the summation over the discrete Matsubara frequencies can be evaluated analytically by the standard contour integral technique or numerically by explicitly summing over them and the momenta p_j. For the former, we need to determine the singularities of the summand F in Eq.(3.16). We outline below briefly the results one obtains for the zero and finite temperature cases.

$T = 0$, $\mu \neq 0$: In order to obtain a general condition for eliminating the spurious $\hat{\mu}^2$-divergences, we first calculate the energy density at zero temperature in the limit $N_T \to \infty$ at finite a. The frequency sum $1/N_T \sum_n$ in Eq.(3.16) gets replaced by the integral $\frac{1}{2\pi}\int_{-\pi}^{\pi} d\omega$ in this limit. Subtracting the vacuum contribution corresponding to $\hat{\mu} = 0$, i.e. $R = 1, \theta = 0$, the energy density at zero temperature is given by

$$\epsilon a^4 = \frac{1}{\pi N^3} \sum_{p_j} \left[\int_{-\pi}^{\pi} F(R, \omega - i\theta) d\omega - \int_{-\pi}^{\pi} F(\omega) d\omega \right] \ . \tag{3.17}$$

For brevity, we suppress from now on the explicit p_j-dependence of the function F although we retain the overall sign to remind of it. Choosing the contour shown in Figure 3.1, the

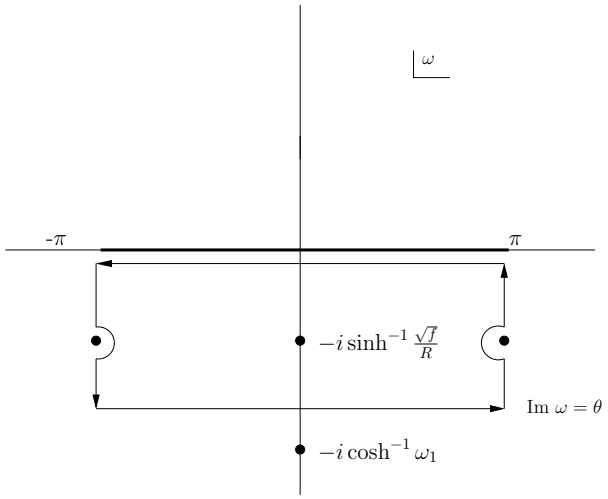

Figure 3.1: Contour chosen for evaluating the energy density for nonzero value of chemical potential at zero temperature. The thick line indicates the Matsubara frequencies while the filled circles denote the poles of $F(R,\omega)$.

expression above can be evaluated in the complex ω-plane as

$$\begin{aligned}\epsilon a^4 &= \frac{1}{\pi N^3}\sum_{p_j}\left[2\pi i\sum_i \text{Res } F(R,\omega_i) - \int_{\pi-i\theta}^{\pi} F(R,\omega)d\omega - \int_{\pi}^{-\pi} F(R,\omega)d\omega\right. \\ &- \left.\int_{-\pi}^{-\pi-i\theta} F(R,\omega)d\omega - \int_{-\pi}^{\pi} F(\omega)d\omega\right] . \qquad (3.18)\end{aligned}$$

The second and fourth terms cancel since F satisfies $F(R,\pi+i\eta) = F(R,-\pi+i\eta)$. Hence, we obtain

$$\epsilon a^4 = \frac{1}{\pi N^3}\sum_{p_j}\left[2\pi R_1\Theta\left(\frac{K(\hat{\mu})-L(\hat{\mu})}{2}-\sqrt{f}\right) + \int_{-\pi}^{\pi} F(R,\omega)d\omega - \int_{-\pi}^{\pi} F(\omega)d\omega\right] , \quad (3.19)$$

where -iR_1 is the residue of the function $F(R,\omega)$ at the pole $-i\ \sinh^{-1}(\sqrt{f}/R)$. It is clear from Eq.(3.19) that the condition $R=1$ cancels the integrals, yielding the canonical Fermi surface form of the energy density. For $R \neq 1$, there will in general be violations of the Fermi surface on the lattice. Moreover, in the continuum limit $a \to 0$, one will in general have the μ^2-divergences for $R \neq 1$ in the energy density. The condition to obtain the correct continuum values of $\epsilon = \mu^4/4\pi^2$ turns out to be $K(\hat{\mu}) - L(\hat{\mu}) = 2\hat{\mu} + O(\hat{\mu}^2)$. That this

effective Domain wall fermion satisfy the same condition as the Overlap [46] suggest that such condition may be generically true for Ginsparg-Wilson fermions. Also that one obtains identical condition in the staggered case [31] suggests that the behavior near the continuum limit dictates this condition. Note also that the form used by Bloch and Wettig [34], namely, $\exp(\pm\hat{\mu})$ for K, L, also satisfies the condition $R = K \cdot L = 1$.

$T \neq 0$, $\hat{\mu} = 0$: In order to choose the appropriate contour in the $T \neq 0$ case, note that the function $F(R = 1, \omega, \vec{p})$ at $\hat{\mu} = 0$ has poles at $\cos^{-1}(\sqrt{d - g^2}) = \pm i \sinh^{-1}\sqrt{f}$. These turn out to contain the physical poles in the continuum limit. As in the Overlap case[46], there are poles at $\cos^{-1}(-\sqrt{d - g^2}) = \pm\pi \pm i \sinh^{-1}\sqrt{f}$ and branch cuts at $\pm\pi \pm i \cosh^{-1}\frac{d}{2g}(\pm i \cosh^{-1}\frac{d}{2g})$ for $\frac{d}{2g} > 0 (< 0)$. However in this case, there are additional(unphysical) poles and cuts at at $\pm i \cosh^{-1}\omega_1$ where $\omega_1 = (d + 4 - 4g)/2(g - 2)$. The definitions of the quantities d,f,g are the same as defined in the previous chapter. Unlike in the Overlap case, however, the contour is not closed just above and below the branch cuts at $\mp\pi \pm i \cosh^{-1}\frac{d}{2g}$ for $\frac{d}{2g} > 0$, but over and below the additional poles at $\mp i \cosh^{-1}\omega_1$. This pole moves to infinity in the $a_5 \to 0$ limit or the Overlap limit and hence do not contribute to the Overlap energy density on the lattice. The contour chosen for evaluating the frequency sum shown in Figure 3.2, is thus slightly different from that chosen for Overlap fermions. The residue of the pole enclosed by the contour for F comes out to be,

$$4\frac{\sqrt{f}}{\sqrt{1+f}} + \frac{\sqrt{1+f}-1}{\sqrt{f(1+f)}}G(M). \tag{3.20}$$

with the first term yielding the continuum value of the energy density in the limit of vanishing lattice spacing a. The energy density expression comes after performing the contour integral comes out to be,

$$\epsilon a^4 = \frac{1}{N^3}\sum_{p_j}\left[4\frac{\sqrt{f}}{\sqrt{1+f}} + \frac{\sqrt{1+f}-1}{\sqrt{f(1+f)}}G(M)\right] \times \frac{1}{e^{N_T \sinh^{-1}\sqrt{f}}+1} + \epsilon_3 + \epsilon_4 \ ,$$

which again turns out to be similar to the Overlap case. Due to a different functional form of F and a different choice of contour, the corresponding lattice correction terms ϵ_3, ϵ_4 which are the line integrals of F along lines 3,4 in the Figure 3.2, are different, leading to different finite size corrections. In the continuum limit the unphysical poles and branch cuts are pushed to infinity and the values of ϵ_3, ϵ_4 vanish, leaving only the contribution of the

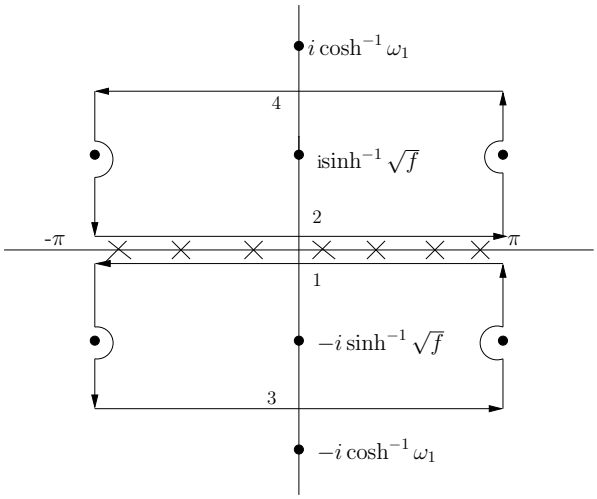

Figure 3.2: Contour chosen for evaluating the energy density at finite temperature. The crosses indicate the Matsubara frequencies while the filled circles denote the poles of $F(\vec{p},\omega)$.

physical poles to the energy density: In the square bracket, only first term gives the usual continuum expression with the other term vanishing as $a \to 0$. The same treatment goes through in presence of $\hat{\mu}$ only the contour has to be shifted along the imaginary ω plane by an amount dependent on $\hat{\mu}$ with the position of the poles in the complex ω-plane remaining unchanged.

3.2.2 $N_5 \to \infty$, $a_5 \to 0$, $L_5 = N_5 a_5 =$ **finite**

In the case when the lattice spacing in the fifth direction $a_5 \to 0$ and the number of sites $N_5 \to \infty$ such that $L_5 = N_5 a_5$ is finite, the effective Domain wall operator reduces to

$$D_{DW} = (1 + \hat{m_q}) + (1 - \hat{m_q})\gamma^5 \tanh(\frac{L_5}{2}\gamma^5 D_W) \tag{3.21}$$

Starting from the above expression we recover the Overlap operator when $L_5 \to \infty$. With this effective Domain wall operator, the energy density can be evaluated [47] as,

$$\epsilon a^4 = \sum_{p_j,n} \frac{4\sinh[\frac{sL_5}{2}]((-h_4h_5\alpha + h^2\gamma)\cosh[\frac{sL_5}{2}] + (h_4h_5\alpha + (h_5^2+s^2)\gamma + 2h_5s^2t)}{sN^3N_T(h^2+(s^2+h_5^2)\cosh[2sL_5]} \\ \frac{\times\cosh(\frac{3sL_5}{2}) - 2s\sinh[\frac{sL_5}{2}](h_5^2t + h_5\gamma + (h^2t + h_4\alpha + 2h_5(h_5t+\gamma))\cosh[sL_5]))}{-2h_5s\sinh[2sL_5])} \,, \tag{3.22}$$

where α and γ are the same as defined previously and t is now defined as,

$$t = \frac{(-\sin^2 ap_4 + h_5\gamma)(-\tanh\frac{L_5s}{2} + \frac{L_5s}{2}\mathrm{sech}^2\frac{L_5s}{2})}{s^2\tanh\frac{L_5s}{2}} \,. \tag{3.23}$$

It was checked that the Overlap energy density is obtained back when $L_5 \to \infty$. We use the expression above for our numerical work presented in section III.

3.2.3 Finite N_5 and a_5

While performing Monte Carlo simulations with Domain wall fermions one needs to work on lattices with finite number of sites in the fifth dimension. For finite N_5, the chiral symmetry is broken and it is important to ascertain the dependence of the correction terms with N_5. Evaluating the matrix $\tanh(N_5/2\ln|T|)$ in Eq.(3.11) various thermodynamic quantities of free Domain wall fermions on the lattice can be evaluated. The energy density in the massless limit then is

$$\epsilon a^4 = \frac{2}{N^3N_T}\sum_{p_j,n}\left(\frac{t^{'}}{t} + \frac{2^{N_5}u^{'}}{2^{2N_5+1}+2^{N_5}u} - \frac{tu^{'}+ut^{'}-xq^{'}-(q-2)x^{'}}{tu-(q-2)x}\right) \tag{3.24}$$

where the quantities u, t and x are functions of h's defined in Eqs.(3.6,3.15) defined as,

$$u = \left(\frac{t-q}{h_5-1}\right)^{N_5} + \left(\frac{t+q}{1-h_5}\right)^{N_5} \,, \quad x = \left(\frac{t-q}{h_5-1}\right)^{N_5} - \left(\frac{t+q}{1-h_5}\right)^{N_5} \,. \tag{3.25}$$

The partial derivatives of the above variables are represented as the same variables with a dash, and are functions of h's, α and γ.

$$
\begin{aligned}
q^{'} &= 2ss^{'} - 2\gamma \ , \\
\frac{u^{'}}{N_5} &= \left(\frac{t-q}{h_5-1}\right)^{N_5-1}\left[\frac{t^{'}-q^{'}}{h_5-1} - \frac{\gamma(t-q)}{(h_5-1)^2}\right] + \left(\frac{t+q}{1-h_5}\right)^{N_5-1}\left[\frac{t^{'}+q^{'}}{1-h_5} + \frac{\gamma(t+q)}{(1-h_5)^2}\right] \ , \\
\frac{x^{'}}{N_5} &= \left(\frac{t-q}{h_5-1}\right)^{N_5-1}\left[\frac{t^{'}-q^{'}}{h_5-1} - \frac{\gamma(t-q)}{(h_5-1)^2}\right] - \left(\frac{t+q}{1-h_5}\right)^{N_5-1}\left[\frac{t^{'}+q^{'}}{1-h_5} + \frac{\gamma(t+q)}{(1-h_5)^2}\right] \ .
\end{aligned}
\tag{3.26}
$$

Again, we shall use these expressions for obtaining the numerical results presented below where we also show the results for quark number susceptibility. The same set of formulae as in Eq.(3.26) remain valid for the calculation of susceptibility where α and γ are replaced by the derivatives α_μ and γ_μ with respect to $\hat{\mu}$, defined as,

$$
\alpha_\mu = \frac{\partial h_4}{\partial \hat{\mu}} = \frac{ia}{a_4}\cos(a_4 p_4 - i\hat{\mu}) \ , \ \gamma_\mu = \frac{\partial h_5}{\partial \hat{\mu}} = -ih_4 (\text{for number density}) \tag{3.27}
$$

3.3 Numerical results at zero density

3.3.1 $N_5 = \infty, a_5 = 1$

The goal of our numerical study is to find the optimum range of M for which the finite lattice spacing corrections are minimum and compare it with that for the Dirac-Neuberger case [46]. We do this in the chiral limit and set $\hat{m}_q = 0$. The lattice energy density given by Eq.(3.16) was computed numerically by summing over the momenta along the spatial and temporal directions. The zero temperature part of the energy density was determined in the limit $N_T \to \infty$ on a lattice with a very large spatial extent N by numerically evaluating the $ap_4 = \omega$ integral. Holding the physical volume constant in units of T by keeping $V^{1/3}T = N/N_T \equiv \zeta$ fixed, we define the continuum limit by $N_T \to \infty$. The thermodynamic limit is then achieved in the limit of large ζ. We first determine the acceptable range of ζ by looking for ζ-independence. The ϵ obtained by subtracting the zero temperature part from the lattice energy density expression was normalized by its continuum value ϵ_{SB}. Figure 3.3 displays the ratio ϵ/ϵ_{SB} as a function of N_T for different values of ζ at a fixed $M = 1.50$. One notices that for $\zeta \geq 3$ the energy density plots lie on top of each other, suggesting the thermodynamic limit to have reached by $\zeta = 4 - 5$. In order to highlight the deviations in the continuum

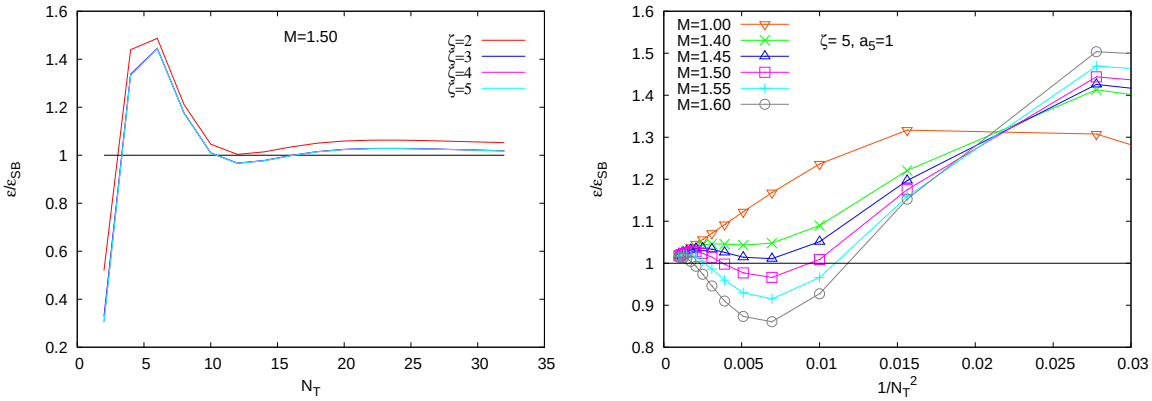

Figure 3.3: The ζ dependence of the energy density of Domain wall fermions for $M = 1.50$, $a_5 = 1$ and in the limit $N_5 \to \infty$ and the variation of energy density of Domain wall fermions with M in the limit $N_5 \to \infty$ and $a_5 = 1$.

limit, the same ratio is exhibited for different M values for $\zeta = 4$ in Figure 3.3 as a function of $1/N_T^2$ for a range of N_T likely to be used in simulations. We choose to define the optimum range of M as the values of M for which the thermodynamic quantities are within 3% of the continuum values for the smallest possible N_T. One sees from the Figure 3.3 that the order $1/N_T^2$ corrections are minimum for M between 1.45-1.50 and $N_T \geq 12$. The correction terms for $M = 1$ are linear in $1/N_T^2$ for $N_T \geq 10$ and are about 20% of the continuum value even for $N_T = 12$. This is similar to that reported earlier for the Overlap fermions [46]. Though the continuum extrapolation with $M = 1$ is easier due to the linear functional form, it is computationally expensive, needing simulations at more values of N_T, each greater than 10. Thus M =1.45-1.50 seems to be an optimum range for lattice simulation of the energy density of domain wall fermions. We have found that odd N_T will give similar results, for both optimum M and in the continuum limit. For small values of N_T however, there are perceptible oscillation in the values of ϵ/ϵ_{SB} for odd and even values making the continuum extrapolation difficult. We have also varied the lattice spacing along the fifth dimension a_5 to find out how the cut-off dependent terms change with it. The correction terms to the energy density for $a_5 = 0.5a$ at small lattice sizes $N_T \leq 10$ are indeed larger than that for $a_5 = a$ for the above mentioned optimum range but for $N_T > 12$ such terms are again within 2-3% of the Stefan Boltzmann value. The optimum M range for which the lattice artifacts

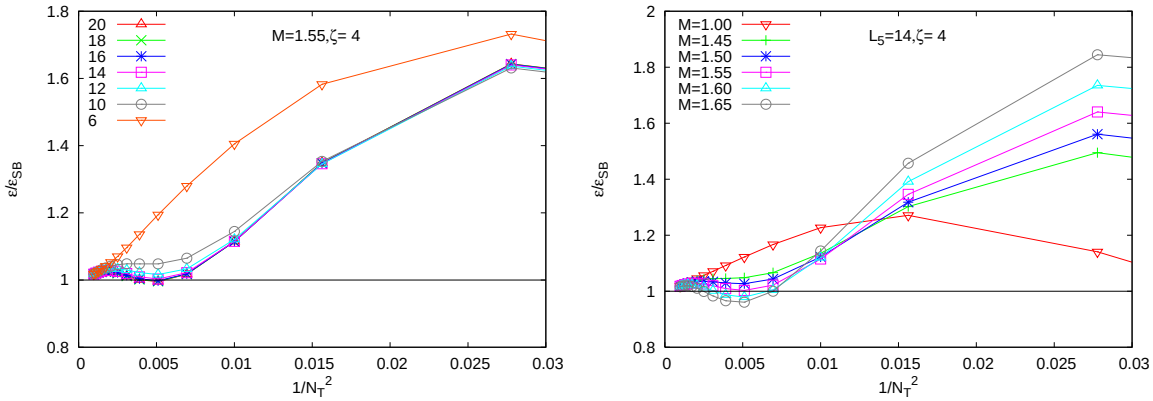

Figure 3.4: The variation of energy density on lattice with N_T for Domain wall fermions for different L_5, as shown by the respective labels, and $M = 1.55$ and the variation of energy density on lattice with $1/N_T^2$ for Domain wall fermions for $L_5 = 14$ and different M.

are minimum shifts to 1.50-1.60. Thus there is a marginal dependence on a_5 for $N_T \geq 10$. Reducing a_5 further does not increase the range much as we demonstrate in the plot for $a_5 \to 0$ in Figure 3.4.

3.3.2 $N_5 \to \infty$, $a_5 \to 0$, $L_5 =$ **finite**

Next we investigated the limit $N_5 \to \infty$, $a_5 \to 0$ such that $L_5 =$ finite in order to estimate numerically the value of L_5 for which we recover the Overlap energy density starting from Eq.(3.22). As can be observed from Figure 3.4, L_5-independent results are obtained for $L_5 \geq 14$ for $M = 1.55$. This was also the case for a range of M around this value. For $L_5 \leq 10$ the convergence towards the ϵ_{SB} value was seen to be very slow for all M and we find that the continuum value is not reached even for lattice size as large as $N_T = 32$. Figure 3.4 displays the results as a function of $1/N_T^2$ for $L_5 = 14$ and various values of M indicated on it. The deviations from the continuum for such L_5 are less than 3 % for the range of M between 1.50-1.60, in agreement with the Overlap results [46].

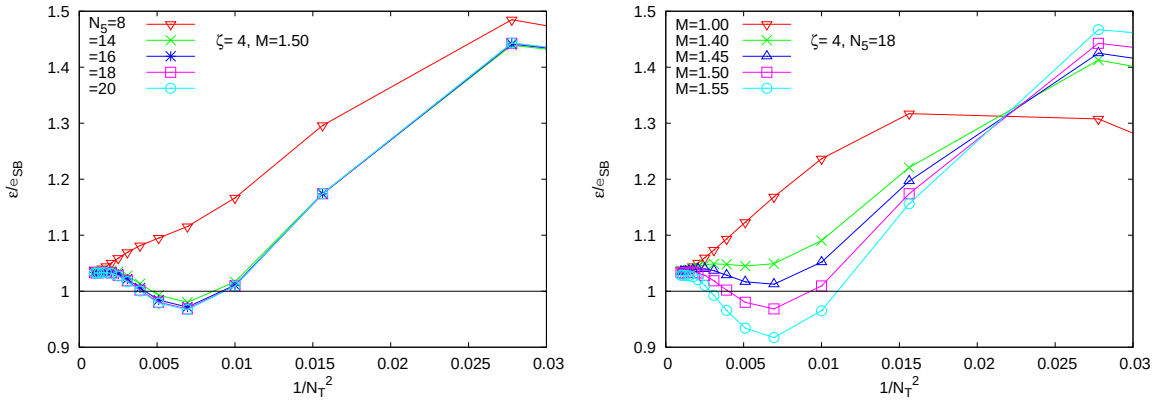

Figure 3.5: The variation of energy density on lattice with $1/N_T^2$ for domain wall fermions at a) different N_5 for $M = 1.50$ and b) $N_5 = 18$ for different M.

3.3.3 Finite N_5 and $a_5 = 1$

The case of finite N_5 with $a_5 = 1$ is clearly of most interest for practical simulations with dynamical fermions. Earlier numerical studies for free Domain wall fermions [48, 32] employed $M = 1.0$ and found somewhat slow convergence of various thermodynamic quantities towards their continuum values. We intend to check whether tuning the value of M results in a faster convergence. For that purpose we have computed the energy density expression for finite N_5 and $a_5 = a$ in Eq.(3.24) by summing over all the discrete momenta. We display those results for ϵ/ϵ_{SB} in Figure 3.5. The Figure 3.5a shows the results for a series of N_5 and a fixed $M = 1.5$. The results are seen to become N_5-independent by $N_5 = 18$, making it an optimum choice for obtaining continuum results on the lattice. The Figure 3.5b shows the M-variation for $N_5 = 18$. The general trend is clearly the same as above with M =1.45-1.50 emerging as the range for which the Stefan-Boltzmann limit is reached to within 3-4% for $N_T \geq 10$. Interestingly, $N_5 = 18$ seems to mimic the $N_5 \to \infty$ limit quantitatively rather well as can be seen by comparing the plots in Figure 3.5. Also the values of ϵ/ϵ_{SB} in the chiral limit, $N_5 \to \infty$ are within 1-2% of the $N_5 = 18$ values

3.4 Numerical results at finite density

It should be noted that in this case T is no longer Hermitian but as long as the condition given in the Eq.(3.12) is satisfied the effective operator in Eq.(3.16) is well defined. We shall restrict the range of $\hat{\mu}$ to ensure that it is so. We choose K and L to be $e^{\pm\hat{\mu}}$ respectively in our numerical computations as suggested in [34]. Our aim again is to find the optimum M for which the continuum results are obtained with least computational effort, and compare it with our the range obtained from the energy density above. We consider two observables here. One is the change in the energy density due to nonzero μ : $\Delta\epsilon(\mu,T) = \epsilon(\mu,T) - \epsilon(0,T)$. In the continuum limit this is

$$\frac{\Delta\epsilon(\mu,T)}{T^4} = \frac{\mu^4}{4\pi^2 T^4} + \frac{\mu^2}{2T^2}. \tag{3.28}$$

Another observable we studied was the quark number susceptibility at $\hat{\mu} = 0$. It is defined for any $\hat{\mu}$ by,

$$\chi = \frac{1}{N^3 a^2 N_T} \left(\frac{\partial^2 \ln\det D}{\partial \hat{\mu}^2} \right)_{a_4} , \tag{3.29}$$

and in the continuum is given by Eq.(2.39). We will focus on $\chi(0)$ here due to its importance in the applications to the heavy ion collisions. We estimated numerically $\Delta\epsilon(\mu,T)$ for $\mu/T = \hat{\mu}N_T$ fixed at 0.5. The Figures 3.6a and b display our results for this observable in the units of T^4 for $N_5 = \infty$ and 18 respectively for the M values indicated. The horizontal line in each case shows the expected result in the continuum limit from Eq.(3.28). From the Figures 3.6a and b it is evident that there are no μ^2/a^2 divergences on the lattice, as expected. The deviations from the continuum limit are due to the M dependent finite size effects. These correction terms are again seen to be small for the same optimum range of $1.45 \leq M \leq 1.50$ for both the cases, as obtained in the zero chemical potential case in section 3.2. The N_5 dependence of the quark number susceptibility at $\hat{\mu} = 0$ is plotted in Figure 3.7. It too exhibits a convergence to the infinite N_5 results for $N_5 \geq 16$, indicating that $N_5 = 18$ can again be used safely to approximate the infinite N_5. Figure 3.7 shows the M-dependence of the quark number susceptibility at $\hat{\mu} = 0$. The $N_5 = 18$ plots show small deviations from the Stefan-Boltzmann value of 1/3 for $1.45 \leq M \leq 1.55$ range and for $N_T \geq 10$. Recent computations of this susceptibility [49] for the interacting Domain wall fermions were performed with $M = 1.8$. Of course, one expects some shift in M due to additive

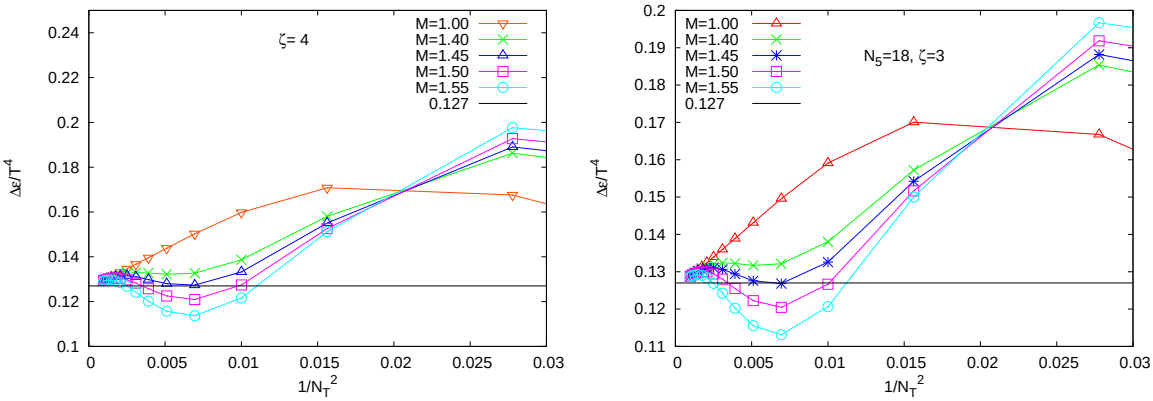

Figure 3.6: The energy density of Domain wall fermions in presence of $\hat{\mu}$ for different M and $\hat{\mu} = 0.5/N_T$ for a) infinite N_5 and for b) $N_5 = 18$.

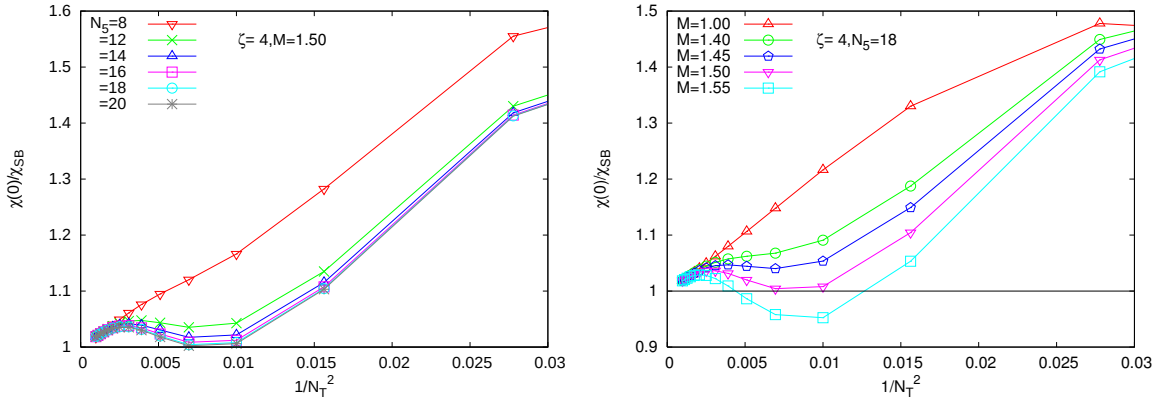

Figure 3.7: The quark number susceptibility as a function of $1/N_T^2$ for N_5 values as indicated for $M = 1.5$ and $\zeta = 4$ and the quark number susceptibility as a function of $1/N_T^2$ for M values as indicated for $\zeta = 4$ and $N_5 = 18$.

renormalization in presence of gauge interactions. The change should however be small for large enough temperature and small gauge field coupling constant where one expects those computations to approach the free quark gas results. In all our plots we find that for the optimum M range, the deviations from the ideal gas results at smaller N_T =4-8 are quite significant but with a relative mild M-dependence for $M > 1.4$. Thus a slightly larger value of M than the optimum range we found may not change the finite size effects drastically for small N_T. What one does need to be careful about though is the extrapolation to the continuum limit. For the optimal range of M and $N_T \geq 10$, the smallness of corrections compared to other errors in the computations may make it a less important issue.

3.5 Improvement of the chiral fermion kernels

In the previous sections we observed that the fermions with exact chiral symmetry on the lattice have large $1/N_T^2$ corrections for small N_T. While we found that the continuum limit for various thermodynamic quantities can be approached faster by choosing the irrelevant parameter M in the range 1.45-1.55, the correction terms for N_T =4-6 are about 50% of the Stefan-Boltzmann result for Domain wall fermions (Figure 3.5) and about the same magnitude as the continuum values for Overlap fermions [46] for such a choice of M too. Here we describe our attempts to improve the convergence to the continuum results for small N_T and even for $M = 1.0$. Having the option of the choice of $M = 1.0$ may be useful since it has been noted previously [23, 50] that the residual mass for such a choice of M is zero for a range of N_5 at the tree level.

3.5.1 Domain wall kernel

The Domain wall operator given in Eq.(3.11) is a matrix-function of the Wilson-Dirac operator as in Eq.(3.5). It is clear that its improvement may lead to a better Domain wall operator, or indeed even a better Overlap operator, one is looking for. Inspired by the attempts to improve the staggered fermions in the so-called Naik-action [51], we add three-link

terms to the D_W as below.

$$
\begin{aligned}
D_W(x,x',\hat{\mu}) = & -\sum_{j=1}^{3}\left(U_j^{\dagger}(x')\frac{1+c_1\gamma_j}{2}\delta_{x,x'+\hat{j}} + U_j(x)\frac{1-c_1\gamma_j}{2}\delta_{x,x'-\hat{j}}\right) \\
- & \frac{a}{a_4}\left(U_4^{\dagger}(x')\frac{1+c_1\gamma_4}{2}\delta_{x,x'+\hat{4}} + U_4(x)\frac{1-c_1\gamma_4}{2}\delta_{x,x'-\hat{4}}\right) + \left(3+\frac{a}{a_4}-M\right)\delta_{x,x'} \\
- & \sum_{j=1}^{3}\frac{c_3\gamma_j}{6}\left(U_j^{\dagger}(x')\delta_{x,x'+3\hat{j}} - U_j(x)\delta_{x,x'-3\hat{j}}\right) - \frac{a}{a_4}\frac{c_3\gamma_4}{6}\left(U_4^{\dagger}(x')\delta_{x,x'+3_{\hat{4}}} - U_4(x)\delta_{x,x'-3_{\hat{4}}}\right)
\end{aligned}
\tag{3.30}
$$

It is clear that the modification amounts to replacing each γ_μ by $(c_1 + c_3/3)\gamma_\mu$ in the non-interacting case. The Wilson mass term, added to remove the doublers, is kept unchanged. Note that the modified D_W-operator is still γ_5-hermitian for arbitrary real values of the coefficients c_1 and c_3. The new domain wall operator can therefore be derived in the same way as Eq.(3.11) was obtained. We fix the coefficients by demanding the dispersion relation for free fermions on the lattice to be the same as in the continuum up to $O(a^4p_j^4)$. We find that all the terms at $O(a^3p_j^3)$ are eliminated for the coefficients $c_1 = 9/8,\ c_3 = -1/8$. We employ them below for the calculation of the thermodynamic quantities.

Following [52], we use $K_3(\hat{\mu}) = K^3(\hat{\mu})$ and $L_3(\hat{\mu}) = L^3(\hat{\mu})$ for introducing $\hat{\mu}$ for the 3-link terms in the modified Domain wall operator. The ratio of quark number susceptibilities, $\chi(0)/\chi_{SB}$, computed using the modified Domain wall operator in presence of $\hat{\mu}$, is plotted as a function of $1/N_T^2$ as in Figure 3.8 along with that for the unimproved Domain wall operator of Eq.(3.11). We used $M = 1$, $\zeta = 4$, $N_5 = 18$ and $a_5 = 1$ for this computation. One clearly notices that the large correction terms ($\sim 45\%$) at N_T =6-8 for the usual Domain wall operator go down to about 7-8 %. Indeed, the size of corrections go down further as N_T increases. Similarly, the energy density of such improved fermions also exhibited smaller, about 15-5%, deviations from the continuum for N_T =6-10, as compared to about 30 % in the Figure 3.5b.

3.5.2 Overlap kernel

From section II, we know that the Overlap operator can be derived as a special limiting case of the Domain wall operator. It would be thus interesting to check how the improvement

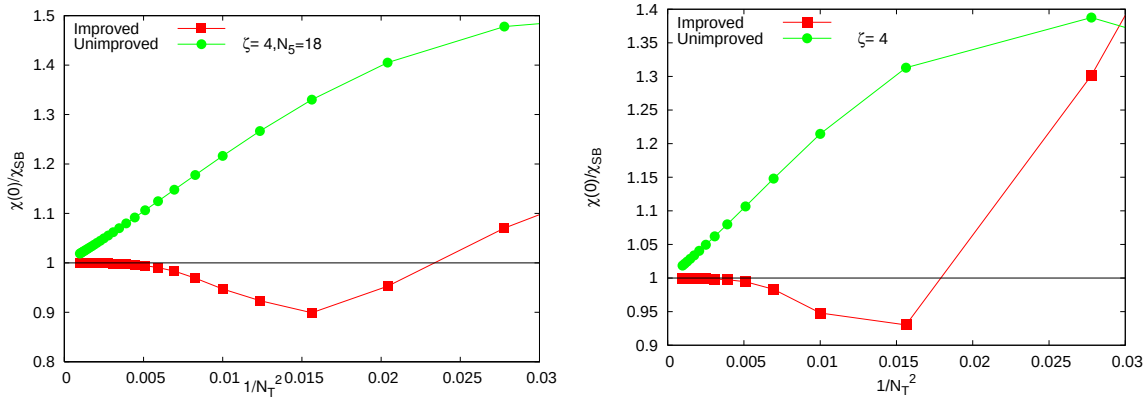

Figure 3.8: The susceptibility of improved and the conventional Domain wall fermions(left panel) and Overlap fermions(right panel) at $M = 1.0$ as a function of $1/N_T^2$.

in the Wilson Dirac operator in Eq. (3.30) fairs in the Overlap case. For that purpose we compute the quark number susceptibility for non-interacting fermions on a $N^3 \times N_T$ lattice numerically with the corresponding improved Overlap operator. The χ/χ_{SB} does have lower $1/N_T^2$ corrections for $N_T = 6, 8$ than for the conventional Overlap operator with $M = 1$ as shown in Figure 3.8. We also observe a faster approach to the continuum result with such improved Overlap operator than with the Neuberger Overlap operator even with optimum $M = 1.55$ reported in [46]. Another advantage is that the thermodynamic quantities calculated from this improved operator are free from oscillations at odd-even values of N_T exhibited [46] by the usual Overlap operator. The improvement in the energy density is marginal up to $N_T = 8$ but substantial for $N_T = 10$ onwards. Similar improvement for 2-D Overlap kernel by replacing the Wilson Dirac operator with different hypercubic operators was observed in [53].

3.6 Summary

Since the chiral violations vanish exponentially with the number of sites N_5 in the fifth dimension, the Domain wall fermions offer a more practical alternative to the Overlap fermions and yet have exact flavour and spin symmetry. We have computed the energy density and susceptibility at zero chemical potential of such fermions numerically for both finite and

infinite N_5. The chiral symmetry is exact in the latter case and a choice M between 1.45-1.50 allows faster convergence to the continuum results. The optimum M range is different from the Overlap fermions because of the presence of additional poles and branch cuts. We have also verified analytically that the energy density has the correct continuum value in the chiral limit. Varying the number of lattice sites in the fifth dimension, we have shown that $N_5 = 18$ is sufficient to restore chiral symmetry.

We found that introducing chemical potential $\hat{\mu}$ in domain wall operator leads to chiral symmetry breaking even for infinite N_5. But if we do allow that, there exist a large class of functions $K(\hat{\mu})$ and $L(\hat{\mu})$, with $K(\hat{\mu}) \cdot L(\hat{\mu}) = 1$, for which there are no $\hat{\mu}$-dependent divergent terms in the physical observables. From the numerical evaluation of the energy density in presence of $\hat{\mu}$, we conclude that the optimum range of M remains the same. The lattice cut-off effects are however very large for small N_T = 4-8. By systematically removing the dominant correction terms to the continuum value of the chiral fermion operators we have achieved a faster rate of convergence to the continuum as well as smaller magnitude of $1/N_T^2$ corrections for small lattice sizes even for $M = 1.0$. This set of optimum parameters is anticipated to produce similar results in full QCD simulations with chiral fermions though an explicit check needs to be done.

Chapter 4

Anomaly at finite density and chiral fermions

4.1 Introduction

Chiral anomalies arise in a theory of massless fermions interacting with the gauge fields. The flavourless axial current of the fermions is classically conserved but is violated at one-loop level, as was shown in the famous calculation of the Adler-Bell-Jackiw(ABJ) triangle diagram for the $U(1)$ case [10, 11]. The anomalous contribution is a universal feature of the theory and is independent of the ultraviolet regulator used for the quantum theory. Fujikawa provided a new insight on anomalies by showing that they arise due to the change of the fermion measure under the corresponding transformation of the fermion fields [12] in the path integral method. For the physically interesting case of two massless flavour QCD ($N_f = 2$), the order of the chiral phase transition depends [13] on the size of the coefficient of the chiral anomaly term. It is of second order, with critical exponents of the $O(4)$ spin model, if the anomaly contribution is sizeable at finite temperature. One could expect a QCD-critical point in the $T - \mu_B$ plane for light quarks in that case. In view of this, it is important to ascertain what change occurs in the anomaly in the presence of finite temperature and densities.

In this chapter we would be addressing both the perturbative and nonperturbative aspects of the chiral anomaly at finite temperature/density. In Sec. 4.2, we compute the

triangle anomaly in the imaginary time formalism of thermal field theory. This method has the advantage that it can be linked to the weak coupling lattice calculations. Lattice QCD deals with the imaginary time Euclidean propagators, and hence anomaly calculation in the Euclidean space-time would be directly relevant for numerical studies. In Sec. 4.2.2, we extend Fujikawa's analysis to finite density in the continuum. We show that the anomaly equation arising due to the change in the measure of the functional integrals under chiral transformation of the fermion fields remains the same at nonzero densities as well. We extend these considerations in Sec. 4.3 to the case of fermions with exact chiral invariance on the lattice. We propose a lattice Overlap Dirac operator with a term linear in the chemical potential μ, i.e., similar to the continuum and also suggest a way to get rid of the spurious divergences in the thermodynamic quantities. This method of introducing chemical potential is completely general and can be used for the staggered fermions as well. Its potential to handle higher order terms in the Taylor expansion in chemical potential μ in full QCD is shown using the staggered fermions for $T > T_c$.

4.2 Anomaly at $T = 0$ and $\mu \neq 0$ in continuum

4.2.1 Perturbative calculation

In this section we calculate the expectation value of the gradient of flavour singlet axial vector current of QCD perturbatively in the presence of finite fermion density to check how the anomaly equation is affected in the presence of a nonzero chemical potential. The lowest order diagrams are the ABJ triangle diagrams shown in Figure 4.1. It is well-known that the higher order diagrams do not contribute to the anomaly equation at zero density, neither do other diagrams like the square and pentagon diagrams. We therefore compute only the triangle diagrams at finite density. Our starting point is the QCD Lagrangian in the Euclidean space with the finite number density term as defined in [54]. In order to maintain consistency with the lattice literature, we have however chosen the Dirac gamma matrices to be Hermitian:

$$\mathcal{L} = -\bar{\psi}(\not{D} + m)\psi - \frac{1}{2}\mathrm{Tr}\ \ F_{\alpha\beta}F_{\alpha\beta} + \mu\bar{\psi}\gamma_4\psi\ , \tag{4.1}$$

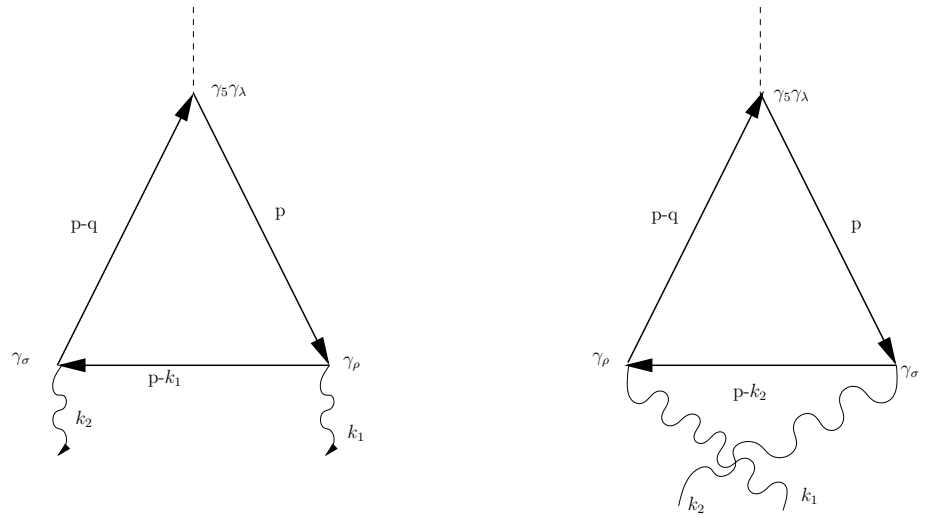

Figure 4.1: The ABJ triangle diagram(left panel) and its crossed counter part(right panel).

where $\not{D} = \gamma_\nu(\partial_\nu - igA^a_\nu T_a)$ with T_a being the generators of the SU(3) gauge group. The ghost terms are not important in such a calculation as these do not directly couple to the fermions. The $\gamma_5 = \gamma_1\gamma_2\gamma_3\gamma_4$ is also Hermitian in our case. The inverse free fermion propagator is seen to acquire a μ dependence and become $[i\not{p} - m + \mu\gamma_4]$. In order to find out whether the chiral current $j_{\mu 5} = \bar{\psi}\gamma_\mu\gamma_5\psi$ for massless quarks is conserved at finite density in one-loop perturbation theory, we compute the quantum mechanical expectation value of the derivative of the chiral current i.e. ,

$$\langle \partial_\mu j_{\mu,5} \rangle = -\frac{1}{2}\int d^4x_1 d^4x_2 \partial_\lambda \langle T\{j_{5,\lambda}(x) j_\rho(x_1) j_\sigma(x_2)\}\rangle A^\rho(x_1) A^\sigma(x_2) \ . \tag{4.2}$$

where the expectation value of the time ordered product of the three currents at one-loop level is the axialvector-vector-vector (AVV) triangle diagram shown in Figure 4.1. Any deviation of this quantity from its classical value would give us the anomaly. Using the Euclidean space Feynman rules, the amplitude of the AVV triangle diagram can be computed. The crossed diagram is the one with the gluon legs exchanged among the two vector (VV) vertices, and it corresponds to the process which is quantum mechanically equally favored.

Denoting by $\Delta^{\lambda\rho\sigma}(k_1, k_2)$ the total amplitude and contracting it with q_λ, Eq.(4.2) can

be written in the momentum space for massless quarks as

$$\begin{aligned} q_\lambda \Delta^{\lambda\rho\sigma} &= (-i) g^2 \mathrm{tr}[T^a T^b] \int \frac{d^4p}{(2\pi)^4} \mathrm{Tr} \quad \left[\gamma^5 \frac{1}{\not{p} - \not{q} - i\mu\gamma^4} \gamma^\sigma \frac{1}{\not{p} - \not{k}_1 - i\mu\gamma^4} \gamma^\rho \right. \\ &- \gamma^5 \frac{1}{\not{p} - i\mu\gamma^4} \gamma^\sigma \frac{1}{\not{p} - \not{k}_1 - i\mu\gamma^4} \gamma^\rho \\ &+ \left. \gamma^5 \frac{1}{\not{p} - \not{q} - i\mu\gamma^4} \gamma^\rho \frac{1}{\not{p} - \not{k}_2 - i\mu\gamma^4} \gamma^\sigma - \gamma^5 \frac{1}{\not{p} - i\mu\gamma^4} \gamma^\rho \frac{1}{\not{p} - \not{k}_2 - i\mu\gamma^4} \gamma^\sigma \right] , \end{aligned} \tag{4.3}$$

with the tr (Tr) denoting trace over color (spin) indices. Combining further the first (second) term of the AVV diagram and the second (first) term of the corresponding crossed diagram respectively, we rewrite the contracted amplitude in terms of functions $f_1(p, k_1)$ and $f_2(p, k_2)$,

$$q_\lambda \Delta^{\lambda\rho\sigma} = (-i)\ \mathrm{tr}[T^a T^b] g^2 \int \frac{d^4p}{(2\pi)^4} \left[f_2(p - k_1, k_2) - f_2(p, k_2) + f_1(p - k_2, k_1) - f_1(p, k_1) \right] \ , \tag{4.4}$$

where the function $f_1(p, k_1)$ is defined as,

$$\begin{aligned} f_1(p, k_1) &= \mathrm{Tr} \quad \left[\gamma^5 \frac{\not{p} - i\mu\gamma_4}{(p_4 - i\mu)^2 + \vec{p}^2} \gamma^\sigma \frac{\not{p} - \not{k}_1 - i\mu\gamma_4}{(p_4 - k_{14} - i\mu)^2 + (\vec{p} - \vec{k}_1)^2} \gamma^\rho \right] \\ &= - \quad \left[\frac{4\epsilon^{\alpha\sigma\beta\rho} p_\alpha k_{1\beta} - 4i\mu\epsilon^{4\sigma\beta\rho} k_{1\beta}}{((p_4 - i\mu)^2 + \vec{p}^2)((p_4 - k_{14} - i\mu)^2 + (\vec{p} - \vec{k}_1)^2)} \right] \ , \end{aligned} \tag{4.5}$$

since Tr $[\gamma^5 \not{p} \gamma^\sigma \not{p} \gamma^\rho] = 0$. f_2 can be obtained by substituting k_2 for k_1 and interchanging the indices ρ and σ in Eq.(4.5). We will use below a common notation f for denoting either in order to sketch the proof further. Although the numerator of Eq.(4.5) has terms up to quadratic order in μ, it should be noted that the μ^2 terms are $\sim \mu^2 \mathrm{Tr}\ [\gamma^5 \gamma^4 \gamma^\sigma \gamma^4 \gamma^\rho] \sim \epsilon^{4\sigma 4\rho}$ and therefore vanish. In order to further evaluate the right-hand side of Eq.(4.4), we note that the integrals are linearly divergent and hence must be regulated by introducing a cut-off scale, Λ. This procedure must be carried out in a gauge invariant manner such that the vector currents are conserved. In momentum space this amounts to

$$k_{1\rho} \Delta^{\lambda\rho\sigma}(k_1, k_2) = k_{2\sigma} \Delta^{\lambda\rho\sigma}(k_1, k_2) = 0 \ . \tag{4.6}$$

We follow the usual text book [55] method to impose these conditions above and compute the anomaly. In order to highlight the differences due to the $\mu \neq 0$ terms, we sketch below the evaluation of just the relevant part of Eq.(4.4). Expanding the first term and combining

it with the second, we rewrite the first two integrals as,

$$\lim_{\Lambda\to+\infty}\int_0^\Lambda \frac{d^4p}{(2\pi)^4}\left[-k_{1\mu}\partial_\mu f_2+\frac{1}{2}k_{1\mu}k_{1\nu}\partial_\mu\partial_\nu f_2+\mathcal{O}(k^3)\right], \tag{4.7}$$

where the derivatives are in the momentum space. The first term of the above integrand can be written as a surface integral using Gauss law,

$$\begin{aligned}
&\lim_{\Lambda\to+\infty}\int_0^\Lambda \frac{d^4p}{(2\pi)^4}k_{1\mu}\partial_\mu f(p,k_2)=\lim_{\Lambda\to+\infty}\frac{k_{1\mu}\Lambda_\mu}{\Lambda}\frac{f(\Lambda,k_2)2\pi^2\Lambda^3}{(2\pi)^4}\\
\sim\quad &\lim_{\Lambda\to+\infty}\left[\frac{4\epsilon^{\alpha\sigma\beta\rho}\frac{\Lambda_\alpha k_{1\mu}k_{2\beta}}{\Lambda}-\frac{4i\mu}{\Lambda}\epsilon^{4\sigma\beta\rho}k_{1\mu}k_{2\beta}}{((1-i\frac{\mu}{\Lambda})^2+1)((1-\frac{k_{24}+i\mu}{\Lambda})^2+(\hat{\Lambda}-\frac{\vec{k}_2}{\Lambda})^2)}\right]\frac{\Lambda_\mu\Lambda^3}{8\pi^2\Lambda^4}\\
=-\quad &\frac{\epsilon^{\alpha\beta\sigma\rho}k_{1\alpha}k_{2\beta}}{8\pi^2}
\end{aligned} \tag{4.8}$$

where we uses the isotropy condition, $\Lambda_\nu\Lambda_\alpha/\Lambda^2=g_{\nu\alpha}/4$. It is clear that the second term of the integrand in Eq.(4.7) when similarly integrated leads to the gradient of $f(p,k_2)$ at the Fermi surface of radius Λ, and therefore vanishes as $\mathcal{O}(\frac{1}{\Lambda})$. Hence this term, and the higher derivative terms, do not contribute in the limit when the cut-off is taken to infinity. The other two terms of Eq.(4.4), as well as the vector current conservation condition Eq.(4.6), can be similarly shown to be μ independent, leading to the canonical result even for $\mu\neq 0$:

$$q_\lambda\Delta^{\lambda\rho\sigma}=-\mathrm{tr}[T^aT^b]\frac{ig^2}{2\pi^2}\epsilon^{\alpha\beta\sigma\rho}k_{1\alpha}k_{2\beta}\ . \tag{4.9}$$

We have thus shown explicitly that the anomaly equation has no corrections due to nonzero μ or, equivalently, at nonzero finite density. It is easy to generalize the same computation to nonzero temperatures. At finite temperature, the temporal part of the momentum gets quantized as the well-known Matsubara frequencies : $p_4=\frac{(2n+1)\pi}{\beta}$. Correspondingly, $\int_{-\infty}^{\infty}\frac{dp_4}{2\pi}$ gets replaced by $\frac{1}{\beta}\sum_n$, where $n=\pm1,\pm2,...,\pm\infty$. The sum over discrete energy eigenvalues, can as usual, be split as a zero temperature contribution along with the finite temperature contributions weighted by the Fermi-Dirac distribution functions for the particles and antiparticles. Note that the finite temperature contributions will fall off to zero in the ultraviolet limit because these are regulated by the distribution functions. Thus,

$$\begin{aligned}
&\int\frac{d^3\vec{p}}{(2\pi)^3}\left[k_1^i\partial_i\left[f(|\vec{p}|)\left(\frac{1}{e^{\beta(|\vec{p}|-\mu)}+1}+\frac{1}{e^{\beta(|\vec{p}|+\mu)}+1}\right)\right]+\{\rho,k_1\leftrightarrow\sigma,k_2\}\right]\\
&=\lim_{|\vec{p}|\to+\infty}\frac{4\pi|\vec{p}|}{(2\pi)^3}\left[(\vec{k}_1\cdot\vec{p})f(|\vec{p}|)\left(\frac{1}{e^{\beta(|\vec{p}|-\mu)}+1}+\frac{1}{e^{\beta(|\vec{p}|+\mu)}+1}\right)+\{\rho,k_1\leftrightarrow\sigma,k_2\}\right]\to 0.
\end{aligned}$$

Such perturbative calculations of the ABJ anomaly were reported earlier in the real time formalism at finite temperature and at both zero [56] and nonzero [57, 58] fermion densities as well as for finite density in Minkowski space-time [59]. We have shown above that these calculations are possible using the imaginary time formalism as well. An imaginary time calculation is useful as this can be generalized to weak coupling calculations in lattice gauge theory.

4.2.2 Nonperturbative calculation

The chiral anomaly in the path integral formalism can also be looked upon as arising due to the change of the measure under chiral transformation of the fermion fields [12]. In this section, Fujikawa's method of anomaly calculation in the path integral formalism, at zero temperature and zero fermion density, is extended to the finite fermion density case. But before analyzing the finite density problem, the method for $\mu = 0$ is summarized to point out the differences that would arise in the finite density case. The partition function for massless fermions interacting with $SU(N)$ gauge theory can be written in Euclidean space as

$$\mathrm{Z} = \int \mathcal{D}\bar{\psi}\mathcal{D}\psi[\mathcal{D}A_\nu]\mathrm{e}^{-\int \mathrm{d^4x}\ \bar{\psi}\not{D}\psi - \mathrm{S_{YM}}} = \int \mathcal{D}\bar{\psi}\mathcal{D}\psi[\mathcal{D}\mathrm{A}_\nu]\mathrm{e}^{-\mathrm{S}} \tag{4.10}$$

where $S_{YM} = 1/2 \int d^4x \left[\mathrm{Tr}\ \ F_{\alpha\beta}(x)F_{\alpha\beta}(x) + 1/\xi(f^a A^a_\mu)^2\right]$ is the free Yang-Mills action with appropriate gauge fixing $f^a A^a_\mu = 0$. The action for the ghost term is included within the gauge field measure and hence denoted within square brackets. This is justified since we are interested in the change of the fermion fields under chiral transformations and the ghost fields do not interact with the fermions. Under the infinitesimal local chiral transformation of the fermion fields, given by

$$\delta\psi(x) = i\alpha(x)\gamma_5\psi(x) \quad \text{and} \quad \delta\bar{\psi}(x) = i\alpha(x)\bar{\psi}(x)\gamma_5\ , \tag{4.11}$$

the action changes as $S \to S - i\int d^4x\ \alpha(x)\partial_\nu j^\nu_5$. The measure changes as a result of the transformation of the fermion fields. The change of measure is,

$$\mathcal{D}\bar{\psi}'\mathcal{D}\psi' = \mathcal{D}\bar{\psi}\mathcal{D}\psi\mathrm{Det}|\frac{\partial(\bar{\psi}', \psi')}{\partial(\bar{\psi}, \psi)}| = \mathcal{D}\bar{\psi}\mathcal{D}\psi\mathrm{e}^{-2\mathrm{i}\int \mathrm{d^4x}\ \alpha(\mathrm{x})\mathrm{Tr}\ \gamma_5} \tag{4.12}$$

where Tr stands for the trace over the spin and the color space. This trace can be computed using the eigenvectors of the operator $\not{D}$, since it is an anti-Hermitian operator. It has purely

imaginary eigenvalues and the corresponding eigenvectors form a complete orthonormal basis. Splitting the trace computation into two parts, the trace over the nonzero eigenvalues can be done easily as follows. Since $\{\gamma_5, \not{D}\} = 0$, for every eigenvector ϕ_m with nonzero eigenvalue $\lambda_m \neq 0$, there is a corresponding eigenvector $\gamma_5\phi_m$ with eigenvalue $-\lambda_m$. Thus for each finite λ_m , $\phi_m^{\pm} = \phi_m \pm \gamma_5\phi_m$ are eigenvectors of γ_5 with eigenvalues ± 1. Since trace is independent of the basis vectors we can also compute the trace of γ_5 in the $\phi_m^{\pm}$ basis. One obtains zero as the result since there are equal number of $\phi_m^{\pm}$ respectively. For the zero eigenmodes, $\not{D}$ and γ_5 commute hence each zero mode has a definite chirality, leading to a +1 contribution for those with $\gamma_5\phi_n = \phi_n$ and a -1 for the opposite chirality. Hence the complete evaluation of the trace gets a nonzero contribution corresponding to the difference between number of the two chiralities:

$$\int d^4x \ \mathrm{Tr}\gamma_5 = \int d^4x \sum_n \phi_n^{\dagger}\gamma_5\phi_n = n_+ - n_-. \tag{4.13}$$

Chiral Jacobian in the presence of μ

The presence of finite chemical potential, μ, in the action can be described as an effective change of the Dirac operator from $\not{D}$ to $\not{D} - \mu\gamma_4 = \not{D}(\mu)$. Under the chiral transformation given in Eq.(4.11) the action still remains invariant as in the zero density case. This is due to the fact that the μ dependent term of the action anticommutes with γ_5: $\{\gamma_5, \mu\gamma_4\} = 0$. Under the transformations given in Eq.(4.11) the fermion measure changes again by the same Jacobian factor $\mathrm{Tr}\gamma_5$. The corresponding $\mathrm{Tr}\gamma_5$ is now evaluated in the space of eigenvectors of the new Dirac operator $\not{D}(\mu)$. This is because the measure is defined by the complete set of states of the Dirac operator which appears in the action. Although $\not{D}(\mu)$ has both an anti-Hermitian and a Hermitian term, it is still diagonalizable. Consider an eigenvector ϕ_m of $\not{D}(0)$ with an eigenvalue λ_m. Let us define two new vectors, ζ_m and υ_m as follows:

$$\zeta_m(\mathbf{x},\tau) = \mathrm{e}^{\mu\tau}\phi_{\mathrm{m}}(\mathbf{x},\tau) \quad , \quad \upsilon_{\mathrm{m}}^{\dagger}(\mathbf{x},\tau) = \phi_{\mathrm{m}}^{\dagger}(\mathbf{x},\tau)\mathrm{e}^{-\mu\tau} \ . \tag{4.14}$$

It is easy to check that ζ_m is the eigenvector of $\not{D}(\mu)$ with the same (purely imaginary) eigenvalue λ_m,

$$\not{D}(\mu)\zeta_m = \lambda_m\zeta_m \ , \tag{4.15}$$

and $\upsilon_m^\dagger$ is the eigenvector of $\not{D}(\mu)^\dagger$ with the eigenvalue $\lambda_m^* = -\lambda_m$,

$$\upsilon_m^\dagger \not{D}^\dagger(\mu) = -\lambda_m \upsilon_m^\dagger. \tag{4.16}$$

Note that the sets of eigenvectors $\{\zeta\}$ and $\{\upsilon\}$ are in one-to-one correspondence with the complete set $\{\phi\}$. Using the completeness relation for the latter,

$$\sum_m \phi_m(x)\phi_m^\dagger(y) \ = \delta^4(x-y) \ , \tag{4.17}$$

we note that

$$\sum_m \zeta_m(x)\upsilon_m^\dagger(y) = \sum_m \phi_m(x)\mathrm{e}^{\mu\tau_\mathrm{x}}\mathrm{e}^{-\mu\tau_\mathrm{y}}\phi_\mathrm{m}^\dagger(\mathrm{y}) = \delta^4(\mathrm{x}-\mathrm{y}) \ . \tag{4.18}$$

Moreover, $\{\zeta\}$ and $\{\upsilon\}$ satisfy the following normality condition,

$$\int \upsilon_m^\dagger(\mathbf{x},\tau)\zeta_m(\mathbf{x},\tau)\ d^4x = \ \int \phi_m^\dagger \mathrm{e}^{-\mu\tau}\mathrm{e}^{\mu\tau}\phi_\mathrm{m}\ \mathrm{d}^4\mathrm{x} = \ \int \phi_\mathrm{m}^\dagger(\mathbf{x},\tau)\phi_\mathrm{m}(\mathbf{x},\tau)\ \mathrm{d}^4\mathrm{x} = 1 \ , \tag{4.19}$$

leading to

$$\upsilon_m^\dagger(\mathbf{x},\tau)\gamma_5\zeta_m(\mathbf{x},\tau) = \phi_m^\dagger \mathrm{e}^{-\mu\tau}\gamma_5\mathrm{e}^{\mu\tau}\phi_\mathrm{m} = \ \phi_\mathrm{m}^\dagger(\mathbf{x},\tau)\gamma_5\phi_\mathrm{m}(\mathbf{x},\tau) \ , \tag{4.20}$$

Using these eigenvector spaces of $\not{D}(\mu)$, the calculation of $\mathrm{Tr}\gamma_5$ goes through in the same way as for $\not{D}(0)$ above. Since the new operator still anticommutes with γ_5 i.e $\{\gamma_5, \not{D}(\mu)\} = 0$, for each eigenvector ζ_m with eigenvalue λ_m there is an eigenvector $\gamma_5\zeta_m$ with the eigenvalue $-\lambda_m$. Thus the trace of γ_5 is zero for all nonzero λ_m. In the basis of the zero modes of $\not{D}(\mu)$, given by ζ_n and $\upsilon_n^\dagger$, the change in the fermion measure is given as,

$$\int d^4x\ \mathrm{Tr}\gamma_5 = \int d^4x \sum_n \upsilon_n^\dagger\gamma_5\zeta_n = \int d^4x \sum_n \phi_n^\dagger \mathrm{e}^{-\mu\tau}\gamma_5\mathrm{e}^{\mu\tau}\phi_\mathrm{n} = \mathrm{n}_+ - \mathrm{n}_-. \tag{4.21}$$

Thus the change in the fermion measure due to the chiral transformations is the same as in the zero density case with no additional μ dependent terms. Hence the anomaly is unaffected in the presence of μ. Some remarks on the proof may be in order. The definition of the vectors ζ_m and υ_m in Eq.(4.14) assumes that neither μ nor τ is infinite. The same assumption is also utilized in various steps in Eqs. (4.18)-(4.21). Clearly at strictly zero temperature, this is not tenable. However, an infinitesimally small temperature suffices for the proof to go through. Moreover, since the result is finally μ-independent, we expect the result to be valid at zero temperature, although our proof is valid only in the limit of zero temperature.

The scaling of the eigenvectors, including the chiral zero modes, by the $\exp(\pm\mu\tau)$ factors can be related to a nonunitary transformation of the fermion fields in the QCD action in the presence of μ, given by

$$\psi^{'}(\mathbf{x},\tau) = \mathrm{e}^{\mu\tau}\psi(\mathbf{x},\tau) \quad , \quad \bar{\psi}^{'}(\mathbf{x},\tau) = \bar{\psi}(\mathbf{x},\tau)\mathrm{e}^{-\mu\tau} \ , \tag{4.22}$$

which makes the action μ-independent:

$$S = \int d^4x \ \bar{\psi}^{'}[\not{D} - \mu\gamma_4]\psi^{'} = \int d^4x \ \bar{\psi}\mathrm{e}^{-\mu\tau} \ [\not{D} - \mu\gamma_4] \ \mathrm{e}^{\mu\tau}\psi = \int \mathrm{d^4x} \ \bar{\psi} \ \not{D} \ \psi \ . \tag{4.23}$$

Note that the fields ψ and $\bar{\psi}$ at the same space-time point scale differently in the transformation in Eq.(4.22) which is permissible [60] in the Euclidean field theory since they are mutually independent fields. Let us also emphasize that the transformation in Eq.(4.22) is not unitary and thus not physical. Indeed, it merely relates the actions in two different physical situations of zero and nonzero μ. One clearly cannot employ it in the evaluation of the partition function due to its nonunitary nature. We have shown above that the transformation suggests how to extend the cancellation argument for nonzero eigenvalues of the Dirac operator for $\mu = 0$ to the nonzero μ case as well and is thus useful. Furthermore, since the transformation commutes with both flavour singlet and nonsinglet chiral transformations, employing it as a prescription to introduce the chemical potential will necessarily lead to a μ dependent action which has the same chiral invariance as for $\mu = 0$. Whether this way to introduce the chemical potential in any theory is the only way to do so without affecting its chiral invariance would be interesting to explore; we conjecture that this is the case.

4.3 Anomaly on the lattice at finite density

The above discussion of the anomaly in the continuum suggests a way to introduce the chemical potential on the lattice. By preserving the transformation (4.22) on the lattice, one may expect to maintain the anomaly to remain μ independent on the lattice as well. Let us consider the naıve massless fermion action on the lattice,

$$S = -\sum_{x,y} \bar{\psi}_x \left[U_4^{\dagger}(y)\frac{\gamma_4}{2}\delta_{x,y+\hat{4}} - U_4(x)\frac{\gamma_4}{2}\delta_{x,y-\hat{4}} + \sum_{i=1}^{3}\frac{\gamma_i}{2}\left(U_i^{\dagger}(y)\delta_{x,y+\hat{i}} - U_i(x)\delta_{x,y-\hat{i}}\right)\right]\psi_y \ . \tag{4.24}$$

Replacing the ψ and $\bar{\psi}$ fields in the above action by ψ' and $\bar{\psi}'$ respectively, using the lattice analogue of the transformation (4.22), we indeed obtain a fermionic action on the lattice at finite density,

$$-\sum_{x,y}\bar{\psi}'_x\left[e^{-\hat{\mu}}U_4^\dagger(y)\frac{\gamma_4}{2}\delta_{x,y+\hat{4}}-e^{\hat{\mu}}U_4(x)\frac{\gamma_4}{2}\delta_{x,y-\hat{4}}+\sum_{i=1}^{3}\frac{\gamma_i}{2}\left(U_i^\dagger(y)\delta_{x,y+\hat{i}}-U_i(x)\delta_{x,y-\hat{i}}\right)\right]\psi'_y\ . \tag{4.25}$$

with a_4 being the lattice spacing in the temporal direction. Unfortunately, the infamous fermion doubling problem is related to the fact that the anomaly on the lattice is canceled exactly for such naıve fermions. The commonly used fermions on the lattice, like the Wilson and the Kogut-Susskind fermions do not have a flavour singlet $U_A(1)$ chiral symmetry, and so there is no anomaly to speak of. Nevertheless, we note that a similar transformation for such fermions does lead to the action popularly used for nonzero chemical potential [28, 29].

The Overlap operator at zero fermion density has exact chiral invariance on the lattice as was discussed in detail in chapter 1. At zero temperature and density, the change in the measure computed on the lattice due to the Luscher transformations was shown to be related to the index of the fermion operator [61, 22, 62] ,

$$\mathrm{Tr}\ [2\gamma_5(1-\frac{1}{2}D_{ov})]=-\mathrm{Tr}\ (\gamma_5 D_{ov})=n_+-n_-=\ 2\ \mathrm{Index}D_{ov}\ , \tag{4.26}$$

where $n_\pm$ are right and left handed fermion zero modes respectively.

Bloch and Wettig [33] proposed a method to incorporate the chemical potential in the Overlap operator It should be noted that the resultant action does not have the property of eliminating the μ-dependence by any transformation like Eq.(4.22) due to the nonlocal nature of D_{ov}.

We have earlier pointed out [46] that the action $S=\sum_{x,y}\ \bar{\psi}_x[D_{ov}(\mu)]_{xy}\psi_y$ is not invariant under Luscher's chiral transformations of Eq.(1.19). The chiral symmetry violation is of the $\mathcal{O}(a)$ and hence the symmetry is restored only in the continuum limit. In that case, the equation $-\mathrm{Tr}\ (\gamma_5 D_{ov}(\mu))=2\ \mathrm{Index}D_{ov}(\mu)$ is valid [33] on the lattice even in the presence of μ, since the fermion measure changes under these transformations by a Jacobian factor $\mathrm{Tr}\ [2\gamma_5(1-1/2D_{ov}(\mu))]$. However that the relevant zero modes are now those of the $D_{ov}(\mu)$, and thus μ dependent, in contrast to our continuum result of the previous section. Moreover altering the symmetry transformations has undesirable physical consequences [63], discussed in detail in the second chapter.

4.3.1 A simple proposal

It is well-known that the Overlap fermion operator can be obtained [18, 45] from the five dimensional domain wall fermions in the limit of infinite extent of the fifth dimension. The Bloch-Wettig proposal above was also shown to arise [34] in this way. It turns out that the chemical potential, μ enters in their action then as the Lagrange multiplier for the number of fermions on *each* slice of the fifth dimension. This means that all the unphysical "bulk" modes are considered with the same weightage in the partition function as the zero modes which eventually correspond to the massless quarks in four dimensions. The subsequent cancellation of the bulk contributions using Pauli-Villars fields to single out the contribution of a single chiral fermion thus becomes μ dependent on the lattice. Motivated from physical consideration, we propose to introduce the chemical potential only to count the fermion confined to the domain wall. Integrating out the fermions in the fifth dimension, one is led to the following action, which one would have written down naively to add a number density term :

$$D_{ov}(\hat{\mu})_{xy} = (D_{ov})_{xy} - \frac{a\hat{\mu}}{2a_4\ M}\left[(\gamma_4+1)U_4^\dagger(y)\delta_{x,y+\hat{4}} - (1-\gamma_4)U_4(x)\delta_{x,y-\hat{4}}\right]\ . \tag{4.27}$$

Here D_{ov} is the same Neuberger-Dirac operator of Eq.(2.1), and $\hat{\mu} = \mu a_4$ is the chemical potential in lattice units. As usual, the volume of the system is defined as $V = N^3a^3$ and the temperature is $T = 1/(N_T a_4)$ on a $N^3 \times N_T$ lattice with lattice spacings a and a_4 in spatial and temporal directions respectively. The term containing the chemical potential is not unique. Improved density operators could be used for faster approach to the continuum limit, e.g., addition of three-link terms. One could have chosen $\hat{\mu}/s$ instead of $\hat{\mu}/M$ as the multiplying factor for the conserved number part. All such choices of actions are constrained by the fact that these have the correct continuum limit. However the finite lattice spacing errors in each of these operators would be different and we comment below on how they may affect the numerical simulations.

Note that our proposal, too, will break exact chiral invariance at the same $\mathcal{O}(a)$ as the Bloch-Wettig proposal. As a result, the anomaly equation on the lattice will get μ -dependent corrections anyway. A significant difference may be the fact that the change in the measure is μ independent for our proposal, as in the case of the continuum. We persist with it in the

following, nevertheless, as it is simpler and easier to implement. Principally, this is due to the fact that one does not have to compute the sign function of a non-Hermitian matrix, with its inherent ambiguities, as in the Bloch-Wettig way of incorporating the chemical potential. The non-Hermitian sign function is numerically also more expensive to simulate for the full interacting case, whenever that becomes more practical.

For noninteracting fermions the $U_\mu = 1$ and the above Neuberger-Dirac operator with the chemical potential term can be diagonalized in momentum space in terms of the functions, $h's$ defined in Eq.(2.8) such that $D_{ov}(\hat{\mu})$ can be written as,

$$D_{ov}(\vec{p}, p_4, \hat{\mu}) = 1 - \sum_{i=1}^{4} i\gamma_i \frac{h_i}{s} - \frac{h_5}{s} - \frac{a\hat{\mu}}{a_4 M}\left[\gamma_4 \cos(a_4 p_4) - i \sin(a_4 p_4)\right] \ . \tag{4.28}$$

The above operator given by Eq.(4.28) can be shown to have correct continuum limit. The number density can be calculated at zero temperature by the contour integral method as was discussed for the Bloch-Wettig version of the Overlap fermions at finite μ in [46]. The major difference one finds is the expected μ/a^2-divergence (μ^2/a^2-divergence) in the number (energy) density in the continuum limit of $a \to 0$. What is perhaps not widely appreciated from such calculations is that the leading term, corresponding to the Stefan-Boltzmann limit, also changes by a *finite* computable part. In the next section, we show through numerical evaluations of the sums, how one can deal with these problems.

4.3.2 Numerical results

We compute two thermodynamic quantities of relevance to the above discussion as well as to the heavy-ion collision experiments: the change in the energy density due to the chemical potential, $\Delta\epsilon(\mu, T) = \epsilon(\mu, T) - \epsilon(0, T)$ and the quark number susceptibility at zero chemical potential, $\chi(0)$. These thermodynamic quantities are computed by taking appropriate derivatives of the partition function $Z = \det D_{ov}$,

$$\chi(0) = \frac{1}{N^3 a^2 N_T}\left(\frac{\partial^2 \ln\det D_{ov}}{\partial\hat{\mu}^2}\right)_{a_4,\hat{\mu}\to 0, a_4=a} \ , \ \epsilon(\hat{\mu}) = -\frac{1}{N^3 a^3 N_T}\left(\frac{\partial \ln\det D_{ov}}{\partial a_4}\right)_{\hat{\mu}N_T,\ a_4=a} \tag{4.29}$$

The quantities computed on the lattice are expected to have a $\Lambda^2 \sim 1/a^2$ dependence on the lattice for the D_{ov} defined in Eq.(4.28). In order to eliminate these spurious Λ^2

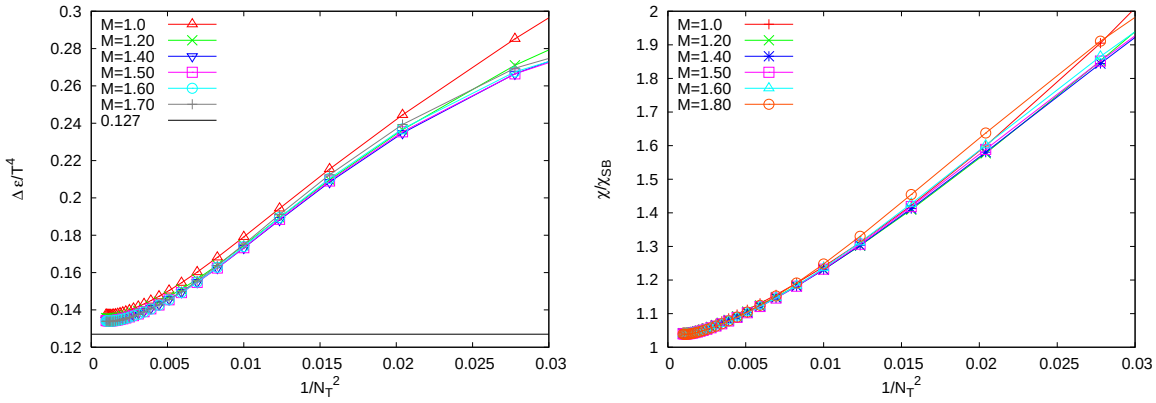

Figure 4.2: The energy density(left panel) and quark number susceptibility (right panel)as a function of $1/N_T^2$ for M values as indicated for $\zeta = 4$.

terms, we follow the same prescription which was used for the energy density computation at zero temperature (which diverges as Λ^4). We compute these thermodynamic quantities at zero temperature and subtract them from the corresponding values computed on the lattice at nonzero temperatures. The zero temperature values were computed numerically on a lattice with a very large temporal extent N_T and fixed a_4 such that $T = 1/(N_T a_4) \to 0$. The Matsubara frequencies then become continuous and hence could be integrated upon numerically.

Figure 4.2 displays the subtracted results for $\Delta\epsilon(\mu, T)$ for $r = \mu/T = \hat{\mu}N_T = 0.5$ and $\chi(0)$. The former is displayed in units of T^4 and has the value 0.127 for $r = 0.5$ in the continuum limit, while the latter is normalized to the ideal gas value $(T^2/3)$. The M values are as indicated along the symbol used. The subtraction constants had to be computed separately for energy density and susceptibility. From a comparison of the plots with the corresponding ones [46] for the Bloch-Wettig case, we find that

- there are no leftover effects of divergences after the zero temperature subtraction,
- there are no oscillations for odd-even values of N_T,
- the M-dependence is much less pronounced, and
- the scaling towards the continuum value is linear with the possibility of an easier

extrapolation.

We also computed the susceptibility using the Wilson fermions and compared the results with those above. We found that for $N_T = 6$ the cut-off effects of the Wilson operator are about 21% larger than the $M = 1.60$ Overlap result shown in the right panel of Figure 4.2. The difference reduces to about 3% at $N_T = 10$. Beyond $N_T = 10$, the approach to the continuum limit is almost identical for both the operators. The Wilson fermions have no chiral symmetry even for $\mu = 0$, which may make them less favored for the QCD critical point searches which are pivoted around the $\mu = 0$ transition.

We have also checked that there are no other divergent terms of the form $\mathcal{O}(a^{-n})$ with $n > 2$ in the number density, by calculating the fourth-order susceptibility since odd orders of susceptibilities vanish at $\mu = 0$. At zero chemical potential, the fourth-order susceptibility is given by,

$$\chi^{(4)}(0) = \frac{1}{N^3 N_T} \left(\frac{\partial^4 \ln \det D_{ov}}{\partial \hat{\mu}^4} \right)_{a_4, \hat{\mu} \to 0} \tag{4.30}$$

A term $\mathcal{O}(a^{-4})$ in the number density will show up as a divergence in this susceptibility, and will need a subtraction too. From Figure 4.3, where we display our results for $\chi^{(4)}(0)$ for $M = 1.5$, we can conclude that there are indeed no divergences to be seen in the large N_T limit. The normalization in this case is also the expected continuum value. It is *not* identical to the Stefan-Boltzmann value of $2\pi^{-2}$. Using the contour integral method it can be easily shown to be $\chi_c^{(4)}(0) = 2/\pi^2(1+1/4)$, with the additional factor of 0.25 coming from the term usually cancelled in the usual prescriptions [28, 29, 30, 31]. We have found the convergence to the continuum value to be strongly M dependent and unfortunately very slow for all values of M, as seen in the plot B of Figure 4.3. Introducing the chemical potential by choosing $\hat{\mu}/s$ as the coefficient of the number density term in Eq.(4.27), instead of the $\hat{\mu}/M$ we used, achieves a milder M dependence and a faster convergence towards the continuum. Perhaps improving the number density term can achieve a still faster convergence.

4.3.3 A new proposal for QCD critical point via Taylor expansion

Inspired by the above experience of dealing with the number density in the linear form, as in Eq.(4.27), we make a proposal valid for all lattice fermion operators. Because of the infamous sign problem for the fermion determinant with nonzero chemical potential, it has

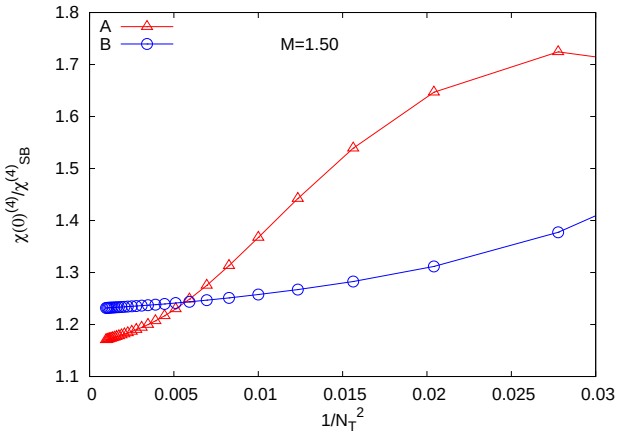

Figure 4.3: The variation of the ratio of the fourth order susceptibility and the corresponding continuum value as a function of $1/N_T^2$ for $\zeta = 4,\ M = 1.5$ for the A) $\hat{\mu}/s$ and B)$\hat{\mu}/M$ way of incorporating the chemical potential.

been proposed to look for the QCD critical point [64] by looking for the radius of convergence of the Taylor expansion [65, 64] of the second order baryon susceptibility, χ_{20} in powers of μ_B/T . This χ_{20} is expected to diverge at the critical point. On a finite lattice however there would be no divergence, only one would observe that the terms of the series are all positive and equal in magnitude. The finite radius of convergence of the series would give as an estimate of the critical point. The radius of convergence estimates require ratios of higher order quark number susceptibilities(QNS). Computations have been done up to the eighth order so far [64, 3], with lattice spacing $1/a \sim 1200$ MeV and pion mass quite close to the realistic one, $M_\pi = 230$ MeV. Extending these calculations to higher order is both necessary and desirable to confirm the results already obtained. Our proposal can permit such an endeavor. We denote $M(\mu)$ to be any generic lattice fermionic operator with the chemical potential μ:

$$S_F = \sum_{x,y} \bar{\Psi}(x) M(\mu; x, y) \Psi(y) = \sum_{x,y} \bar{\Psi}(x) D(x, y) \Psi(y) + \mu a \sum_{x,y} N(x, y) \tag{4.31}$$

Here D can be the staggered, Overlap, Wilson-Dirac or any other suitable fermion operator, and $N(x, y)$ is the corresponding point-split and gauge invariant number density. Eq.(4.27) provides a concrete example of the above for the Overlap fermions. Any improve-

ments in the fermion operator D or the number density N are generically included as long as the classical continuum limit is the same and μ appears linearly.

It is easy to see that only the first derivative of M with μ is nonzero. All others are zero. Thus denoting by $M^{'}$ the first derivative of M with respect to μ and adding more primes in the superscript for successively higher orders,

$$M' = \sum_{x,y} N(x,y), \qquad \text{and} \qquad M'' = M''' = M''''... = 0 \ , \tag{4.32}$$

for our proposal to incorporate μ in contrast to the popular $\exp(\pm\mu a)$ prescription where *all* derivatives are nonzero:

$$M' = M'''... = \sum_{x,y} N(x,y) \qquad \text{and} \qquad M'' = M'''' = M''''''... \neq 0 \ . \tag{4.33}$$

As a consequence, the various nonlinear susceptibility expressions, or equivalently the expressions for Taylor series coefficients, are a lot simpler and have a lot fewer terms. For example, let us write down a fourth-order coefficient [by combining Eqs.(A.4), (A.7) and (A.8) of [64]] :

$$\chi^{(4)} = \frac{T}{V}\left[\left\langle \mathcal{O}_{1111} + 6\mathcal{O}_{112} + 4\mathcal{O}_{13} + 3\mathcal{O}_{22} + \mathcal{O}_4 \right\rangle - 3\left\langle \mathcal{O}_{11} + \mathcal{O}_2 \right\rangle^2\right]. \tag{4.34}$$

Here the notation $\mathcal{O}_{ij...l}$ stands for the product, $\mathcal{O}_i\mathcal{O}_j\cdots O_l$. The expressions for $\mathcal{O}_n$, n=1,4 for our proposal above are,

$$\begin{aligned}
\mathcal{O}_1 &= \text{Tr } M^{-1}M', \\
\mathcal{O}_2 &= -\text{Tr } M^{-1}M'M^{-1}M', \\
\mathcal{O}_3 &= 2 \text{ Tr } (M^{-1}M')^3, \\
\mathcal{O}_4 &= -6 \text{ Tr } (M^{-1}M')^4,
\end{aligned} \tag{4.35}$$

in contrast with those for the usual case given in [64] :

$$\begin{aligned}
\mathcal{O}_1 &= \text{Tr } M^{-1}M', \\
\mathcal{O}_2 &= -\text{Tr } M^{-1}M'M^{-1}M' + \text{Tr } M^{-1}M'', \\
\mathcal{O}_3 &= 2 \text{ Tr } (M^{-1}M')^3 - 3 \text{ Tr } M^{-1}M'M^{-1}M'' + \text{Tr } M^{-1}M''', \\
\mathcal{O}_4 &= -6 \text{ Tr } (M^{-1}M')^4 + 12 \text{ Tr } (M^{-1}M')^2M^{-1}M'' - 3 \text{ Tr } (M^{-1}M'')^2 \\
&- 4 \text{ Tr } M^{-1}M'M^{-1}M''' + \text{Tr } M^{-1}M''''.
\end{aligned} \tag{4.36}$$

The eighth-order term needs $\mathcal{O}_8$, which has 18 terms in the usual case whereas it will simply be $\mathcal{O}_8 = -5040$ Tr $(M^{-1}M')^8$ for our proposal. The number of matrix inversions required to compute the higher order susceptibilities is also drastically reduced in this way of incorporating the chemical potential. Each derivative comes with the inverse of Dirac operator in the expression of QNS, and the inversion is the most expensive step in a lattice calculation. Hence as argued in [47], considerable amount of time would be saved in computing higher order QNS using the operator used here. For the eighth-order susceptibility computation we need to compute only eight matrix inversions as compared to the twenty required in the standard prescription, thus saving 60% of the computer time. For higher order susceptibilities, the number of matrix inversions is reduced by at least half, enabling us to compute even higher orders of the Taylor series of thermodynamic quantities and thus constrain the radius of convergence and allow for a precise estimation of the critical point.

Of course, there is a price to pay, and we would be demonstrating in the next section that it is not very big. All the coefficients that one evaluates this way will have the remnants of the terms which are otherwise eliminated by the usual prescriptions [28, 29, 30, 31]. It has been seen that in all such methods the artifacts once eliminated from the free theory by suitable change in the fermion action, do not appear in the interacting theory. We expect that the free theory artifacts are the dominant ones appearing in the expressions of higher order QNS computed in QCD as well with the fermion operator where μ enters linearly. Removal of the free theory artifacts will give us physical results for higher order QNS in the interacting theory. To check the validity of this proposal we use staggered fermions in the subsequent work. The choice of the staggered fermions is motivated from the fact that it has a remnant chiral $U(1)$ symmetry on the lattice and also easier to implement on the lattice. The staggered fermion operator at finite density that we would be considering is,

$$D(\mu)_{xy} = D(0)_{xy} + \frac{\mu a}{2}\eta_4(x)\left[U_4^\dagger(y)\delta_{x,y+\hat{4}} + U_4(x)\delta_{x,y-\hat{4}}\right], \eta_4(x) = (-1)^{x_1+x_2+x_3}. \tag{4.37}$$

The QNS for two quark flavours is defined as,

$$\chi_{ij}(\mu_u, \mu_d) = \frac{T}{V}\frac{\partial^{i+j} \ln Z(T, \mu_{u,d}, m)}{\partial\mu_u^i \mu_d^j} = \frac{T}{V}\frac{\partial^{i+j} \langle Tr \ln D(\mu_{u,d}, m)\rangle}{\partial\mu_u^i \mu_d^j}\ , \tag{4.38}$$

where Z is the QCD partition function. The Dirac operator used in this work, has a term linear in μ, hence second and higher order derivatives of this operator with respect to μ

vanishes. All the QNS are computed at zero baryon density so we do not encounter any "sign problem".

4.4 Results for Quark number susceptibilities

4.4.1 Free Theory

The different orders of quark number susceptibilities can be computed analytically for the free fermions. It is important since it allows us to have an estimate of the possible cut-off effects in the QNS and compare with the existing methods. In this case the staggered Dirac operator in presence of $\hat{\mu} = \mu a_4$ can be written as,

$$D(\hat{\mu}) = i\sum_{j=1}^{3}\eta_j \sin(ap_j) + \eta_4(\sin a_4p_4 + i\hat{\mu}\ \cos a_4p_4) + \hat{m}_q\ . \tag{4.39}$$

The susceptibilities can be calculated using Eq.(4.38). For example the number density expression on the lattice is of the form,

$$na^3 = \frac{1}{N^3N_T}\sum_{\vec{p},n}\frac{(\sin\omega_n + i\hat{\mu}\cos\omega_n)\cos\omega_n}{f + (\sin\omega_n + i\hat{\mu}\cos\omega_n)^2} \tag{4.40}$$

where $f = \sin^2 ap_1 + \sin^2 ap_2 + \sin^2 ap_3 + \hat{m}_q^2$. The above expression can be evaluated by the standard trick of converting the sum over energy eigenvalues to a contour integral. In this method,

$$\begin{aligned} na^3 &= \frac{i}{N^3}\sum_{\vec{p}}\int_{-\pi+i\theta}^{\pi+i\theta}\frac{d\omega}{2\pi}\frac{\sqrt{1-\hat{\mu}^2}\sin\omega\cos(\omega - i\theta)}{f + (1-\hat{\mu}^2)\sin^2\omega} = \frac{i}{N^3}\sum_{\vec{p}}\int_{-\pi+i\theta}^{\pi+i\theta}\frac{d\omega}{2\pi}F(\omega) \\ &= \frac{i}{N^3}\sum_{\vec{p}}\left[\oint F(\omega)d\omega - \int_{\pi}^{-\pi} - \int_{-\pi}^{-\pi+i\theta} - \int_{\pi+i\theta}^{\pi}\right] \\ &= \frac{i}{N^3}\sum_{\vec{p}}\left[-i\sum Residues + \int_{-\pi}^{\pi}\frac{d\omega}{2\pi}\frac{\sin\omega(\cos\omega + i\hat{\mu}\sin\omega)}{f + (1-\hat{\mu}^2)\sin^2\omega}\right]\ , \end{aligned} \tag{4.41}$$

where $F(\omega)$ is the integrand appearing in the expression of number density and $\tan\theta = \hat{\mu}$. The second term in the last expression does not exist for the standard prescription [28]. This additional term gives rise to lattice artifacts in the expressions of number density which are

absent in the standard prescription upto $\mathcal{O}(\hat{\mu}^3)$. The integral can be evaluated exactly for $\hat{m}_q = 0$ as,

$$n = \frac{\mu^3}{3\pi^2} + \frac{\mu^5 a^2}{6\pi^2} + \frac{\mu^7 a^4}{24\pi^2} + .. + \left[\frac{2\left(1-\sqrt{2}\right)\mu}{3\pi^2 a^2} + \frac{\left(-8+5\sqrt{2}\right)\mu^3}{3!\ \pi^2} + \frac{\left(-100+\frac{125}{\sqrt{2}}\right)\mu^5 a^2}{5!\ \pi^2} + ... \right] \tag{4.42}$$

where the terms in the square bracket are the additional zero temperature contribution arising in our method that are absent in the standard prescription. In the zero temperature limit and for a fixed lattice spacing, the number of sites in the temporal direction, $N_T \to \infty$. The energy eigenvalues are no longer quantized and are continuous in the range $[\frac{-\pi}{a}, \frac{\pi}{a}]$. The energy sum converts into an integral. The zero temperature values of the different susceptibilities can be explicitly evaluated on a finite lattice by integrating over the continuous energy modes as,

$$\chi_{20} = -\frac{1}{4\ N^3} \sum_{\vec{p}} \left(1 - \sqrt{\frac{f}{1+f}} \right) \ , \tag{4.43}$$

$$\chi_{40} = -\frac{3}{4\ N^3} \sum_{\vec{p}} \left(2 - \frac{3+2f}{1+f} \sqrt{\frac{f}{1+f}} \right) \ , \tag{4.44}$$

$$\chi_{60} = -\frac{15}{N^3} \sum_{\vec{p}} \left(2 - \frac{15+20f+8f^2}{4(1+f)^2} \sqrt{\frac{f}{1+f}} \right) \ , \tag{4.45}$$

To estimate and compare the cut-off effects, we compute the QNS for free fermions on a $24^3 \times 6$ lattice using the operator in Eq.(4.37). The expressions for χ_{n0} would have zero temperature $\mathcal{O}(a^{n-4})$ lattice artifacts which have to be subtracted to give physical values on the lattice. These zero temperature artifacts given in Eqs.(4.43), (4.44), & (4.45) are evaluated numerically by summing over the momentum modes.

When compared with the results obtained from the standard Hasenfratz-Karsch(H-K) operator, the QNS computed with the operator in Eq.(4.37) have smaller cut-off effects as evident in Figure 4.4.

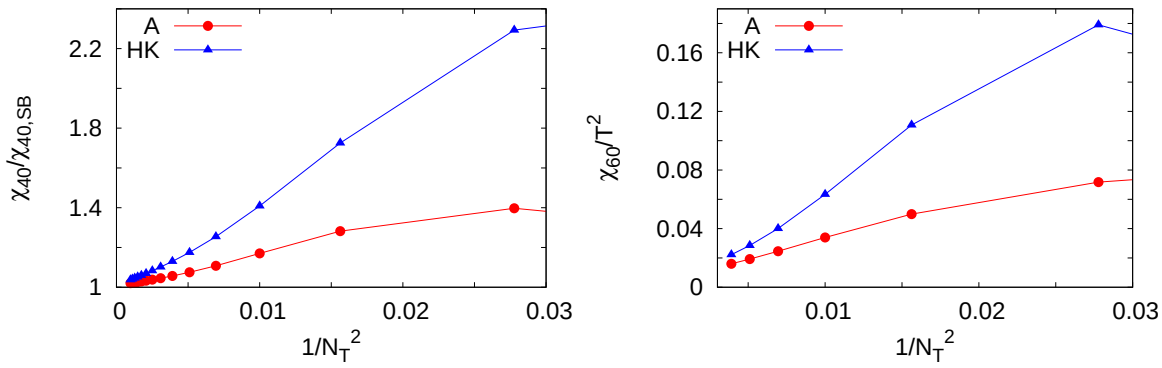

Figure 4.4: The comparison of fourth order (left panel) and the sixth order susceptibility (right panel) computed using the standard H-K method and the operator in Eq.(4.37).

4.4.2 $N_f = 2$ QCD

In this section we compute the baryon number susceptibilities for two flavour QCD on a $24^3 \times 6$ lattice. Wilson action is used for the gluon sector and for the fermion sector we have used the staggered fermion operator as given in Eq.(4.37). We would be considering exact isospin symmetry, therefore $\mu_u = \mu_d = 3\mu_B$, where μ_B is the baryon chemical potential. For lattice simulations, one need to set the temperature scale. First, the variation of the Polyakov loop susceptibility is studied as a function of the bare coupling constant for fixed $m/T_c = 0.1$. The value of the coupling constant at which the susceptibility of the bare Polyakov loop peaks, is labeled as g_c. The scale was set by measuring the plaquette values at $T = 0$, to extract a renormalized gauge coupling α_s in $\overline{MS}$ scheme. Once it is done then the lattice spacing can be expressed in terms of the renormalized coupling. This would allow conversion of lattice spacing a into a physical length scale in order to extract $T_c/\Lambda_{\overline{MS}}$ [66]. In order to estimate zero temperature lattice artifacts, one should ideally perform QCD simulations on a symmetric lattice of size 24^4 for each value of the coupling constant. But then the estimated gain in time could be reduced in generating configurations on the symmetric lattice. To remove such terms without any additional computational cost we propose the following two subtraction schemes:

- A: We subtract the zero temperature value of χ_{20} for free fermions computed by numerically summing over the momentum modes on a 24^3 lattice with infinite temporal

extent.

- B: We subtract χ_{20} for free fermions computed numerically on a 24^4 lattice.

We expect that the free theory artifacts would approximately be similar in magnitude to that in the interacting theory in the high temperature regime. This is motivated from the fact that we know in the perturbative regime that there are no additional divergences appearing at finite temperature and density in the expression for pressure. This is evident from the right panel of Figure 4.5, where the ratio of $\chi_{20}/\chi_{20,SB}$ is independent of the subtraction scheme at temperatures $T > T_c$, where the SB value was computed on a finite lattice. In the left panel of Figure 4.5, the values of χ_{20} using the method A are consistent with the existing results computed using H-K prescription which we label as GG [3]. The method B gives smaller cut-off errors and consistent with those using improved fermion actions like p4 and Asqtad [67, 68]. For $T < T_c$, the results from the methods A and B are consistent with each

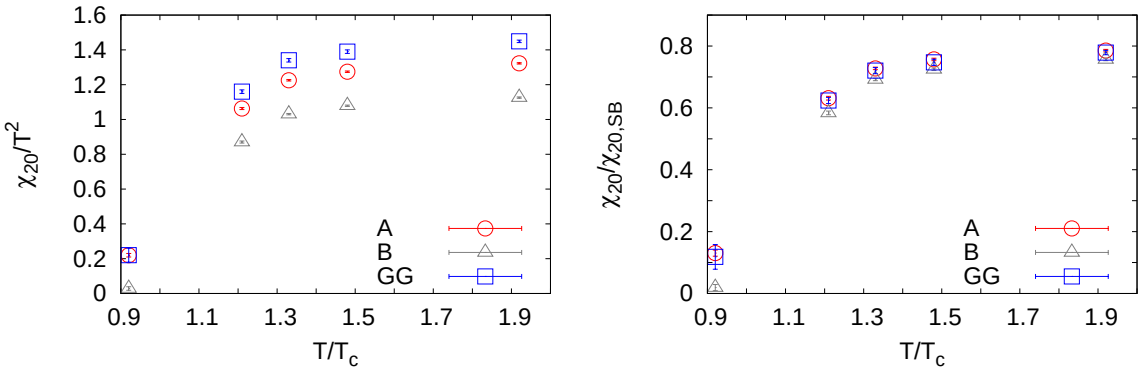

Figure 4.5: The second order QNS(left panel) and the ratio of $\chi_{20}/\chi_{20,SB}$(right panel) as a function of T/T_c.

other but do not agree with the GG results within errorbars. So the results are prescription dependent in this phase. Henceforth we would be only investigating the properties of the higher order susceptibilities for $T > T_c$ only. We would be following the subtraction scheme A, since the free theory divergences are accurately determined in this method. The ratio of χ_{4B} normalized by the corresponding SB value on the lattice is shown in the left panel of Figure 4.6. From the free theory plots we know that the $N_T = 6$ SB value computed using method A is about 1.8 times smaller than the corresponding HK result. Hence the

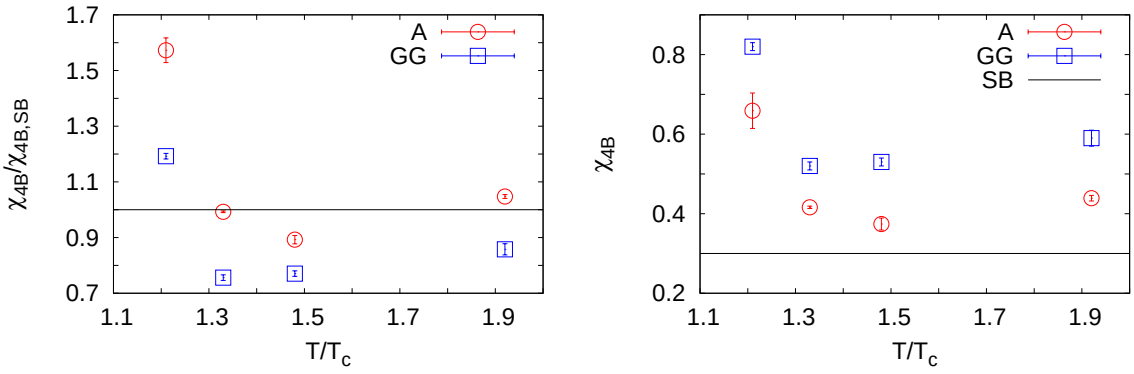

Figure 4.6: The ratio $\chi_{4B}/\chi_{4B,SB}$(left panel) and deviation of the fourth order baryon number susceptibility from continuum value 0.3(right panel) as a function of T/T_c.

ratio $\chi_{4B}/\chi_{4B,SB}$ has visible dependence on the subtraction scheme near the vicinity of T_c. At the highest temperatures, the results are closest to each other implying that the interacting theory results are close to the free theory ones. This is also evident from the plot of χ_{4B} in the interacting theory. The SB value referred here is the continuum value. The deviation from the continuum theory at the highest temperatures is of the same magnitude as observed for the free theory implying that at these temperatures the QGP consists of almost non-interacting quark quasi-particles. The sixth and eighth order susceptibilities are also prescription independent as seen in Figure 4.7. The rapid fall of these quantities towards zero again confirm the non-interacting quasi-particle nature of QGP at $T > 1.5T_c$.

The off-diagonal susceptibilities measure the correlations between the quasi-particles in the QCD medium. It also gives an estimate of how strongly interacting the medium is because these quantities are zero for ideal fermi gas. The lowest off-diagonal susceptibility is χ_{11} which measures the correlation between the u and d quarks in the medium. The χ_{11} should be identical for both the operators used and provides a consistency check for our results. The rapid drop of χ_{11} towards zero at $T > 1.2T_c$ signify rapid decorrelation among the quark flavours(Figure 4.8). This indicates that the quasi-particles in this phase are not composite particles but carrying the quantum number of quarks. This would imply that no new terms would arise due to correlations between the flavours, and there would be no further subtraction required for the fourth order off-diagonal QNS shown in the right panel of Figure 4.8. The χ_{22} is a sensitive indicator of the critical point as it peaks sharply at T_c,

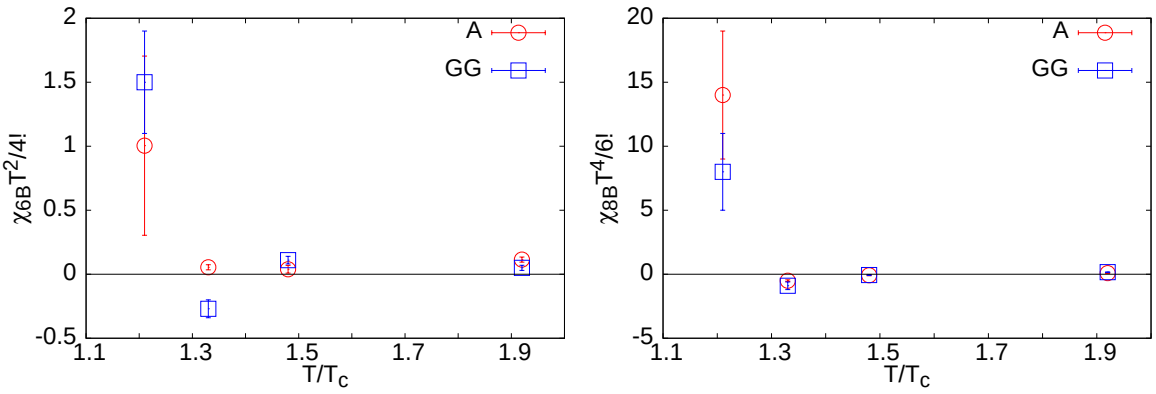

Figure 4.7: The sixth (left panel) and the eighth order(right panel) baryon number susceptibility as a function of T/T_c.

the same point at which the Polyakov loop susceptibility peaks whereas the χ_{31} remains close to zero for $T > T_c$, again signaling almost no correlation between the light quark flavours.

Next we check the ratios of susceptibilities. These ratios are important for estimating the radius of convergence of the Taylor series of χ_{20}. From the Figure 4.9 it is evident that ratios of both diagonal and off-diagonal susceptibilities are quite robust and independent of the prescription for a range of temperatures $T > T_c$. This would imply that the radius of convergence estimates using method A would be similar to that computed in GG. It would be interesting to check whether the same conclusions are valid for $T < T_c$.

4.5 Summary

We have shown perturbatively from the computation of the triangle diagrams at zero temperature that the anomaly equation does not have any finite density correction terms. We have extended our calculations to the nonperturbative case where we have used Fujikawa's method to show that the anomaly relation is unaffected in the presence of a finite chemical potential. This has an important implication for the lattice field theory in designing the lattice Dirac operator for nonzero μ: it should lead to a μ-independent anomaly relation on the lattice. The recent Bloch-Wettig proposal for chiral fermion operators at finite density violates the chiral invariance on the lattice itself. While a μ-dependent modification of the

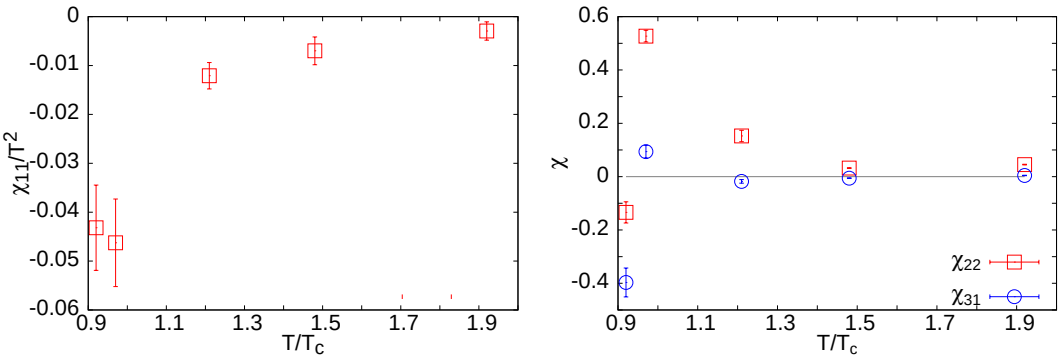

Figure 4.8: The second order(left panel) and the fourth order(right panel) off-diagonal QNS as a function of T/T_c.

chiral transformation can restore the chiral invariance, it leads to a μ-dependent anomaly relation unlike in the continuum theory. Such a modification has other physical consequences discussed in [63].

We have proposed a physically more justified way of introducing μ in the Overlap Dirac operator. In this method the chiral symmetry is explicitly broken as well, but the contribution to the anomaly relation from the measure is likely to remain μ independent, with the lattice corrections to the anomaly relation falling off as a power law in the continuum limit. It has the expected μ^2/a^2-type divergences in the continuum limit. We showed how a simple subtraction scheme can take care of them in the free case. This prescription is easily generalizable for other lattice fermion operators as well. We have computed the baryon number susceptibilities for two flavour QCD using the staggered Dirac operator given in Eq.(4.37). We have suggested two methods for removing these artifacts for $T > T_c$, which would allow for faster computation of these quantities than the conventional method. It has the advantage that the number of fermion matrix inversions goes down drastically when computing the higher order quark number susceptibilities. The higher order susceptibility computations are clearly important to accurately locate the critical point in the T-μ_B phase space for QCD. Our proposal would save much of the computational effort required for obtaining higher order susceptibilities, even for the staggered fermions. These methods however, are not expected to work for $T < T_c$ and we have to estimate the subtraction term for the interacting theory on a symmetric lattice for each value of the coupling constant.

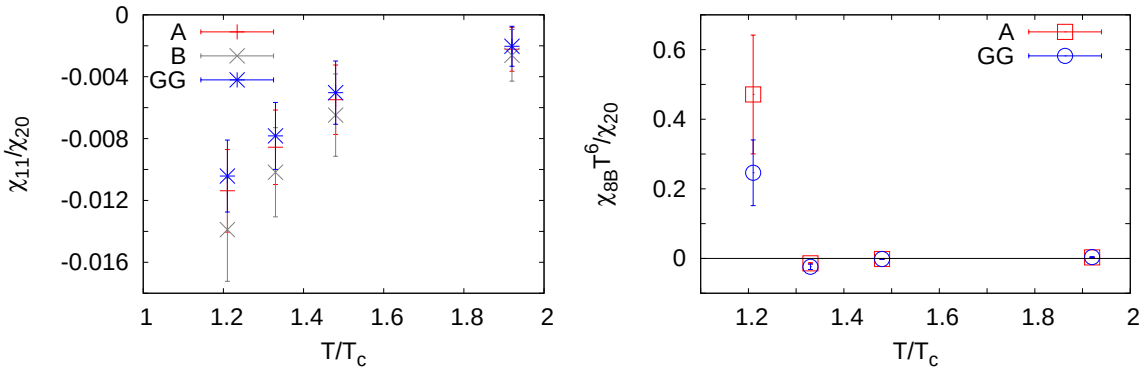

Figure 4.9: The second order off-diagonal χ_{11}/T^2(left panel) and ratio of second and eighth order susceptibility(right panel) as a function of T/T_c.

But we expect that the operator used in our work would still be efficient for continuum extrapolation for eighth and higher order QNS, which we would like to check in a future study.

Chapter 5

Overlap fermions at finite chemical potential

5.1 Introduction

Introducing chemical potential in the Overlap operator in the Lagrangian formalism has the main problem that a conserved number density cannot be defined. This has to do with the non-linearity of the Overlap operator. One way to circumvent this problem is to look at the Overlap operator [17] as a superposition between the ground states of two many body Hamiltonians. In this method one can construct suitable number density operators in terms of the many-body creation and annihilation operators. The chemical potential can be coupled to such number density term. Standard Overlap operator at finite density [33] do not have exact chiral symmetry on the lattice. In the Hamiltonian method by introducing external chiral sources we elucidate the meaning of explicit chiral invariance of the Overlap operator at finite density.

In Sec. 5.2 we review the Hamiltonian formalism for Overlap fermions at zero chemical potential. In the subsequent sections we motivate how to introduce the chemical potential in this formalism and show that the Overlap partition function with massless fermion sources has exact chiral invariance even at finite μ. In the last section of this chapter we show that different methods of introducing μ in the Overlap operator lead to μ^2/a^2 lattice artifact in the expression of free energy and discuss two proposals to remove these unphysical terms on

the lattice for full QCD simulations.

5.2 Review of Overlap formalism at zero fermion density

If we have fermions in a five dimensional Euclidean spacetime with a single domain wall profile, we can consider the fifth dimension as timelike and construct the Hamiltonian $\mathcal{H} = \gamma_5(D + M(s))$, D being the four dimensional Dirac operator and s being the coordinate along the fifth dimension. If the domain wall in the fifth dimension is of the form $M(s) = -M, s > 0$ and $M(s) = \Lambda, s < 0$, then the overlap between the ground states $|+\rangle$ and $|-\rangle$ of the two many body Hamiltonians $\mathcal{H}_+ = \gamma_5(D - M)$ and $\mathcal{H}_- = \gamma_5(D + \Lambda)$, respectively, gives us a chiral fermion for $s \to \infty$. On a lattice the continuum Dirac operator is replaced by the lattice Dirac operator, which in the Weyl notation is given as,

$$\mathcal{D}_W = \begin{pmatrix} B & C \\ C^\dagger & -B \end{pmatrix}$$

In the above equation, B is the Wilson term to remove the doublers and C is the nearest neighbour hopping term given as,

$$\begin{aligned} B &= \frac{1}{2}\sum_\mu \left(2 - T_\mu - T_\mu^\dagger\right) \\ C &= \frac{1}{2}\sum_\mu \sigma_\mu \left(T_\mu - T_\mu^\dagger\right) \\ (T_\mu\phi)(x) &= U_\mu(x)\phi(x+\hat{\mu}) \end{aligned}$$

with σ matrices are in $d = 4$.

$$\sigma_1 = \begin{pmatrix} 0 & 1 \\ 1 & 0 \end{pmatrix};\ \ \sigma_2 = \begin{pmatrix} 0 & -i \\ i & 0 \end{pmatrix};\ \ \sigma_3 = \begin{pmatrix} 1 & 0 \\ 0 & -1 \end{pmatrix};\ \ \sigma_4 = \begin{pmatrix} i & 0 \\ 0 & i \end{pmatrix}\ . \tag{5.1}$$

The Hamiltonian is now denoted as $H_w = \gamma_5\mathcal{D}_W$. H_w is a $2n \times 2n$ matrix where $n = 3 \times N^3 \times N_T$ and the gauge field is in the zero topological sector. The overlap formalism is designed to work in all topological sectors and this is one of the important features of the formalism. But, we can restrict ourselves to the zero topological sector to simplify the

discussion. All results can be trivially extended to all topological sectors. Also we would be considering the partition function at fixed gauge field background in this chapter. Let the Dirac Hamiltonian be diagonalized by a matrix U,

$$H_w U = U\Lambda, \tag{5.2}$$

with

$$U = \begin{pmatrix} \alpha & \gamma \\ \beta & \delta \end{pmatrix}; \quad \Lambda = \mathrm{diag}(\lambda_1^+, \cdots, \lambda_n^+, -\lambda_1^-, \cdots, -\lambda_n^-). \tag{5.3}$$

and $\lambda_i^\pm > 0$ for all i. On a lattice the parameter M in the Hamiltonian $\mathcal{H}_+$ is chosen to be between 0 & 2 on the lattice and $\mathcal{H}_+$ is denoted as H_w. The parameter Λ in $\mathcal{H}_-$ is usually chosen to be ∞ [69] and for this choice $\mathcal{H}_- \sim \gamma_5$. These Hamiltonians can be expressed in the second quantized form in terms of creation and annihilation operators,

$$\mathcal{H}_{R,L} = -a^\dagger_{R,L} H_w a_{R,L} \ , \ \Gamma_{R,L} = -a^\dagger_{R,L}\gamma_5 a_{R,L} \ . \tag{5.4}$$

with $a_{R,L}, a^\dagger_{R,L}$ obeying canonical anti-commutation relations separately for the R and L sets. The $\mathcal{H}$ is not diagonal in the basis of the operators a and a unitary matrix can provide suitable rotation to the basis in which H_w is diagonal,

$$b_{R,L} = U^\dagger a_{R,L} \tag{5.5}$$

and it follows that $b_{R,L}, b^\dagger_{R,L}$ also obey canonical anti-commutation relations. We can write

$$b_{R,L} = \begin{pmatrix} u'_{R,L} \\ d'_{R,L} \end{pmatrix}; \quad a_{R,L} = \begin{pmatrix} u_{R,L} \\ d_{R,L} \end{pmatrix}, \tag{5.6}$$

then

$$\mathcal{H}_{R,L} = -\sum_{i=1}^{n} \lambda_i^+ u'^\dagger_{R,L_i} u'_{R,L_i} + \sum_{i=1}^{n} \lambda_i^- d'^\dagger_{R,L_i} d'_{R,L_i} \ . \tag{5.7}$$

Let $|0\rangle$ be the vacuum state that is annihilated by all the destruction operators. Then the lowest state of $\mathcal{H}_{R,L}$ is

$$|+\rangle_{R,L} = u'^\dagger_{R,L_n} u'^\dagger_{R,L_{n-1}} \cdots u'^\dagger_{R,L_2} u'^\dagger_{R,L_1} \ .|0\rangle \tag{5.8}$$

In addition,

$$|-\rangle_{R,L} = u^\dagger_{R,L_n} u^\dagger_{R,L_{n-1}} \cdots u^\dagger_{R,L_2} u^\dagger_{R,L_1} |0\rangle \tag{5.9}$$

is the lowest state of $\Gamma_{R,L}$. It is to be noted that we are working in a fixed gauge field background for which such states are defined. The generating functional for a vector like theory with massless fermions is the overlap between these two lowest energy states [69],

$$Z(\bar{\xi}_R, \bar{\xi}_L, \xi_R, \xi_L) = {}_R\langle -|e^{\bar{\xi}_R d_R + \xi_R u_R^\dagger}|+\rangle_{RL}\langle +|e^{\xi_L d_L^\dagger + \bar{\xi}_L u_L}|-\rangle_L \ . \tag{5.10}$$

The sources, $\bar{\xi}_R$, $\bar{\xi}_L$, ξ_R and ξ_L are all Grassmann variables and they anti-commute with the fermionic operators. The properties of the generating functional are listed below,

- The phase choice for $|+\rangle_{R,L}$ are tied together since they are the ground states of identical many body operators. The same is true for $|-\rangle_{R,L}$. Therefore, the generating functional is unambiguous and does not not depend upon the phase choice present in the unitary matrix, U, that diagonalizes H_w.

- It does not depend on the ordering of the operators since the two terms in the exponent commute with each other in both factors.

- d_R and $u_R^\dagger$ are the propagating degrees of freedom in the first factor since $\langle -|u_R$ and $\langle -|d_R^\dagger$ are both zero. The converse holds for the second factor.

- In the absence of sources, it gives the fermion determinant for massless fermions as

$$ {}_R\langle -|+\rangle_R \ \ {}_L\langle +|-\rangle_L = \det\alpha \det\alpha^\dagger. \tag{5.11}$$

  where we have used (5.5) and an identity derived in [70].

- The generating functional is invariant under global chiral transformations:

$$\xi_R \to e^{i\varphi_R}\xi_R; \quad \bar{\xi}_R \to \bar{\xi}_R e^{-i\varphi_R}; \quad \xi_L \to e^{i\varphi_L}\xi_L; \quad \bar{\xi}_L \to \bar{\xi}_L e^{-i\varphi_L}. \tag{5.12}$$

- The propagator for the right-handed and left-handed fermions are

$$G_R^{ij} = \frac{{}_R\langle -|u_{Rj}^\dagger d_{Ri}|+\rangle_R}{{}_R\langle -|+\rangle_R}; \quad G_L^{ij} = \frac{{}_L\langle +|d_{Lj}^\dagger u_{Li}|-\rangle_L}{{}_L\langle +|-\rangle_L} \tag{5.13}$$

  and they obey the relation

$$G_R^\dagger = G_L. \tag{5.14}$$

Since the propagators of left and right handed fermions in the last item above are related by hermitian conjugation as opposed to anti-hermitian conjugation, our definitions are for the hermitian Dirac operator obtained by a multiplication of the conventional anti-hermitian Dirac operator by γ_5. This is a consequence of defining the generating functional for the left-handed fermions the way we did as opposed to the way it is defined in [69] where the highest states of the two many-body Hamiltonians were used.

The generating functional can be written in the operator form as,

$$Z(\bar{\xi}_R, \bar{\xi}_L, \xi_R, \xi_L) = \left[e^{\bar{\xi}_R \beta\alpha^{-1}\xi_R} \det \alpha\right] \left[e^{\bar{\xi}_L \left[\beta\alpha^{-1}\right]^\dagger \xi_L} \det \alpha^\dagger\right]. \tag{5.15}$$

The derivation of the above expression was detailed in [69]. The main steps in the above derivation is outlined for completeness and would be referred to in the derivation for the finite density case in Sec. 5.4. We can express the exponent of Eq.(5.10) in terms of new operators $Q^\pm$ as,

$$\bar{\xi}_R d_R + \xi_R u_R^\dagger = Q_R^- + Q_R^+ \tag{5.16}$$

where

$$Q_R^+ = \bar{\xi}_R (\delta^{-1})^\dagger d'_R + \xi_R u'^\dagger_R \alpha^{-1}; \quad Q_R^- = -\bar{\xi}_R (\gamma\delta^{-1})^\dagger u_R - \xi_R d_R^\dagger \beta\alpha^{-1}, \tag{5.17}$$

and we have used Eqs.(5.3), (5.5) and (5.6). Since we can also write Q_R^+ as

$$Q_R^+ = \bar{\xi}_R d_R + \xi_R u_R^\dagger - Q_R^- \tag{5.18}$$

it follows that

$$\left[Q_R^-, Q_R^+\right] = -\bar{\xi}_R \left(\beta\alpha^{-1} - (\gamma\delta^{-1})^\dagger\right) \xi_R, \tag{5.19}$$

Using the identity

$$e^{A+B} = e^A e^B e^{-\frac{1}{2}[A,B]} \tag{5.20}$$

where $[A, B]$ is a c-number, we can show that the exponent in Eq.(5.10) is

$$e^{\bar{\xi}_R d_R + u_R^\dagger \xi_R} = e^{Q_R^-} e^{Q_R^+} e^{\frac{1}{2}\bar{\xi}_R \left(\beta\alpha^{-1} - (\gamma\delta^{-1})^\dagger\right)\xi_R}. \tag{5.21}$$

Since

$${}_R\langle -| e^{Q_R^-} = {}_R\langle -|; \quad e^{Q_R^+} |+\rangle_R = |+\rangle_R, \tag{5.22}$$

it follows that

$${}_R\langle -| e^{\bar{\xi}_R d_R + u_R^\dagger \xi_R} |+\rangle_R = e^{\frac{1}{2}\bar{\xi}_R \left(\beta\alpha^{-1} - (\gamma\delta^{-1})^\dagger\right)\xi_R} {}_R\langle -|+\rangle_R = e^{\bar{\xi}_R \beta\alpha^{-1}\xi_R} \det \alpha, \tag{5.23}$$

and we have used the unitarity property $U^\dagger U = 1$ to show

$$(\gamma\delta^{-1})^\dagger + \beta\alpha^{-1} = 0. \tag{5.24}$$

For the left handed sector we can similarly follow the above steps to get an expression of the overlap in terms of the left handed fields,

$$\xi_L d_L^\dagger + \bar{\xi}_L u_L = Q_L^- + Q_L^+ \tag{5.25}$$

where

$$Q_L^+ = \bar{\xi}_L(\alpha^{-1})^\dagger u_L' + \xi_L d_L'^\dagger \delta^{-1}; \quad Q_L^- = -\bar{\xi}_L(\beta\alpha^{-1})^\dagger d_L - \xi_L u_L^\dagger \gamma\delta^{-1}, \tag{5.26}$$

and we have used Eqs.(5.3), (5.5) and (5.6). Since we can also write Q_L^+ as

$$Q_L^+ = \xi_L d_L^\dagger + \bar{\xi}_L u_L - Q_L^- \tag{5.27}$$

it follows similarly as for the right handed sector that

$$\left[Q_L^+, Q_L^-\right] = -\bar{\xi}_L \left((\beta\alpha^{-1})^\dagger - \gamma\delta^{-1}\right) \xi_L, \tag{5.28}$$

and

$$e^{\xi_L d_L^\dagger + \bar{\xi}_L u_L} = e^{Q_L^+} e^{Q_L^-} e^{\frac{1}{2}\bar{\xi}_L\left((\beta\alpha^{-1})^\dagger - \gamma\delta^{-1}\right)\xi_L}. \tag{5.29}$$

Since

$${}_L\langle +| e^{Q_L^-} = {}_L\langle +|; \quad e^{Q_L^-}|-\rangle_L = |-\rangle_L, \tag{5.30}$$

the determinant for the left handed chiral fermions can be simplified to be,

$${}_L\langle +| e^{\xi_L d^\dagger + \bar{\xi}_L u}|-\rangle_L = e^{\frac{1}{2}\bar{\xi}_L\left((\beta\alpha^{-1})^\dagger - \gamma\delta^{-1}\right)\xi_L}\, {}_L\langle +|-\rangle_L = e^{\bar{\xi}_L(\beta\alpha^{-1})^\dagger \xi_L} \det \alpha^\dagger. \tag{5.31}$$

5.3 The massless Overlap Dirac operator

For the numerical implementation of the overlap formalism, it is important to express the determinant in Eq.(5.15), in terms of an effective Dirac operator. In principle, one has to perform an exact diagonalization of H_w which is needed for the computation of U and Eq.(5.15). But there exists an Overlap Dirac operator for vector like theories [18] which can represent the overlap determinant. Considering the unitary operator,

$$V = \gamma_5 sgn(H_w). \tag{5.32}$$

It follows from Eqs.(5.2) and (5.3) that,

$$\frac{1+V}{2}U = \begin{pmatrix} \alpha & 0 \\ 0 & \delta \end{pmatrix}; \quad \frac{1-V}{2}U = \begin{pmatrix} 0 & \gamma \\ \beta & 0 \end{pmatrix}, \tag{5.33}$$

and therefore

$$G_o = \frac{1-V}{1+V} = \begin{pmatrix} 0 & -(\beta\alpha^{-1})^\dagger \\ \beta\alpha^{-1} & 0 \end{pmatrix}, \tag{5.34}$$

is the massless Overlap Dirac propagator. Since [69] the unitary operator U has the property that

$$\det U = \frac{\det \alpha}{\det \delta^\dagger}\ , \tag{5.35}$$

we have the identity,

$$\det \alpha \det \alpha^\dagger = \det \delta \det \delta^\dagger, \tag{5.36}$$

and therefore,

$$\det \alpha \det \alpha^\dagger = \det \frac{1+V}{2}. \tag{5.37}$$

The massless Overlap Dirac operator is given by

$$D_o = \frac{1+V}{2}. \tag{5.38}$$

Our generating functional in Eq.(5.15) can be written as

$$Z(\bar{\xi}, \xi) = \det D_o e^{-i\bar{\xi}\gamma_4 G_0 \xi}. \tag{5.39}$$

We can use Eqs.(5.34) and (5.37) along with an efficient implementation of V to compute the generating functional. One essential ingredient of the overlap formalism is that the operator appearing in the determinant in Eq.(5.37) is not identical to the operator used to compute the propagator in Eq.(5.34). This is a generic feature of the chiral fermions.

5.4 Introduction of the chemical potential

Consider the generating functional

$$Z(\bar{\xi}_R, \bar{\xi}_L, \xi_R, \xi_L; \hat{\mu}_R, \hat{\mu}_L) = {}_R\langle -|e^{\bar{\xi}_R d_R + \xi_R u_R^\dagger + u_R^\dagger \hat{\mu}_R d_R}|+\rangle_{RL}\langle +|e^{\xi_L d_L^\dagger + \bar{\xi}_L u_L - d_L^\dagger \hat{\mu}_L u_L}|-\rangle_L, \tag{5.40}$$

where $\hat{\mu}_R(\mu_R)$ and $\hat{\mu}_L(\mu_L)$ are operators that parametrically depend on the chemical potentials, μ_R and μ_L.

In order to obtain a formula for the generating functional in terms of the determinant of the many body operators, we start by noting that

$$\int d\zeta_R d\bar{\zeta}_R e^{-\bar{\zeta}_R \hat{\mu}_R d_R - \zeta_R u_R^\dagger + \bar{\zeta}_R \zeta_R} = e^{u_R^\dagger \hat{\mu}_R d_R} \tag{5.41}$$

and

$$\int d\bar{\zeta}_L d\zeta_L e^{-\bar{\zeta}_L \hat{\mu}_L u_L - \zeta_L d_L^\dagger - \bar{\zeta}_L \zeta_L} = e^{-d_L^\dagger \hat{\mu}_L u_L}. \tag{5.42}$$

Therefore,

$$\begin{aligned} Z(\bar{\xi}_R, \bar{\xi}_L, \xi_R, \xi_L; \mu_R, \mu_L) &= \det \alpha \det \alpha^\dagger \\ &\quad \int d\zeta_R d\bar{\zeta}_R e^{\bar{\zeta}_R \zeta_R + \left(\bar{\xi}_R - \bar{\zeta}_R \hat{\mu}_R\right) \beta \alpha^{-1} (\xi_R - \zeta_R)} \\ &\quad \int d\bar{\zeta}_L \zeta_L e^{-\bar{\zeta}_L \zeta_L + \left(\bar{\xi}_L - \bar{\zeta}_L \hat{\mu}_L\right) \left[\beta \alpha^{-1}\right]^\dagger (\xi_L - \zeta_L)} \\ &= \det \alpha \det \left(1 + \hat{\mu}_R \beta \alpha^{-1}\right) \det \alpha^\dagger \det \left(1 - \hat{\mu}_L \left[\beta \alpha^{-1}\right]^\dagger\right) \\ &\quad e^{\bar{\xi}_R \frac{1}{\alpha \beta^{-1} + \hat{\mu}_R} \xi_R} e^{\bar{\xi}_L \frac{1}{\left[\alpha \beta^{-1}\right]^\dagger - \hat{\mu}_L} \xi_L} \end{aligned} \tag{5.43}$$

The generating functional is invariant under the chiral transformation given in Eq.(5.12) since the introduction of the chemical potential does not mix the two chiral sectors. To be consistent with the continuum definition of the chemical potentials, we require

$$\hat{\mu}_R(0) = 0; \qquad \hat{\mu}_L(\mu) = -\hat{\mu}_R^\dagger(-\mu). \tag{5.44}$$

The fermion determinant is not real and positive for a real quark chemical potential, $\mu_R = \mu_L = \mu$, but it is real and positive for an isospin chemical potential, $\mu_R = -\mu_L = \mu$. These are standard properties in the continuum correctly reproduced in the overlap formalism.

There are several choices for $\hat{\mu}_R(\mu)$ which would be addressed in detail when we analyze the thermodynamics of free fermions.

5.5 The massless Overlap Dirac operator with a chemical potential

Let the operator containing the quark chemical potentials be denoted as,

$$N = \begin{pmatrix} 0 & \hat{\mu}_R \\ \hat{\mu}_L & 0 \end{pmatrix}$$

. Using Eqs.(5.34) and (5.37) it can be deduced that the determinant part in the Eq.(5.43) can be expressed in terms of the sign function without diagonalizing the operator U,

$$\begin{aligned} \det\alpha \det\alpha^\dagger \det\left(1+\hat{\mu}_R\beta\alpha^{-1}\right) \qquad & \det\left(1-\hat{\mu}_L\left[\beta\alpha^{-1}\right]^\dagger\right) = \det\left[\frac{1+V}{2}+N\frac{1-V}{2}\right] \\ = \quad & \det\frac{1+V}{2}\det\left[1+N\frac{1-V}{1+V}\right] . \end{aligned} \tag{5.45}$$

The propagator can also be expressed in terms of four dimensional operator as,

$$G_o(\hat{\mu}_R,\hat{\mu}_L) = \left[\frac{1+V}{1-V}+N\right]^{-1} . \tag{5.46}$$

The partition function for the Overlap fermions in presence of a finite chemical potential is thus,

$$Z(\bar{\xi},\xi;\hat{\mu}_R,\hat{\mu}_L) = \det D_o(\hat{\mu}_R,\hat{\mu}_L)e^{-i\bar{\xi}\gamma_4 G_o(\hat{\mu}_R,\hat{\mu}_L)\xi}. \tag{5.47}$$

5.6 Thermodynamics of free fermions at finite density

In order to work out the energy density and quark number susceptibility for free massless quarks, it is best to work in momentum space since the corresponding fermion Hamiltonian can be diagonalized exactly. Let us assume that we have converted to creation and annihilation operators in momentum space by the appropriate unitary transformation. We will work on a $N^3\times N_T$ lattice. The allowed discrete spatial momenta are p_k in the range $[-\pi,\pi]$. The Matsubara frequencies in the N_T direction are $\omega_n = \frac{(2n+1)\pi}{N_T}$; $n = 0,\cdots,N_T-1$ and we will assume that N_T is even. The hermitian Wilson-Dirac operator for a fixed momentum takes the form

$$H_w = \begin{pmatrix} -h_5 & c \\ c^\dagger & h_5 \end{pmatrix} \tag{5.48}$$

where

$$c = i\sum_k \sigma_k \sin p_k - \sin\omega_n;$$
$$cc^\dagger = c^\dagger c \;\; = \;\; \sum_k \sin^2 p_k + \sin^2\omega_n. \tag{5.49}$$

The positive eigenvalues come in one doubly degenerate pair, $\lambda = \sqrt{h_5^2 + cc^\dagger}$, per momentum block and the corresponding pair of orthonormal eigenvectors are

$$\frac{1}{\sqrt{2\lambda(\lambda+h_5)}}\begin{pmatrix} c \\ \lambda + h_5 \end{pmatrix}. \tag{5.50}$$

Note that λ and h_5 are even functions of ω_n at a fixed p_k. Assuming a vector like chemical potential, we write

$$N = \begin{pmatrix} 0 & n(\mu,\omega_n) \\ -n^*(-\mu,\omega_n) & 0 \end{pmatrix}, \tag{5.51}$$

per momentum block where $n(0,\omega_n) = 0$. We write,

$$n(\mu,\omega_n) = n_r(\mu,\omega_n) + i n_i(\mu,\omega_n)\ , \tag{5.52}$$

where $n_{r,i}(\mu,\omega_n)$ are both real functions. The free energy density is given by

$$F(\mu,N_T)a^4 = -\frac{1}{N^3 N_T}\sum_{n,p_k}\left\{-2\ln(2\lambda) + \ln\left(g^2+h\right)\right\}\ , \tag{5.53}$$

where

$$g = \lambda - h_5 + n(\mu,\omega_n)n^*(-\mu,\omega_n)(\lambda+h_5) - [n(\mu,\omega_n) + n^*(-\mu,\omega_n)]\sin\omega_n\ , \tag{5.54}$$

and

$$h = [n(\mu,\omega_n) - n^*(-\mu,\omega_n)]^2 f\ , \quad f = \sum_{k=1}^{3}\sin^2 p_k. \tag{5.55}$$

The quark number susceptibility,

$$\chi = -\left.\frac{\partial^2 F}{\partial\mu^2}\right|_{\mu=0} \tag{5.56}$$

can be evaluated to be,

$$\chi a^2 = \frac{1}{N^3 N_T}\sum_{n,p_k}\frac{4(q^2-r^2)\left(\sin^2\omega_n - f\right) - 4v(\lambda-h_5)\sin\omega_n}{(\lambda-h_5)^2}\ , \tag{5.57}$$

where

$$q(\omega_n) = \left.\frac{\partial n_i(\mu,\omega_n)}{\partial(\mu a)}\right|_{\mu=0}; \quad r(\omega_n) = \left.\frac{\partial n_r(\mu,\omega_n)}{\partial(\mu a)}\right|_{\mu=0}; \quad v(\omega_n) = \left.\frac{\partial^2 n_r(\mu,\omega_n)}{\partial^2(\mu a)}\right|_{\mu=0}. \tag{5.58}$$

The sum over n can be non-zero only if $4(q^2 - r^2)$ is an even function of ω_n and v is an odd function of ω_n. The two choices we have made are,

$$n(\mu,\omega_n) = \frac{1}{2M}\begin{cases} i\mu a & \text{local} \\ \sin\omega_n - \sin(\omega_n - i\mu a) & \text{H-K} \end{cases}. \tag{5.59}$$

For the local case,

$$q = \frac{1}{2M}; \quad r = 0; \quad v = 0\ . \tag{5.60}$$

For the H-K case,

$$q = \frac{\cos\omega_n}{2M}; \quad r = 0; \quad v = -\frac{\sin\omega_n}{2M}\ . \tag{5.61}$$

We can make a modification to the H-K insertion such that $v = 0$ but keep q to be the same. This corresponds to

$$\hat{\mu}_R(\mu) = \frac{i}{2M}\sinh\frac{\mu a}{2}(T_4 + T_4^\dagger) \Rightarrow n(\mu,\omega_n) = \frac{i}{M}\cos\omega_n \sinh\frac{\mu a}{2}. \tag{5.62}$$

Keeping only the forward derivative will result in

$$n(\mu,\omega_n) = \frac{i}{M}e^{i\omega_n}\sinh\frac{\mu a}{2}, \tag{5.63}$$

with

$$q = \frac{\cos\omega_n}{2M}; \quad r = -\frac{\sin\omega_n}{2M}; \quad v = 0. \tag{5.64}$$

This leads us to consider the restricted class of operators,

$$\hat{\mu}_R^j(\mu) = \frac{i}{M}\sinh\frac{\mu a}{2}T_4^j \Rightarrow n^j(\mu,\omega_n) = \frac{i}{M}e^{ij\omega_n}\sinh\frac{\mu a}{2}, \tag{5.65}$$

with

$$q = \frac{\cos j\omega_n}{2M}; \quad r = -\frac{\sin j\omega_n}{2M}; \quad v = 0; \quad q^2 - r^2 = \frac{\cos 2j\omega_n}{(2M)^2}. \tag{5.66}$$

This motivates us to study the quantity I_j related to the quark number susceptibility,

$$I_j(N_T, M) = \frac{1}{N^3 N_T M^2}\sum_{n,p_k}\frac{\cos(j\omega_n)\left(\sin^2\omega_n - \sum_{k=1}^3\sin^2 p_k\right)}{(\lambda - h_5)^2},\ j = even\ , \tag{5.67}$$

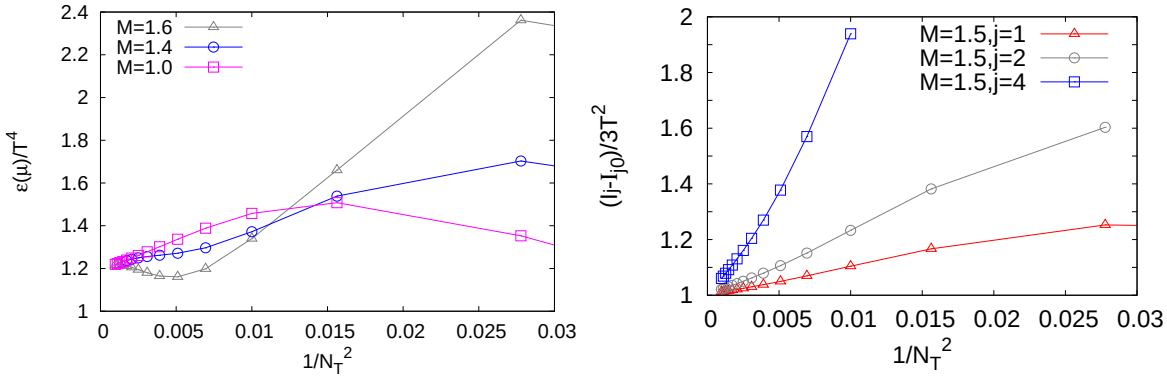

Figure 5.1: The energy density(left panel) and the I_j(right panel) for the Overlap fermions as a functions of $1/N_T^2$ for different M.

and we conjecture that

$$I_j(N_T, M) = I_j(\infty, M) + \frac{1}{3N_T^2} + O\left(N_T^{-4}\right). \tag{5.68}$$

where $I_j(\infty, M)$ is the additional zero temperature lattice artifact that diverges in the continuum limit, appearing in our formalism.

The computations of the energy density and the quark number susceptibility, which is related to the quantity I_j, were done for the free fermions to check their dependence on the irrelevant parameter M. As discussed earlier for the free theory computations, the ratio $\xi = V^{1/3}T = N/N_T$ was fixed for each thermodynamic quantity. When this ratio tends to infinity, the thermodynamic limit is recovered. In numerical simulations, $\xi = 4$ approximates the thermodynamic limit quite well in this case too. Then taking the large N_T limit ensures continuum limit. The energy density was computed on the lattice using the local method of inserting μ. The zero temperature values of the energy density and I_j, were computed on a lattice of the same volume and an infinite temporal extent. These subtracted values normalized by the corresponding Stefan-Boltzmann values, are shown as a function of $1/N_T^2$ for different values of the irrelevant parameter M in Figure 5.1. The thermodynamic quantities have a smoother approach towards the continuum limit with the cut-off errors significantly less than the staggered and even the Bloch-Wettig fermions.

5.7 Summary

We have discussed the problem of introducing the chemical potential within the overlap formalism. In this formalism the chemical potential is coupled only to the physical chiral fermions and the overlap definition of the topological charge is unaffected by the value of μ on the lattice. A large class of number density operators can be coupled to the chemical potential. Each one of them results in a divergent quark number susceptibility but all of them have the correct continuum limit after the divergent contribution is subtracted. For full QCD the quark number susceptibility can be computed by taking the difference between its value on a finite temperature lattice and zero temperature lattice for the same value of lattice gauge couplings and lattice quark masses [47]. This will remove the zero temperature divergences and enable a proper study of the fluctuations close to the transition temperature. We can also consider the linear combination,

$$\hat{\mu}_R(\mu) = \sum_{j=1}^{\infty} c_j \hat{\mu}_R^j(\mu). \tag{5.69}$$

The associated free fermion quark number susceptibility for this choice of the number density operator will be

$$\chi(N_T, M) = \sum_{j_1, j_2=1}^{\infty} c_{j_1} c_{j_2} I_{j_1+j_2}(N_T, M). \tag{5.70}$$

As per the conjecture in (5.68), the quark number susceptibility will give the correct $\frac{1}{3N_T^2}$ behavior as long as

$$\sum_j c_j = 1. \tag{5.71}$$

In order to have no divergence, we need to tune the coefficients, c_j, such that

$$\sum_{j_1, j_2=1}^{\infty} c_{j_1} c_{j_2} I_{j_1+j_2}(\infty, M) = 0, \tag{5.72}$$

and this is only one condition and we have infinite number of coefficients. Therefore, we can find a large class of number density operators that have the correct finite behavior in the free fermion limit. Addition of gauge fields cannot give rise to new divergences as long as all couplings and masses are properly renormalized. $c_1 = \alpha$ and $c_2 = (1 - \alpha)$ can be used with α chosen to cancel the free fermion divergence. This will provide one good choice for the

number density operator in the full interacting theory. The disadvantage in this approach is that one has to tune α to cancel the divergence.

Dynamical simulations of Overlap fermions are currently being performed both at zero temperature [72] and finite temperature [73]. It would be interesting to compute the quark number susceptibility in such simulations using the operators presented in this work and compare them with the complimentary approach of [33].

Chapter 6

Conclusions

In the recent years, the lattice QCD results on the location of the critical point in QCD phase diagram using Taylor expansion of the baryon number susceptibility [3, 4], are beginning to converge. The accurate theoretical estimation of the critical point has gained more importance in view of the fact that there are dedicated large scale experimental facilities in Brookhaven National laboratory(BNL), USA especially aimed at the critical point search. There are also future experiments to start at FAIR, GSI, Germany and at NICA, Russia designed for this purpose. Current theoretical predictions on the critical point are obtained using staggered fermions which have partial chiral symmetry but explicitly broken flavour and spin symmetry on the lattice. The existence of the critical point needs two light quark flavours and correct magnitude of the anomaly term. It is associated with the restoration of chiral symmetry. To make a more precise prediction for the critical point, which can be put to test experimentally, it is desirable to use fermions with exact chiral symmetry as well as having the correct anomaly on the lattice. It would thus be important to understand whether the existing Overlap and Domain wall fermion operators [33, 34] at finite baryon chemical potential have exact chiral symmetry on the lattice. As discussed in the introductory chapter, it is computationally very expensive to implement the chiral fermion operators, like the Overlap operator, for lattice QCD simulations. The aim of this thesis work was to understand the different aspects of QCD at finite temperature and density with the chiral fermion operators on the lattice.

In the second chapter of this thesis, we studied the thermodynamics of free Overlap

fermions finite temperature and density. We derived analytically the possible cut-off effects of the Overlap operator at the tree level by computing thermodynamic quantities of the free Overlap fermions. The branch cuts in the expressions of different thermodynamic quantities, which are absent for the commonly used Wilson/staggered fermions, give rise to additional cut-off effects on a finite lattice. Though these terms do not contribute in the continuum limit, these may have sizeable effects on reasonably small lattice sizes. These cut-off effects can be minimized by a suitable choice of the irrelevant parameter M present in the Overlap operator. We have shown numerically that by fine tuning the value of M in the range 1.50-1.60, it is possible to reduce the deviations due to the finite lattice cut-off effects to within 3-4% of the continuum, on reasonable lattice sizes for both at zero and finite fermion density. Our results are only at the tree level. Since M is an irrelevant parameter, we expect that it would not be changed drastically in full QCD. It would be nevertheless interesting to check how much this optimum M range would change in presence of interactions. Unfortunately we also found that the existing Overlap operator at finite density (Bloch-Wettig operator) [33] does not have exact chiral symmetry on the lattice. The chiral symmetry gets broken at order a and no exact order parameter can be defined on the lattice. If one changes the symmetry transformations to restore exact chiral invariance on the lattice, these become μ dependent. This leads to unphysical consequences like the non-unitary transformation of fermion fields and dependence of the topological charge on μ, which is discussed in detail in chapter four.

In the third chapter, we studied analytically as well as numerically, the thermodynamics of free Domain wall fermions, both at zero and finite fermion density. We have shown that if the number of sites along the fifth dimension $N_5 \geq 18$, we recover a single chiral fermion on the lattice. We have found out analytically that there are additional pole and branch cut contributions to the thermodynamic quantities for Domain wall fermions. These quantities are M dependent and the optimum M range for the Domain wall fermions for which lattice results were within 3-4% of the continuum was found to be $1.45 < M < 1.50$. It was also shown that Domain wall fermion operator for $N_5 \geq 18$, does not have exact chiral symmetry at finite chemical potential. as may be expected. One can also perform tree level improvement of the Wilson-Dirac operator appearing in the argument of the sign function in the Overlap operator. Similar improvements are shown to work for the Domain wall fermions

as well. In this chapter we have demonstrated that through tree level improvements one can reduce the cut-off effects of the thermodynamic quantities of chiral fermions, to within 10% for lattice sizes of $N_T = 6$ commonly used for full QCD simulations.

In the fourth chapter, we used the non-perturbative Fujikawa's method, to prove that the flavour singlet axial anomaly has no additional μ-dependent contribution in the continuum. In addition, we have also checked there are no finite temperature and density corrections to the chiral anomaly even perturbatively, using the imaginary time formalism. This result is in agreement with the existing results on chiral anomaly at finite T and μ using the real time formalism [57, 58, 59]. This implies that the topological charge of the chiral fermions at finite density is μ-independent in the continuum. The chiral fermion operators on the lattice at $\mu = 0$, have all those properties that any chiral fermion operator would have in the continuum. It is well known that the Overlap fermions have a lattice analog of chiral transformation called Luscher transformation [22] under which the action remains invariant. These also satisfy the index theorem on the lattice [61]. We would expect that the Overlap operator at finite μ should have the topological charge independent of μ as in the continuum. We have showed that in order to maintain chiral invariance of the Bloch-Wettig Overlap operator at finite μ, the topological charge should be explicitly μ dependent unlike in the continuum. We tried to motivate a physically more appropriate method of introducing the chemical potential in the Overlap fermion operator. The chemical potential is coupled to only those *physical* fermions that are confined on the 4D domain-wall. This amounts to adding a μN term to the Dirac operator, where N is the point-split number density operator. Under the Luscher transformation, the path integral measure remains independent of μ as in the continuum but the action no longer remain invariant. This method of introducing chemical potential can be generalized to other lattice fermion operators as well. In this prescription however, there would be additional lattice artifacts of order $\mathcal{O}(a^{n-4})$ appearing in the expression of the quark number susceptibilities(QNS) χ_n, which has to be removed to obtain the correct continuum limit.

Since a full QCD computation with the Overlap fermions would be expensive, we have used staggered fermions to compute higher order QNS for two flavour QCD using this method. It was aimed at checking whether these lattice artifacts can be effectively removed by subtracting the free theory contribution since we expect no additional divergences to

appear in a renormalized theory. We have shown that for $T > T_c$, these artifacts have dominant contribution from the free fermions and removing them gives us results which are in reasonable agreement with the existing results obtained using the standard prescription [28]. It remains to be checked whether the values of QNS for $T < T_c$, obtained using the free theory subtraction scheme are in agreement with the standard prescription or with the subtraction scheme where these artifacts are computed on a large symmetric lattice of the same volume and at each gauge coupling. Currently the main challenges in estimating the higher order QNS are computing large number of inverses of the Dirac operator that increases with the successive order of the QNS and delicate cancellation between different terms at each order to give correct values of QNS on the lattice. In this method, the number of matrix inversions are reduced drastically, compared to the standard prescription [28] since μ appears linearly in the action. This would allow us to extend the computations of the QNS to the tenth or even twelfth order. Moreover the cut-off effects in the expression of the QNS computed using our method are considerably reduced compared to the standard method, allowing for more precise estimate of the radius of convergence.

In an attempt to construct an Overlap operator at finite density which has exact chiral symmetry, we have used the first principle Hamiltonian formalism in presence of fermion sources. Here, the determinant of the Overlap operator can be expressed as a superposition of the ground states of two many body Hamiltonians. In the fifth chapter, we have shown that appropriate number operators can be constructed on the lattice in terms of the many body creation operators, which can be coupled with μ. The chiral fermions can be created from the ground states of the two many body Hamiltonians and introduced as Grassmann source terms at the action level. The action in terms of these massless fermions remain invariant under the chiral transformation of sources even in the presence of finite chemical potential. This is the most important result of the fifth chapter. We have constructed partition functions of the Overlap fermions at finite μ with exact chiral symmetry, which can be used to compute different thermodynamic quantities. The second order susceptibility computed using these operators have $\mathcal{O}(1/a^2)$ artifacts and we have suggested two methods to remove these lattice artifacts to get physically relevant value for full QCD.

To summarize, in this thesis we have shown that the existing Overlap and Domain wall fermion operators do not have exact chiral invariance at finite density. We have proved

non-perturbatively that in the continuum QCD, the flavour singlet axial anomaly remains the same even if we turn on a finite μ. This allowed us to motivate for better methods of introducing chemical potential in the lattice chiral fermion operators. We have introduced the chemical potential in the Hamiltonian formalism and tried to understand the meaning of chiral symmetry in the context of Overlap fermions at finite μ in terms of the external fermion sources. Through extensive studies of the thermodynamic quantities of free Overlap/Domain wall fermions, we have tried to understand the cut-off effects of these operators on the lattice. We have shown that it is possible to reduce the cut-off effects through tree level improvement of the Dirac operator or by suitable fine tuning of the irrelevant parameter M present in these operators.

Bibliography

[1] K. Nakamura *et al.* (Particle Data Group), *J. Phys.* G 37, 075021 (2010).

[2] J. Adams *et al.*, *Nucl. Phys.* A757, 102 (2005).

[3] R. V. Gavai and S. Gupta, *Phys. Rev.* D78, 114503 (2008).

[4] C. Schmidt, *Prog. Theor. Phys. Suppl.* 186, 563 (2010).
C. Schmidt, PoS CPOD2009, 024 (2009).

[5] M. A. Stephanov, *Phys. Rev. Lett.* 102, 032301 (2009).

[6] S. Gupta, PoS CPOD2009, 025 (2009).

[7] M. M. Aggarwal *et al.*, *Phys. Rev. Lett.* 105, 022302 (2010).

[8] R. V. Gavai and S. Gupta, *Phys. Lett.* B696, 459 (2011).

[9] B. Mohanty, `e-Print: arXiv:1106.5902` [nucl-ex], to appear in proceedings of Quark Matter 2011.

[10] S. L. Adler, *Phys. Rev.* 177, 2426 (1969).

[11] J. Bell and R. Jackiw, *Nuovo. Cim.* A60, 47 (1969).

[12] K. Fujikawa, *Phys. Rev.* D21, 2848 (1980).

[13] R. D. Pisarski and F. Wilczek, *Phys. Rev.* D29, 338 (1984).

[14] K. G. Wilson, *Phys. Rev.* D10, 2445 (1974).

[15] S. B. Nielsen and M. Ninomiya, *Nucl. Phys.* B 185, 20 (1981).

[16] J. Kogut and L. Susskind, *Phys. Rev.* D11, 395 (1975).

[17] R. Narayanan and H. Neuberger, *Phys. Rev. Lett.* 71, 3251 (1993);
H. Neuberger, *Phys. Lett.* B 417, 141 (1998).

[18] H. Neuberger, *Phys. Rev.* D57, 5417 (1998).

[19] D. B. Kaplan, *Phys. Lett.* B288, 342 (1992).

[20] P. Hernandez, K. Jansen and M. Luscher, *Nucl. Phys.* B552, 363 (1999).

[21] P. H. Ginsparg and K. G. Wilson, *Phys. Rev.* D25, 2649 (1982).

[22] M. Luscher, *Phys. Lett.* B428, 342 (1998).

[23] P. M. Vranas, *Phys. Rev.* D57, 1415 (1998).

[24] M. Cheng *et al.*, *Phys. Rev.* D81, 054510 (2010).

[25] Y. Kikukawa and A. Yamada, `e-Print : hep-lat/9810024`;
P. Hasenfratz *et al.*, *Nucl. Phys.* B643, 280 (2002).

[26] J. E. Mandula, `e-Print: arXiv:0712.0651` [hep-lat].

[27] R. V. Gavai, private communication.

[28] P. Hasenfratz and F. Karsch, *Phys. Lett.* 125B, 308 (1983).

[29] J. Kogut *et al.*, *Nucl. Phys.* B 225, 93 (1983).

[30] N. Bilic and Rajiv V. Gavai, *Z. Phys.* C23, 77 (1984).

[31] R. V. Gavai, *Phys. Rev.* D32, 519 (1985).

[32] P. Hegde *et al.*, *Eur. Phys. J.* , C55, 423 (2008).

[33] J. Bloch and T. Wettig, *Phys. Rev. Lett.* 97, 012003 (2006).

[34] J. Bloch and T. Wettig, *Phys. Rev.* D76, 114511 (2007).

[35] F. Karsch, E. Laermann and A. Peikert, *Phys. Lett. B* 478, 447 (2000).

[36] E. Laermann and O. Philipsen, *Ann. Rev. Nucl. Part. Sci.* 53, 163 (2003).

[37] K. Rajagopal and F. Wilczek, in "At the Frontier of Particle Physics / Handbook of QCD", Vol. 3, M. Shifman, ed., (World Scientific), p2061.

[38] W. Bietenholz, *Eur. Phys. J.* C6, 537 (1999).

[39] C. Gattringer and L. Liptak, *Phys. Rev.* D76, 054502 (2007).

[40] W. Bietenholz *et al.*, *Nucl. Phys. Proc. Suppl.* 53, 921 (1997); W. Bietenholz and U. J. Wiese, *Phys. Lett. B.* 426, 114 (1998).

[41] W. Bietenholz and I. Hip, *Nucl. Phys.* B570, 423 (2000).

[42] H. J. Rothe, "Lattice Gauge Theories: An introduction", (World Scientific), Second edition (1998).

[43] Thesis of Debasish Banerjee, 2011, Tata Institute of Fundamental Research, India.

[44] Y. Shamir, *Nucl. Phys.* B406, 90 (1993).

[45] R. G. Edwards and U. M. Heller, *Phys. Rev.* D63, 094505 (2001).

[46] D. Banerjee, R. V. Gavai and S. Sharma, *Phys. Rev.* D78, 014506 (2008).

[47] R. V. Gavai and S. Sharma, *J. Phys.* G 35, 104097 (2008).

[48] G. T. Flemming, *Nucl. Phys. Proc. Suppl.* 94, 393 (2001).

[49] P. Hegde, F. Karsch and C. Schmidt, `e-Print arxiv:0810.0290`[hep-lat].

[50] S. Capitani, *Phys. Rev.* D75, 054505 (2007).

[51] S. Naik, *Nucl. Phys.* B316, 238 (1989).

[52] R. V. Gavai, *Nucl. Phys. Proc. Suppl.* 119, 529 (2003).

[53] W. Bietenholz and I. Hip, *Nucl. Phys.* B570, 423 (2000).

[54] M. Kapusta, *Finite Temperature Field Theory* , Cambridge University Press, Cambridge, England, (1985), pp. 124-125.

[55] A. Zee, *Quantum Field Theory in a Nutshell* , Princeton University Press, Princeton, NJ, (1980), pp. 244-248.

[56] H. Itoyama and A. H. Meuller, *Nucl. Phys.* B 218, 349 (1983).

[57] Z. Qian, R. Su and P. K. N. Yu, *Z. Phys.* C63, 651 (1994).

[58] S. Gupta and S. N. Nayak, `e-Print hep-ph/9702205`.

[59] S. D. Hsu, F. Sannino and M. Schwetz, *Mod. Phys. Lett.* A16, 1871 (2001).

[60] We thank Parthasarathi Mitra of SINP Kolkata for pointing this out to us, which led to the transformation we used in Eq. (4.14).

[61] P. Hasenfratz, V. Laliena and F. Neidermeyer, *Phys. Lett.* B 427, 125 (1998).

[62] K. Fujikawa, *Nucl. Phys.* B 546, 480 (1999).

[63] D. Banerjee, R. V. Gavai and S. Sharma, *PoS (LATTICE 2008)*, 177.

[64] R. V. Gavai and S. Gupta, *Phys. Rev.* D71, 114014 (2005).

[65] C. R. Allton *et al.*, *Phys. Rev.* D66, 074507 (2002);
C. R. Allton *et al.*, *Phys. Rev.* D68, 014507 (2003);
R. V. Gavai and S. Gupta, *Phys. Rev.* D68, 034506 (2003).

[66] S. Gupta, *Phys. Rev.* D64, 034507 (2001).

[67] M. Cheng *et al.*, *Phys. Rev.* D79, 074505 (2009).

[68] C. DeTar *et. al.* , *Phys. Rev.* D81, 114504 (2010).

[69] R. Narayanan and H. Neuberger, *Nucl. Phys.* B 443, 305 (1995).

[70] R. Narayanan and H. Neuberger, *Nucl. Phys.* B 412, 574 (1994).

[71] R. G. Edwards, U. M. Heller, R. Narayanan, Phys. Rev. **D59**, 094510 (1999).

[72] S. Hashimoto, PoS **LATTICE2008**, 011 (2008).

[73] G. Cossu *et al.* [JLQCD Collaboration], PoS **LATTICE2010**, 174 (2010).